Distribution Agreement

In presenting this thesis or dissertation as a partial fulfillment of the requirements for an advanced degree from Emory University, I hereby grant to Emory University and its agents the non-exclusive license to archive, make accessible, and display my thesis or dissertation in whole or in part in all forms of media, now or hereafter known, including display on the world wide web. I understand that I may select some access restrictions as part of the online submission of this thesis or dissertation. I retain all ownership rights to the copyright of the thesis or dissertation. I also retain the right to use in future works (such as articles or books) all or part of this thesis or dissertation.

Signature:

_____ _____

Laura E. Mariani Date

The Role of Arl13b and Non-Canonical Sonic Hedgehog Signaling in Joubert Syndrome

By

Laura E. Mariani
Doctor of Philosophy

Graduate Division of Biological and Biomedical Science
Neuroscience

_____
Tamara Caspary, PhD
Advisor

_____
Gary Bassell, PhD
Committee Member

_____
Ping Chen, PhD
Committee Member

_____
Randy Hall, PhD
Committee Member

_____
Rick Kahn, PhD
Committee Member

Accepted:

_____
Lisa A. Tedesco, PhD
Dean of the James T. Laney School of Graduate Studies

_____
Date

The Role of Arl13b and Non-Canonical Sonic Hedgehog Signaling in Joubert Syndrome

By

Laura E. Mariani
BS, MS, Brandeis University, 2006

Advisor: Tamara Caspary, PhD

An abstract of
a dissertation submitted to the Faculty of the
James T. Laney School of Graduate Studies of Emory University
in partial fulfillment of the requirements for the degree of
Doctor of Philosophy in the Graduate Division of Biological
and Biomedical Sciences, Neuroscience, 2015

Abstract

The Role of Arl13b and Non-Canonical Sonic Hedgehog Signaling in Joubert Syndrome

By Laura E. Mariani

The human ciliopathy Joubert Syndrome (JS) can be caused by mutations in *ARL13B*, a gene that codes for a cilia-associated protein regulating canonical, transcriptional Sonic hedgehog (Shh) signaling. While many symptoms and signs of JS can be easily explained by defects in cilia and/or canonical Shh signaling, the key diagnostic criterion of JS is of unknown molecular etiology. In order to receive a diagnosis of JS, patients must exhibit an anatomical malformation of the hindbrain white matter known as the molar tooth sign (MTS), which involves abnormal axon guidance in the projection neurons that give rise to the superior cerebellar peduncle (SCP). Indeed, JS patients show aberrant axon guidance in many brain regions. The mechanism through which cilia-associated proteins can affect axon guidance is unknown. However, in addition to its canonical functions, Shh signaling can act through a non-canonical pathway to regulate axon guidance in some neurons. This dissertation tests the hypothesis that mutations in *ARL13B* give rise to JS-associated anatomical abnormalities by misregulating Shh-dependent axon guidance.

I first examine how *Arl13b* mutations affect Shh signaling in mouse embryonic fibroblasts. Previous work has shown that total loss of Arl13b significantly disrupts transcriptional Shh signaling. In this study, I show differential effects of JS-causing mutations and other mutations in *Arl13b* on cilia and Shh signaling. Using an assay of Shh-dependent fibroblast migration, I give the first evidence that shows Arl13b is involved in non-canonical Shh signaling. Surprisingly, I find that Arl13b need not be present in cilia in order to execute some of its functions, and that mutations disrupting cilia localization of Arl13b have counterintuitive effects on canonical (cilia-associated) and non-canonical (cilia-independent) Shh signaling.

I next ask whether Arl13b is specifically involved in the development of axons in neurons known to use Shh as a guidance cue, and whether perturbing Arl13b or Shh signaling in hindbrain projection neurons can recapitulate the phenotypes seen in JS. Using mouse genetic models and cultured neurons, I show that a) loss of Arl13b in the mouse brain produces phenotypes consistent with JS, b) loss of either Arl13b or the Shh pathway protein Smoothened (Smo) in the neurons of the SCP produces defects in midline crossing, and c) loss of Arl13b affects axonal development in spinal commissural neurons, which use Shh as a guidance cue.

In summation, this work indicates that Arl13b plays multiple roles in regulating both canonical and non-canonical Shh signaling and suggests a mechanism through which JS-causing mutations in *ARL13B* can affect the development of white matter tracts leading to the MTS.

The Role of Arl13b and Non-Canonical Sonic Hedgehog Signaling in Joubert Syndrome

By

Laura E. Mariani
B.S., M.S., Brandeis University, 2006

Advisor: Tamara Caspary, PhD

A dissertation submitted to the Faculty of the
James T. Laney School of Graduate Studies of Emory University
in partial fulfillment of the requirements for the degree of
Doctor of Philosophy in the Graduate Division of Biological
and Biomedical Sciences, Neuroscience, 2015

Acknowledgements

It is with great pleasure that I acknowledge the following people who have contributed to my success in the pursuit of a PhD. Many labmates have supported me through the years, notably our lab "mom" Alyssa Long and my fellow graduate students Sarah Bay, Nicole Umberger, Christy Larkins, Chen-Ying Su, Chao Lin, Sarah Suciu, Julie Fritz, and Ana Portelinha. My classmates in the Emory Neuroscience Graduate Program have been like family, particularly my 2008 cohort, and I thank them for creating a remarkable community that has allowed me to survive and thrive. Credit is also due to my actual family, including Gary Mariani, Stacy Mariani, Al Mariani and Gloria Lay, who instilled in me the values that sustain everything I do, and to whose memory I dedicate this dissertation.

I must thank many excellent collaborators, without whom my ideas could never have come to fruition. Frédéric Charron inspired all of my hypotheses about non-canonical Shh signaling and, along with Julien Ferent, gave generously of his time and expertise to help test those hypotheses. Maarten Bijlsma has been an ideal collaborator and contributed all of the experimental data related to Shh-dependent fibroblast migration. Shella Keilholz, Jaekeun Park, Sarah Suciu and Katherine Bryant provided copious assistance with mouse *ex vivo* DTI protocol development and data analysis. Several Emory core facilities, including the Molecular Cloning Core, Viral Vector Core, and not one but two FACS cores (one at the Emory School of Medicine and one at the Emory+Children's Pediatric Research Center) provided essential technical services.

I acknowledge my dissertation committee (Gary Bassell, Ping Chen, Randy Hall and Rick Kahn) for their support, feedback, and, most importantly, patience through the years. I also thank the Neuroscience Program leadership, including DGSes Ron Calabrese, Leonard Howell, and Malu Tansey, Program Directors Yoland Smith, Shawn Hochman, and David Weinshenker, and Program Administrators Sonia Perez Hayden and Gary Longstreet, who shepherded me through all the important milestones in my graduate career.

Finally, I must give credit to my mentor, Tamara Caspary, who gave me the guidance and freedom I needed as I grew and matured not just as a scientist but as a human being over the past eight years. Tamara, for recognizing my strengths, correcting my errors, forgiving my mistakes, and always reminding me to "just do the experiment," I thank you.

Table of Contents

List of Tables and Figures

List of Symbols and Abbreviations

cm	centimeter
g	gram
kDa	kilodalton
mg	milligram
mL	milliliter
mM	millimolar
mm	millimeter
µL	microliter
µm	micrometer
µM	micromolar
CiLS	Cilia localization signal
e	Embryonic day
DCN	Deep cerebellar nuclei
FACS	Fluorescence assisted cell sorting
FBS	Fetal bovine serum
GliA	Gli activator
GliR	Gli repressor
GNP	Granule neuron precursor
MEF	Mouse embryonic fibroblast
MTS	Molar tooth sign
JS	Joubert Syndrome
p	Postnatal day
PBS	Phosphate-buffered saline

SCP	Superior cerebellar peduncle
Shh	Sonic hedgehog
Smo	Smoothened

Chapter 1

Introduction

Cilia are mysterious. These tiny organelles, long considered vestigial in vertebrate cells, have in recent years inspired an increasing number of studies in genetics, cell biology, and developmental biology. After the surprising discovery that defects in cilia can cause polycystic kidney disease (Pazour et al., 2000), the serendipitous revelation that cilia are involved in vertebrate Sonic hedgehog (Shh) signaling (Huangfu et al., 2003), and the establishment of an ever-expanding list of human ciliopathies (reviewed in: Brown and Witman, 2014; Lee and Gleeson, 2011; Yuan and Sun, 2013), we have come to appreciate the importance of cilia in a variety of biological processes. Still, much remains to be explained about the molecular mechanisms underlying the signaling functions of cilia, and how the disruption of cilia-dependent processes leads to the broad array of phenotypes observed in ciliopathy patients.

This dissertation focuses on one ciliary protein, Arl13b, which has been linked to the ciliopathy Joubert Syndrome (JS; Cantagrel et al., 2008). Previous research from the Caspary lab has shown that Arl13b regulates Shh signaling at multiple points in the pathway (Caspary et al., 2007; Larkins et al., 2011), suggesting a mechanism for the Shh-dependent phenotypes in JS patients. Other JS features, particularly the characteristic hindbrain malformation known as the molar tooth sign (MTS; described in Maria et al., 1999), are more difficult to explain. Mutations in *ARL13B* and other cilia-related genes give rise to defects in the white matter tracts of JS patients, but it is not clear how gene products found at the neuronal cilium can affect the distal axons that form these tracts.

In this dissertation, I put forth the hypothesis that the white matter tracts affected in JS normally undergo Shh-dependent axon guidance and that mutations in Arl13b disrupt this process. My hypothesis reconciles the known role of Arl13b and other cilia proteins in Shh

signaling with the discovery that Shh can serve as an axon guidance cue for some neurons (Charron et al., 2003; Fabre et al., 2010). Because the site of Shh-dependent axon guidance is understood to be the growth cone, I posit that Arl13b must play a role in cellular signaling processes occurring outside of the primary cilium. To test my hypothesis, I conducted a series of experiments exploring the cilia-dependent and cilia-independent functions of Arl13b in Shh signaling, as well as the effects of perturbing Arl13b and Shh signaling in the specific axonal tracts affected in JS.

In chapter 3, I show that Arl13b is involved in Shh-dependent fibroblast migration, a process that can occur even in cells lacking cilia (Bijlsma et al., 2007; Bijlsma et al., 2012). This chapter assesses the importance of different Arl13b protein domains in ciliogenesis and Shh signaling, defines the effects of JS-causing *Arl13b* mutations on Shh signaling, and explores the relationship between Arl13b's presence in cilia and its role in regulating Shh signaling.

In chapter 4, I look more directly at the role of Arl13b in axon guidance through *in vivo* neuroanatomical studies. By analyzing mice with mutations in *Arl13b*, the critical Shh pathway component *Smoothened* (Smo), or both, I draw conclusions about the importance of Arl13b in white matter tracts known to use Shh as a guidance cue. These studies also allow me to determine whether white matter tracts affected in JS, such as the superior cerebellar peduncles (SCPs), display JS-like abnormalities in mice with *Arl13b* and/or *Smo* mutations. This chapter also includes data from an ongoing collaboration examining the role of Arl13b in axon guidance *in vitro*.

The following Introduction provides relevant background information and a more detailed rationale for my experiments. Section 1.1 explains what is currently known about the pathology and etiology of JS and puts JS in context with other ciliopathies. Section 1.2 describes the importance of cilia in Shh signaling and outlines previous research on the functions of Arl13b. (This section includes a portion of the more detailed discussion of cilia, Shh signaling, and neural tube development that I originally published as a chapter in *Cilia and Nervous System*

Development; see Mariani and Caspary, 2013.) Section 1.3 covers transcription-independent Shh signaling in fibroblasts and axons, and how these phenomena differ from canonical, cilia-centric, transcriptionally-dependent Shh signaling. Section 1.4 outlines lingering questions that exist at the nexus of these three topics. As a whole, this dissertation synthesizes the current research in the field of cilia, Shh signaling, and ciliopathies, and gives new insights into the molecular etiology of a complex human disease.

1.1 Joubert Syndrome: A ciliopathy caused by *ARL13B* mutations

Although syndromic human diseases caused by dysfunctional cilia have been clinically recognized for many decades, these disorders have only been linked to cilia – and, therefore, to each other – more recently. Kartagener Syndrome, now more descriptively known as primary ciliary dyskinesia (PCD), was the first human disease shown to arise from cilia dysfunction (Afzelius, 1976). However, PCD symptoms are mostly attributed to problems with motile cilia, such as those that line the airway to assist the flow of mucus. Bardet-Biedl Syndrome was the first human disease to be linked to non-motile primary cilia (Ansley et al., 2003). Since this discovery, more than 20 other ciliopathies have been identified. The signs and symptoms of ciliopathies affect a wide variety of different organs and tissues, emphasizing the importance of cilia in essentially every vertebrate cell type. The phenotypic features of individual ciliopathies also exhibit significant overlap, reflective of their common etiology. The relationships between ciliopathies can be better understood at a molecular level when we consider that many ciliopathy gene products form functional networks with one another, and that in some cases, closely-related ciliopathies can be caused by mutations within the same gene (Figure 1.1). In this way, JS is a model ciliopathy – it shares symptoms and causative mutations with many other ciliopathies, making it an appealing choice for studies that seek to reveal common features across the spectrum of cilia-related diseases.

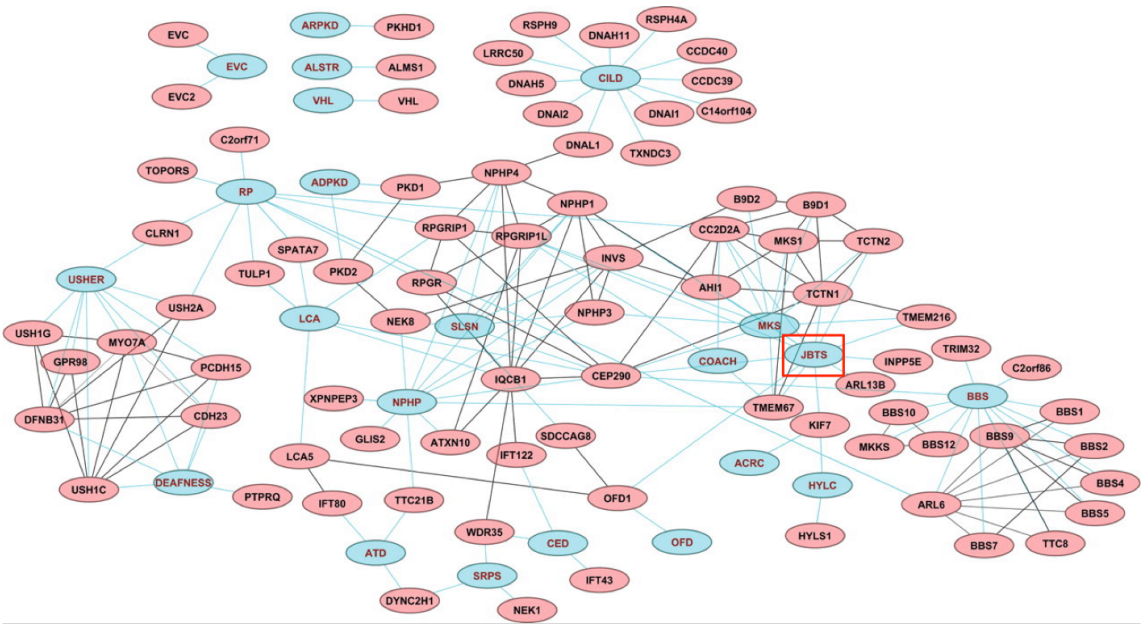

Figure 1.1 Ciliopathy interaction network. This network illustrates the high degree of interaction between ciliary proteins (pink ovals) associated with phenotypically overlapping human ciliopathies (blue ovals). Joubert Syndrome (JBTS, in red box) is closely associated with other ciliopathies both molecularly and phenotypically. Other abbreviations: ACRC, Acrocallosal syndrome; ALSTR, Alstrom Syndrome; ARPKD, Autosomal Recessive Polycystic Kidney Disease; ATD, asphyxiating thoracic dystrophy; BBS, Bardet-Biedl syndrome; CED, Cranioectodermal Dysplasia; CILD, primary ciliary dyskinesia; COACH, Cerebellar vermis hypo/aplasia, Oligophrenia, Ataxia, Coloboma and Hepatic fibrosis; EVC, Ellis-van Creveld syndrome, HYLS, Hydrolethalus syndrome; LCA, Leber Congenital Amaurosis; MKS, Meckel-Gruber syndrome; NPHP, nephronophthisis; OFD, Oro-Facio-Digital syndrome, RP, Retinitis Pigmentosa; SLSN, Senior Løken syndrome; SRP, Short-Rib-Polydactyly; USHER, Usher syndrome; VHL, Von Hippel Lindau disease.
Figure from van Reeuwijk et al., 2011.

Joubert Syndrome is named after pediatric neurologist Marie Joubert, who first described the disorder (Joubert et al., 1969). A diagnosis of "classic" JS requires the presence of infant hypotonia that develops into ataxia, developmental delay and/or intellectual disability, and a neuroanatomical abnormality of the hindbrain known as the molar tooth sign (MTS). The MTS involves hypoplasia or agenesis of the cerebellar vermis, deepening of the interpeduncular fossa, and elongated, thickened, and abnormally oriented superior cerebellar peduncles (SCPs). On an axial MRI, these features combine to create a tooth-like shape visible near the pons/midbrain junction. Although these are the only three criteria for a JS diagnosis, many JS patients also display oculomotor defects (apraxia, nystagmus) and abnormal breathing rhythms (alternating hyperpnea and apnea). Additional symptoms that may occur in JS include retinal dystrophy, renal

disease, hepatic disease, and orofaciodigital abnormalities – patients with these features are often classed as having Joubert Syndrome and Related Disorders (JSRD).

The true prevalence of JS is difficult to discern. Previously published statistics range from 1:80,000 to 1:100,000, but these may be underestimates (Brancati et al., 2010a; Parisi et al., 2007). Furthermore, because the ciliopathies share many common characteristics and closely related etiologies, it may be more appropriate to consider the combined prevalence of all ciliopathies – which is in the range of 1:1000 (Davis and Katsanis, 2012) – when considering the potential impact of research on JS. An improved understanding of the etiology of JS will likely have relevance for other ciliopathies, and will shed new light upon the importance of cilia and cilia-dependent processes for normal embryonic development.

1.1.1 Genetics of JS

Causative mutations for JS have been identified in 23 genes (Parisi and Glass, 2012; Romani et al., 2014; Thomas et al., 2014; Tuz et al., 2014), all of which encode proteins related to primary cilia. Though all JS genes are associated with cilia, their gene products range from the Wnt regulator AHI1/Jouberin (Dixon-Salazar et al., 2004) to the small GTPase ARL13B (Cantagrel et al., 2008), and there are many gaps in our understanding of the function of these diverse cilia proteins. JS is one of the most genetically diverse ciliopathies and many genes known to cause JS have also been associated with other ciliopathies. For example, mutations in *CEP290* can cause nephronophthisis, Meckel-Gruber Syndrome, Senior-Loken Syndrome, and Bardet-Biedl Syndrome in addition to JS (reviewed in Davis and Katsanis, 2012). At times, members of a single family possessing the same genetic mutation will have disparate symptoms, leading to distinct diagnoses of either JS or a different ciliopathy. This has made it particularly difficult to determine exactly how mutations in cilia-associated genes lead to the characteristic features of diseases like JS.

Of the 23 genes implicated in JS to date, two seem especially sensitive to mutations: *ARL13B* and *INPP5E*. Clinicians have identified patients homozygous for deletions and/or truncating mutations in other JS genes (reviewed in: Barkovich et al., 2009; Parisi and Glass, 2012; Valente et al., 2008) but not in *ARL13B* or *INPP5E.* Instead, patients with *ARL13B* or *INPP5E* mutations all possess at least one hypomorphic allele, preserving at least some protein function (Bielas et al., 2009; Cantagrel et al., 2008).

1.1.2 Shh-dependent features of JS

Although the molecular etiology of ciliopathies is not completely understood, the relationship between cilia and Shh signaling clearly underlies certain ciliopathy features. JS is no exception: many JS-associated phenotypes are consistent with defects in well-characterized forms of canonical Shh signaling.

Shh acts as a mitogen in the developing cerebellum. Cerebellar Purkinje cells secrete Shh ligand, which is detected by developing granule neuron precursor cells (GNPs) and activates pro-mitotic factors such as cyclin D1/D2. This Shh-dependent proliferation causes a huge expansion in the number of GNPs during embryonic and early postnatal development, such that by the time the cerebellum has fully developed (around p21 in mice), mature granule neurons are the most abundant cell type in the entire brain (reviewed in: Roussel and Hatten, 2011). Because granule neurons make up such a large portion of the cerebellum, perturbations in Shh signaling (and therefore, GNP proliferation) can lead to changes in the overall size and shape of the cerebellum, including the number and arrangement of cerebellar folia (Corrales et al., 2004). Modest to moderate changes in cerebellar Shh signaling may even explain inter-species differences in cerebellar structure: increasing the level or duration of Shh signaling in mice leads to the formation of an additional fissure in the cerebellum that is normally only found in rats (Corrales et al., 2006). Meanwhile, reductions in Shh signaling, including those caused by perturbation of cilia-associated genes, lead to hypoplasia or agenesis of the cerebellum (Chizhikov et al., 2007).

These phenotypes are consistent with the cerebellar vermis hypoplasia seen in JS patients as part of the MTS.

In addition to neurodevelopmental signs of abnormal Shh signaling, JS patients can have other phenotypes consistent with Shh defects. Orofaciodigital abnormalities, although not required for a JS diagnosis, are seen in some patients with JSRD. 8-19% of patients with JSRD exhibit polydactyly (Brancati et al., 2010b; Doherty, 2009), in which extra digits form in response to abnormal levels of Shh signaling in the developing limb (reviewed in: Anderson et al., 2012). Shh is also critical for craniofacial patterning. Defects in Shh signaling cause a range of craniofacial midline patterning defects, from holoprosencephaly and cyclopia to cleft lip/palate (Hu and Helms, 1999; Hu et al., 2015). Some JS patients exhibit cleft lip, lobulated tongue, or midline lip groove, and many clinicians have noticed a characteristic pattern in the facial features of JS patients, some of which may be attributable to abnormalities in Shh-dependent craniofacial development (Braddock et al., 2007). Finally, ciliopathy patients (particularly Bardet-Biedl Syndrome patients) often present with obesity, although obesity has been observed in only one JS case (Thomas et al., 2015). The factors contributing to obesity are complex, but Shh signaling may be involved: Shh signaling blocks white (but not brown) adipogenesis (Pospisilik et al., 2010; Suh et al., 2006) and cilia-dependent Shh signaling through Smo and Ampk can regulate cellular metabolism in both muscle and brown fat (Teperino et al., 2012).

Given the relationship between cilia and Shh signaling, as well as the clear relationship between Shh-dependent developmental processes and many features of JS, it seems plausible that Shh signaling may underlie other features of JS that remain to be explained. This dissertation therefore focuses on elucidating the relationship between Shh signaling and the more poorly-characterized neuroanatomical features of JS.

1.1.3 Unexplained features of JS

The MTS is a fundamental diagnostic criterion for JS, but little is known about the etiology of this hindbrain malformation. This is especially significant in light of the fact that many severe symptoms of JS arise from defects in the hindbrain: cerebellar dysfunction commonly causes ataxia, while life-threatening breathing problems are linked to hindbrain nuclei such as the parafacial respiratory group and pre-Bötzinger complex (reviewed in: Onimaru et al., 2006). It is unclear how the genetic mutations that cause JS lead to such a stereotyped defect in the anatomy and functional circuitry of the hindbrain.

Formation of the MTS clearly involves abnormal axon guidance in the cells comprising the SCP. Radiological studies as well as post mortem analysis of JS patient brains have confirmed midline crossing defects in the SCPs as well as the central pontine tract and the medullary pyramids of the corticospinal tract (Juric-Sekhar et al., 2012; Maria et al., 1999; Yachnis and Rorke, 1999). These abnormal anatomical features are associated with physiological and behavioral phenotypes in JS: failure of such tracts to decussate is correlated with inappropriate bilateral activation of sensorimotor cortex as measured by fMRI (Parisi et al., 2004) and can make it difficult for patients to activate muscles on one side of the body without inappropriate muscle contractions of the contralateral side (mirror movement synkinesis; reviewed in Engle, 2010). Furthermore, abnormal decussation at the optic chiasm is likely to underlie some ophthalmic features associated with JS, such as nystagmus and asymmetric visual evoked potentials (Khan et al., 2008).

Many other abnormalities have been observed in subsets of JS brains, including fragmented deep cerebellar nuclei (DCN) and hypoplasia of the solitary, trigeminal, and dorsal column nuclei. However, because only a small number of patient brains have been carefully analyzed for neuropathology, it is not clear which of these anatomical abnormalities are associated with which neurological symptoms of JS.

1.2 Cilia proteins and Sonic hedgehog signaling

Primary cilia are linked to a variety of biochemical pathways, with the Sonic hedgehog (Shh) signaling pathway being especially notable for its fundamental connection to cilia structure and function (reviewed in: Berbari, O'Connor, Haycraft, & Yoder, 2009; Eggenschwiler & Anderson, 2007; Wong & Reiter, 2008). Without primary cilia, canonical Shh signaling cannot occur (Huangfu and Anderson, 2005; Huangfu et al., 2003), and genetic mutations that disrupt ciliogenesis, intraflagellar transport (IFT), and other important cilia functions typically cause defects in Shh signaling as well. Many such mutations are incompatible with life because Shh is so important for embryonic development, but in animal models these mutations have revealed much about the complex interaction between cilia and developmental signaling.

Shh plays many roles in the developing nervous system (reviewed in: Sánchez-Camacho and Bovolenta, 2009; Hatten and Roussel, 2011), where it was first shown to possess an essential function in patterning the embryonic spinal cord, also known as the neural tube (Chiang et al., 1996; Echelard et al., 1993). During development, there is a gradient of Shh activity in the neural tube that confers different cell fates upon neural progenitors at distinct positions along the dorsoventral axis. The resulting progenitor domains are highly consistent among embryos and also highly sensitive to changes in Shh activity (reviewed in: Jessell, 2000; J Briscoe and Ericson, 2001; Lupo et al., 2006; Dessaud et al., 2008), making the pattern of the ventral neural tube an informative readout of any perturbations to the Shh signaling pathway. Indeed, such perturbations are what revealed the initial link between cilia and Shh signaling (Huangfu et al., 2003).

In recent years, descriptive *in vivo* studies on the relationship between cilia and Shh activity in the neural tube have been complemented by cellular and molecular experiments that give a more mechanistic explanation of the role of cilia in Shh signaling. We now know that Shh signals are transduced via a series of proteins that dynamically enter and exit the primary cilium in a ligand-dependent manner (Corbit et al., 2005; Haycraft et al., 2005; Rohatgi et al., 2007), ultimately resulting in either the activation or repression of Shh target genes. If the primary cilium

is absent or abnormal, Shh signaling is adversely affected (Huangfu and Anderson, 2005; Huangfu et al., 2003; Liu et al., 2005). Furthermore, an entire suite of specialized molecules regulates the traffic and transport of Shh pathway components and other ciliary proteins into and within cilia (Haycraft et al., 2005; Kovacs et al., 2008; Liu et al., 2005; May et al., 2005; Seo et al., 2011). Disruption of any aspect of this molecular system can lead to Shh signaling defects and developmental abnormalities. This section of the Introduction focuses on the relationship between cilia and canonical Shh signaling, primarily focusing on how studies of abnormal neural patterning in mouse have informed our understanding of the role cilia proteins play in regulating Shh signaling.

1.2.1 Canonical Shh signaling pathway components

In canonical Shh signaling, cells respond to Shh ligand through a multi-step molecular cascade that results in the expression of Shh target genes. Ultimately, Shh signaling regulates target gene expression via the Gli family of transcription factors, which can act either as transcriptional activators or repressors (Bai et al., 2004; Ding et al., 1998; Lei et al., 2004; Litingtung and Chiang, 2000; Matise et al., 1998). Other critical regulators of Gli transcriptional activity include the Shh receptor, Patched1 (Ptch1) (Denef et al., 2000; Marigo et al., 1996; Taipale et al., 2002); the major effector of Shh activity, Smoothened (Smo) (Alcedo et al., 1996; Stone et al., 1996; vandenHeuvel and Ingham, 1996); the Gli inhibitor, Suppressor of Fused (Sufu) (Ding et al., 1999; Kogerman et al., 1999; Svärd et al., 2006); an atypical kinesin, Kif7 (Cheung et al., 2009; Endoh-Yamagami et al., 2009; Liem et al., 2009); and protein kinase A (PKA) (Epstein et al., 1996; Hammerschmidt et al., 1996; Pan et al., 2009; Tuson et al., 2011). As the Shh signal is transduced, all of the aforementioned proteins localize to primary cilia in a highly regulated manner.

In the absence of Shh, Ptch1 inhibits Smo, thereby acting as a brake on Shh signaling (see Figure 1.2, left; Denef et al., 2000; Taipale et al., 2002). (Ptch2 can also serve as a Shh receptor

and plays a role in regulating early developmental patterning, see Alfaro et al., 2014.) When Shh binds to Ptch1, the inhibition of Smo is relieved, triggering activation of Gli proteins and transcription of Shh target genes. The opposing functions of Ptch1 and Smo in Shh signaling become clear when these proteins are ablated in mice. *Ptch1*$^{-/-}$ embryos exhibit a ventralized neural tube in which cells throughout the tissue express markers of the floor plate, indicating a maximal level of Shh signaling in the absence of the inhibitory receptor (Goodrich et al., 1997). *Smo*$^{-/-}$ embryos, on the other hand, are insensitive to Shh ligand and fail to develop any Shh-dependent cell types in the neural tube (Wijgerde et al., 2002). Similar experiments in mouse genetics have used neural tube patterning phenotypes to examine the role of many other proteins in the Shh pathway, as I will describe in more detail later in this Introduction.

Under normal conditions, Shh-dependent neural patterning arises from differing levels of Gli activator (GliA) and repressor (GliR) activity along the dorsoventral axis of the neural tube (Lei et al., 2004; Motoyama et al., 2003; Sasaki et al., 1999). Ultimately, because Shh pathway activity mirrors the gradient of Shh ligand across the dorsoventral axis, the end result of this tightly regulated signaling cascade is that GliA levels are high in the ventral neural tube, whereas GliR predominates in the dorsal neural tube. These opposing gradients of activator and repressor establish the progenitor domains in the ventral neural tube.

In vertebrates, the Gli family of transcription factors consists of three members: Gli1 functions solely as a transcriptional activator, while Gli2 and Gli3 contain both activator and repressor domains (Bai et al., 2002; Ding et al., 1998; Park et al., 2000; Persson et al., 2002). Gli2 serves as the primary activator and cleaved Gli3 the primary repressor of Shh target genes in the mammalian neural tube (Sasaki et al., 1999). The regulation of Gli2 and Gli3 is critical for the proper transduction of Shh signaling. In the absence of Shh activity, Gli3 is proteolytically cleaved into its repressor form (GliR) through a PKA-dependent mechanism (Wang et al., 2000), and Gli2 is targeted for degradation. Sufu binds to Glis in the absence of Shh signaling, serving both to stabilize the Gli proteins and inhibit their activation (see Figure 1.2; Chen et al., 2009;

Tukachinsky et al., 2010; Wang et al., 2010). When Shh is present, the ensuing Shh signaling cascade blocks the cleavage of Gli3 into GliR and stabilizes full-length Gli2, which can then be converted into its activator form (GliA) through an as-yet-unknown mechanism. The atypical kinesin Kif7 is necessary for the formation of both GliA and GliR via a cilia-dependent process (Cheung et al., 2009; Endoh-Yamagami et al., 2009; Liem et al., 2009). In addition, PKA regulates not just the processing of Gli3 into GliR, but also the activation of Gli2 (Tuson et al., 2011).

The functions of individual Gli proteins in neural tube patterning have been studied through genetic ablation experiments. *Gli1*$^{-/-}$ mice are phenotypically normal, indicating that Gli1 is dispensable for Shh signaling in mammals. In fact, *Gli1* is itself a Shh target gene, and all Gli1 expression requires Shh signaling (Bai et al., 2002). In the absence of Gli1, the other Gli proteins (primarily Gli2) compensate for its function. *Gli2*$^{-/-}$ mouse embryos, in contrast, display reduced Shh activity: the highest levels of Shh activity cannot be achieved without Gli2. This indicates Gli2's role as the primary activator of Shh target gene transcription in the neural tube (Ding et al., 1998; Matise et al., 1998; Park et al., 2000). Finally, *extra toes (Xt)* mouse embryos, which carry a protein null mutation in *Gli3*, show an expansion of the Shh-responsive domain of the neural tube in the absence of the primary repressor (Persson et al., 2002). Epistasis experiments indicate that Gli3 does have some role as an activator, however; *Gli2*$^{-/-}$*;Gli3*$^{Xt/Xt}$ double mutant embryos completely lack Shh-dependent v3 progenitor cells in the neural tube, suggesting the v3 progenitors that are present in *Gli2*$^{-/-}$ embryos are induced by GliA derived from Gli3 (Motoyama, 2003). This exquisite sensitivity to such slight changes in the balance of GliA and GliR highlights the neural tube as an excellent system for testing hypotheses about canonical Shh signaling through genetic manipulations.

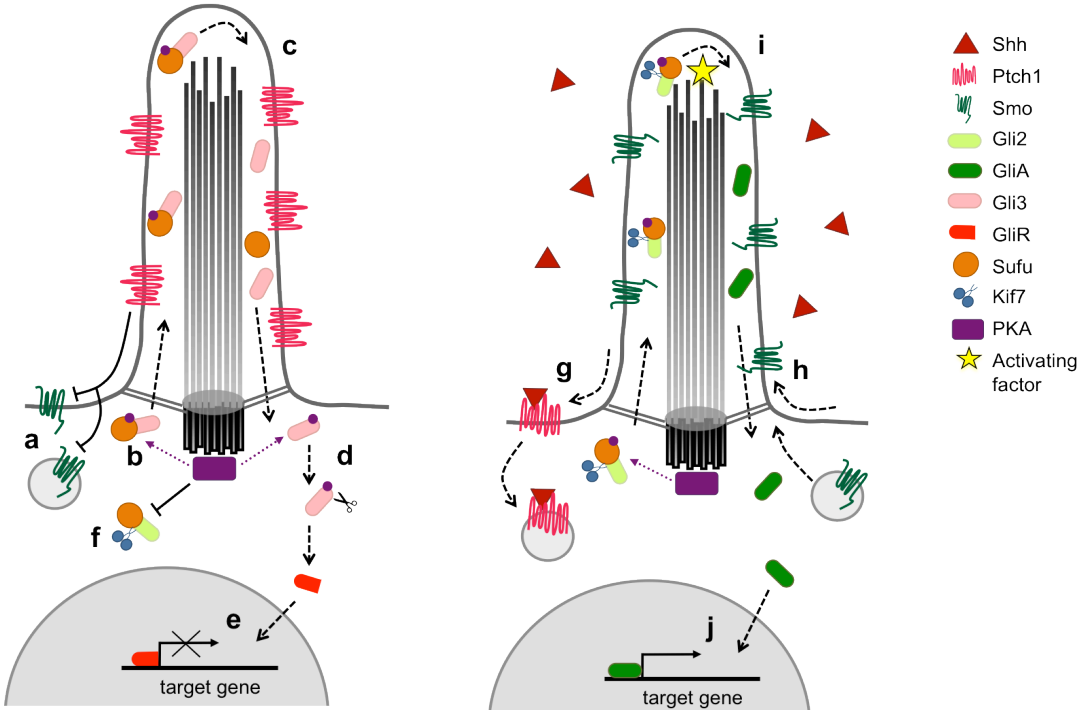

Figure 1.2 Localization of major Shh pathway proteins within cilia. In the absence of Shh ligand (left panel), the Shh receptor Ptch1 is localized to the ciliary membrane, which inhibits the ciliary entry of Smo. Studies have reported that Smo is localized either to the plasma membrane or to intracellular vesicles (or, perhaps, both) in the absence of Shh signaling (**a**). Without Shh stimulation, Gli transcription factors, particularly Gli3, are converted to their repressor form. Gli3 is bound to Sufu, which is regulated via phosphorylation (purple circles) by PKA to promote its ciliary localization (**b**). The Sufu/Gli3 complex must be trafficked to the tip of the cilium in order for Gli3 to dissociate from Sufu and promote the formation of GliR (**c**), although it is not known whether this dissociation occurs within the cilium or after the complex exits the cilium. Gli3 itself is also phosphorylated by PKA (purple circles) at the base of the cilium to promote its cleavage by the proteasome into GliR (**d**). Processed GliR then translocates to the nucleus, where it represses the transcription of Shh target genes (**e**). At the same time, PKA and Kif7 together inhibit the ciliary localization and activation of Gli2 (**f**). In the presence of Shh (right panel), Ptch1 binds to the ligand and is internalized (**g**). The removal of Ptch1 from the ciliary membrane allows Smo to enter the cilium via lateral transport, targeted vesicle fusion, or both (**h**). Activated ciliary Smo promotes the enrichment of Gli proteins at the tip of the cilium, where they are activated to form GliA through a currently unknown mechanism (**i**). GliA then translocates to the nucleus where it initiates transcription of Shh target genes (**j**). (Figure from Mariani and Caspary, 2012)

1.2.2 Molecular mechanisms of Shh signaling in cilia

Primary cilia are seen on virtually every type of vertebrate cell and are required for canonical Shh signaling. The connection between primary cilia and Shh signaling is unique to vertebrates (reviewed in: Huangfu and Kathryn V Anderson, 2006; P. W. Ingham et al., 2011) and was first revealed through *in vivo* analysis of mouse mutants with defects in cilia genes. Recent experiments have uncovered more about the molecular biology of cilia-dependent Shh

signaling within individual cells. All major components of the Shh signaling pathway are known to localize in or near primary cilia, and Shh pathway proteins are trafficked in and out of cilia depending on the activation state of the pathway (Figure 1.2). In general, disrupting ciliogenesis or ciliary protein transport also leads to disruption of Shh signaling.

Cell biology experiments point to an extremely complex mechanism through which a large number of effectors regulate Shh signaling in cilia. These molecules can be disrupted independently of one another, leading to abnormal Shh signaling activity through similar, overlapping, but ultimately distinct mechanisms. In such cases, the mouse neural tube again makes an appealing system for analyzing the roles of individual molecules in the regulation of the Shh pathway, since we can observe shifts in the patterning of neural progenitor domains when a gene is manipulated in embryos and use the patterning phenotype to make inferences about the effects of the mutation on canonical Shh signaling.

Shh signaling activity depends on the proper localization of the pathway's component proteins to primary cilia: Ptch1, Smo, Gli2, Gli3, Sufu, and Kif7 are all known to move into and out of the cilium during Shh signaling (Corbit et al., 2005; Haycraft et al., 2005; Liem et al., 2009; Rohatgi et al., 2007; Tukachinsky et al., 2010). It is not currently known whether other Shh signaling proteins, including the receptors Boc, Cdo, and Gas1, as well as Shh inhibitors Ptch2 and Hhip1, are localized to cilia. Still, without primary cilia, no canonical Shh signaling can occur. Cilia are required for the formation of both GliA and GliR (Haycraft et al., 2005; Huangfu and Anderson, 2005; Liu et al., 2005; May et al., 2005); cells without cilia receive no transcriptional signals from the Shh pathway. Despite this, neural progenitors requiring only low levels of Shh signaling are still observed in some mutants with no cilia (Huangfu and Anderson, 2005). The progenitors form due to the loss of GliR-dependent repression of their cell fates. This situation is distinct from $Shh^{-/-}$ embryos, for example, in which ventral neural progenitors do not develop because GliA is never induced by Shh signaling, but GliR is still produced (Chiang et al., 1996). Epistasis experiments show that $Shh^{-/-};Gli3^{-/-}$ double mutants are still capable of producing

some ventral progenitors; the loss of GliR derepresses the Shh pathway under these conditions (Persson et al., 2002). In contrast, mutants that lack cilia are much less sensitive to *Gli3* ablation (Huangfu et al., 2003). These experiments provide yet another example of how genetic studies can untangle the complex relationships between the genes required for cilia function and Shh signaling.

Under baseline conditions, cilia-dependent mechanisms are required to properly regulate the Shh pathway. In the absence of Shh, Ptch1 is enriched in the membrane of the primary cilium (Rohatgi et al., 2007). The presence of Ptch1 inhibits the accumulation of Smo in the ciliary membrane, although a small amount of Smo constantly shuttles through the cilium, even in the presence of Ptch1 (Kim et al., 2009; Ocbina and Anderson, 2008). Gli2 and Gli3 are also found in cilia in the absence of Shh ligand, and Gli proteins must travel into and out of primary cilia to be properly converted into GliR (Haycraft et al., 2005).

When Shh binds Ptch1, the bound ligand prevents Ptch1's inhibition of Smo (Kim et al., 2015) and an unknown process causes Ptch1 to exit the cilium. The ensuing signaling cascade leads to Smo becoming enriched in cilia (Corbit et al., 2005; Rohatgi et al., 2007). The exact mechanism of Smo's movement into cilia remains a matter of debate, although there is some evidence that Smo moves from the plasma membrane into the cilium via lateral transport (Milenkovic et al., 2009), and other studies point to a mechanism by which vesicular Smo is targeted to the cilium (Wang et al., 2009). Another possibility is that Smo uses several mechanisms for its transport into cilia. A recent study supporting the multiple-mechanisms model identified a novel protein, LZTFL1, as a negative regulator of ciliary traffic of Smo (Seo et al., 2011). LZTFL1 mediates the interaction between Smo and a protein coat complex known as the BBSome. The BBSome is responsible for targeting a variety of membrane-associated receptors to the ciliary membrane. When LZTFL1 is knocked down, the ciliary localization of BBSome proteins and of Smo increases, irrespective of Shh signaling activity. However, further ciliary enrichment of Smo can still be seen under LZTFL1-depleted conditions upon treatment with a

Shh pathway agonist. This implies that, while some Smo traffic is mediated by the BBSome and repressed by LZTFL1 in the absence of Shh, Smo is also targeted to the ciliary membrane through LZTFL- and BBSome-independent mechanisms. Other experiments have also revealed that the ciliary enrichment of Smo upon Shh stimulation depends on kinesin-based transport (specifically, Kif3a) and β-arrestins (Kovacs et al., 2008). Further study will determine whether these data can be reconciled into a single model of Smo transport.

Pharmacological evidence shows that although Smo moves into the cilium as a consequence of Shh pathway activation, the mere presence of Smo in the cilium is not sufficient to transduce the Shh signal and trigger the formation of GliA: Smo must also be activated (Wang et al., 2009). The two-step process of Smo-dependent Shh signaling (translocation and activation) has yet to be fully explained. Smo is a G protein-coupled receptor (Ayers and Thérond, 2010; Ruiz-Gómez et al., 2007) and responds to several small molecules in pharmacological screens. Therefore, one appealing model posits that a yet-unknown endogenous ligand – possibly a cholesterol-derived oxysterol (Nachtergaele et al., 2012) – regulates Smo activation, and that Ptch1 inhibits Smo by blocking its access to this ligand, as well as blocking its accumulation in cilia.

The presence of activated Smo in the cilium causes enrichment of Gli proteins at the tip of the cilium, inhibits GliR formation, and triggers the formation of GliA (Chen et al., 2009; Wen et al., 2010). The processing of Gli proteins into GliA and GliR requires transport of Gli proteins into and out of the primary cilium. It is not known how traffic through the primary cilium regulates the conversion of full-length Gli proteins into activator or repressor, but experiments thus far have indicated that the process involves the core Shh pathway proteins Sufu, Kif7, and PKA (Chen et al., 2009; Chen et al., 2011; Tukachinsky et al., 2010). Because the balance of GliA and GliR ultimately determines the output of the Shh signaling pathway, proper regulation of Gli proteins is key, and the disruption of Gli processing and/or activation leads to signaling defects that cause abnormal neural patterning *in vivo*.

Sufu, Kif7, and PKA act at the primary cilium to regulate Gli processing and activation. Sufu binding inhibits the transcriptional functions of Gli proteins. Sufu can act in a cilia-independent manner to inhibit Gli proteins by sequestering them from the nucleus, but it also moves into and out of cilia with the Glis, becoming enriched in cilia upon Shh stimulation. For GliR or GliA to form, Gli proteins must first dissociate from Sufu. This dissociation requires kinesin-dependent traffic of the Sufu/Gli complex to primary cilia (Humke et al., 2010; Tukachinsky et al., 2010). In addition to inhibiting the formation of GliR and GliA, Sufu serves to stabilize Gli proteins: genetic ablation of Sufu leads to degradation of Gli2 and Gli3. Gli3 is more affected by loss of Sufu than Gli2; *Sufu* null embryos exhibit a ventralized neural tube phenotype due to the alteration in the balance of GliA and GliR that results from Gli3 degradation (Wang et al., 2010).

Kif7, an atypical kinesin, normally localizes to the base of the cilium, where it is ideally positioned to regulate the access of Shh pathway proteins to the ciliary compartment. Kif7 serves as a negative regulator of Shh signaling downstream of Smo. Upon activation of the Shh pathway, Kif7 moves to the tip of the cilium concomitantly with Gli proteins, indicating that it may regulate the transport and activation of Gli2, as well as the processing of Gli3 into GliR (Endoh-Yamagami et al., 2009; Liem et al., 2009). One model suggests that, as a motor protein, Kif7 may inhibit Gli activation by moving Gli proteins away from the cilium in the absence of signals from Shh (Liem et al., 2009). Further experiments are needed to test this model. Notably, the role of Kif7 in Shh signaling was initially disputed, as cell-based assays of Kif7 knockdown did not show a significant effect on Shh pathway output (Varjosalo et al., 2006). Thus, *in vivo* analysis of neural tube patterning proves to be a more sensitive method for examining subtle effects of perturbations to the Shh pathway.

PKA phosphorylates Sufu, thereby promoting Sufu's ciliary localization (Chen et al., 2011). However, analysis of $PKA^{-/-}$ mutants reveals a more severe neural tube patterning phenotype than $Sufu^{-/-}$ mutants, indicating that PKA is affecting Gli activity and Shh signaling

through Sufu-independent mechanisms, in addition to regulating Sufu. Specifically, PKA is localized to the base of the primary cilium, where it regulates the ciliary entry of Gli proteins, the production of GliR from Gli3, and the activation of Gli2 (Tuson et al., 2011). When a Shh signaling component plays multiple roles in regulating the pathway, as PKA does, this complicates the interpretation of experiments in which a single molecule is perturbed. Yet it is not surprising for one effector to interact with multiple steps of a signaling cascade, especially when all the major signaling components localize to a small organelle like the cilium. Indeed, evidence suggests that Arl13b has a similar multi-faceted regulatory role in Shh signaling.

The dynamic regulation of Shh pathway proteins in primary cilia points to the central nature of cilia and ciliary protein traffic in Shh signaling, and explains why many ciliopathies can cause classic Shh signaling defects, such as polydactyly. Still, many of the Shh-related proteins described above also perform functions in cellular compartments other than the cilium. Some of these functions regulate non-canonical Shh signaling (to be discussed further in section 1.3).

1.2.3 Arl13b and Shh signaling

The small GTPase Arl13b plays a unique role in the regulation of canonical Shh signaling. Wild-type Arl13b protein localizes to cilia, leaving it poised to interact with Shh pathway components. The *hennin* (*hnn*) mutant mouse has a protein null mutation in *Arl13b* that leads to loss of the most ventral cell types in the neural tube (floor plate) and an expansion of more mediolateral cell types (pMN). Epistasis experiments show that the $Arl13b^{hnn}$ phenotype is caused by abnormal regulation of Gli2 (Caspary et al., 2007). Specifically, the highest levels of GliA are never reached, while a constitutive moderate level of GliA drives the expression of Shh target genes throughout most of the neural tube. Gli3, meanwhile, appears to be relatively unaffected by loss of Arl13b. An intact gradient of Gli3-derived GliR regulates the residual patterning in the $Arl13b^{hnn}$ neural tube, but $Arl13b^{hnn};Gli3^{-/-}$ double mutants have essentially no dorsoventral neural tube patterning. The importance of Gli3 in maintaining proper neural

patterning is further highlighted by the fact that conditional deletion of *Arl13b* early in development causes a temporary disruption of neural patterning that recovers over time, but mutant embryos experiencing conditional deletion of both *Arl13b* and *Gli3* fail to display the same recovery (Su et al., 2012).

At the cellular level, Arl13b regulates multiple components of the Shh signaling pathway in cilia. *Arl13b*^{hnn} cells have short cilia with defects in the microtubule ultrastructure of the ciliary axoneme (Caspary et al., 2007). Indeed, Arl13b plays a critical role in cilia formation and is one of the primary targets of the FoxJ1 and Rfx family transcription factors that regulate ciliogenesis (Lu et al., 2014). Although the defects in *Arl13b*^{hnn} cilia are not as severe as those seen in some other cilia mutants, such as cells with mutations in anterograde IFT components, the abnormal structure of primary cilia could contribute to the misregulation of the Shh pathway in cells lacking Arl13b. Furthermore, many of the proteins that make up the Shh signaling pathway show abnormal localization patterns in *Arl13b*^{hnn} cells (Larkins et al., 2011). Specifically, Ptch1 is found in the cilium even after cells are treated with Shh ligand, and Smo is enriched in cilia even in the absence of Shh. Meanwhile, Sufu, Gli2, and Gli3 fail to become enriched at the tip of the cilium upon Shh treatment in cells lacking Arl13b. Because Gli2 activation requires its transport to the tip of the cilium (Liu et al., 2015; Santos and Reiter, 2014), the abnormal ligand-dependent traffic of Shh pathway proteins may explain why GliA function is impaired in *Arl13b*^{hnn} mutants. It is not yet clear whether the abnormal transport of Shh pathway proteins in *Arl13b*^{hnn} cells arises from the structural defects in mutant cilia, or whether Arl13b has a specific function in regulating protein traffic.

1.3 Non-canonical Shh signaling

Although Shh is best characterized as a morphogen or mitogen that works by activating or repressing the transcription of target genes, components of the Shh pathway can regulate a wide array of cellular functions, some of which occur in a transcriptionally-independent manner

(reviewed in Brennan et al., 2012). In particular, Shh acts as an axon guidance cue in spinal cord commissural neurons, retinal ganglion cells, and enteric neurons (Charron et al., 2003; Jin et al., 2015; Sánchez-Camacho and Bovolenta, 2008). Shh can also serve as a chemoattractant for migrating fibroblasts (Bijlsma et al., 2007; Bijlsma et al., 2012). These non-canonical forms of Shh signaling share some commonalities with the canonical signaling described in chapter 1.2, but differ from canonical signaling and from each other in significant ways. Importantly, non-canonical signaling seems to occur outside and independent of the primary cilium. However, the exact mechanisms governing non-canonical Shh signaling are incompletely understood, and the cell migration and axon guidance phenotypes seen in some ciliopathies suggest that cilia-related proteins may regulate these non-canonical processes.

1.3.1 Shh-dependent axon guidance

Shh was first shown to function as an axon guidance cue in commissural neurons of the developing spinal cord (Charron et al., 2003). Along with Netrin, Shh secreted from the floor plate serves as a chemoattractant for these neurons and acts through the Shh receptors Boc and Cdo. After commissural neurons have crossed the midline, they undergo a shift in their receptor expression profile and are no longer attracted to floor plate cues (this enables them to continue projecting toward targets beyond the midline). Shh is also involved in the guidance of post-crossing commissural axons, meaning that it switches from an attractive to a repulsive cue. After commissural axons cross the midline, they begin to express the Shh receptor Hhip1, which mediates the chemorepulsive response to Shh (Bourikas et al., 2005; Wilson and Stoeckli, 2013).

Shh can also serve as an axon guidance cue in other neurons. At the optic chiasm, midline Shh acts through Boc to repel retinal ganglion cell axons destined to form the ipsilateral optic tract (Fabre et al., 2010). In the enteric nervous system, Shh also acts as a chemorepulsive cue. Enteric axons embedded between layers of smooth muscle normally encircle the outer portion of the intestines, but in Shh mutant mice, axons project deep into the intestinal villi. Jin and

colleagues found that Shh secreted by the gut epithelium binds to the Shh receptor Gas1 and prevents axons from invading the villi of normal intestines (Jin et al., 2015).

With the exception of post-crossing commissural neurons, which cease to express Smo, studies of Shh-dependent axon guidance all confirm that Smo is as essential for non-canonical Shh signaling as it is for the canonical, transcriptionally-dependent arm of the pathway. Smo mediates the chemoattractive response to Shh in commissural neurons; pharmacological or genetic ablation of Smo interferes with axon guidance (Charron et al., 2003). Furthermore, Shh-responsive retinal ganglion cells express Smo in their growth cones and Shh-mediated growth cone collapse in these cells is blocked by the Smo inhibitor SANT-1 (Fabre et al., 2010). Downstream of Smo, Src family kinases are responsible for mediating the cytoskeletal rearrangements required for growth cone turning in commissural neurons (Yam et al., 2009). In the enteric nervous system, Shh-dependent chemorepulsion downstream of Gas1 signals through the Smo-coupled Gαi protein Gnaz (Jin et al., 2015). While all of these data emphasize the importance of Smo signaling locally at the growth cone, the mechanism regulating the traffic and activation of Smo in axons is not yet known.

1.3.2 Shh-dependent fibroblast migration

In addition to regulating axon guidance, non-canonical Shh signaling can drive chemotaxis of fibroblasts. Mouse embryonic fibroblasts will migrate toward a source of Shh via a transcription- and translation-independent mechanism. Shh initiates cytoskeletal rearrangements in migrating fibroblasts via leukotriene synthesis (Bijlsma et al., 2007), Gαi signaling, and PI3K activation (Polizio et al., 2011). However, the Src family kinases that regulate Shh-dependent axon guidance in commissural neurons are not required for Shh-dependent fibroblast migration (Bijlsma et al., 2012).

Shh-dependent migration acts through Smo, but, importantly, Smo does not have to localize to primary cilia in order to mediate chemotaxis. Non-ciliary forms of Smo actually

potentiate fibroblast migration toward Shh, and the cilium itself is dispensable for Shh-dependent migration. As previously reported (Bijlsma et al., 2012), "defective ciliary localization motifs in Smo or defective ciliogenesis resulted in altered intracellular trafficking of Smo to sites other than the primary cilium. These altered itineraries correlated with reduced capacity for Shh-mediated transcriptional signaling, but enhanced chemotactic responsiveness. This suggests that the ciliary localization machinery plays a role in the transport of Smo to sites where it can mediate transcriptional signaling, and away from sites where it can mediate chemotactic signaling."

A variety of evidence thus indicates that Shh signaling can occur at multiple locations within a Shh-responsive cell. The varying downstream events resulting from Smo activation in canonical vs. non-canonical signaling seem at least in part to depend upon the localization of the Smo protein to the cilium, the growth cone, or the migratory leading edge. What is less clear is whether any other Shh pathway components and/or cilia-associated proteins aside from Shh receptors and Smo play a role in extraciliary, non-canonical Shh signaling.

1.4 Unanswered questions in Joubert Syndrome etiology and Shh signaling

Little is known about the molecular etiology of neuroanatomical defects in JS. It is not known whether Shh-dependent axon guidance regulates development of the affected white matter tracts, but several lines of evidence suggest that Shh may contribute to the characteristic hindbrain malformations in JS. Other JS phenotypes, including cerebellar hypoplasia, craniofacial abnormalities, and polydactyly, are related to abnormal Shh signaling. Furthermore, the products of many JS-associated genes, including *ARL13B*, *KIF7*, *RPGRIPL1*, *TCTN1*, and *TCTN2*, regulate Shh signaling (Caspary et al., 2007; Cheung et al., 2009; Endoh-Yamagami et al., 2009; Liem et al., 2009; Reiter and Skarnes, 2006; Vierkotten et al., 2007).

If Shh signaling does contribute to normal hindbrain white matter development and perturbations to Shh signaling cause the white matter defects characteristic of JS, this raises a number of questions. Because all known JS-causing mutations are found in cilia-associated genes

but non-canonical Shh signaling appears to be largely cilia-independent, this model requires JS-associated gene products to affect cellular functions outside of the cilium. There is some evidence that ciliopathy-associated proteins, including Arl13b, can affect signaling that occurs outside of cilia. However, no one has yet found evidence that key distinguishing features of ciliopathies can arise from cilia-independent mechanisms. This model therefore questions our fundamental understanding of ciliopathies and suggests new layers of complexity in the disease phenotypes arising from mutations in *ARL13B* and other traditionally cilia-associated genes.

1.4.1 Hindbrain development

It is clear that hindbrain development in JS patients is disrupted, but much remains to be learned about the normal developmental processes regulating the formation of the hindbrain. In particular, the factors regulating axon guidance of the major cerebellar white matter tracts are clearly impacted by mutations causing JS, but it is not known whether these defects arise from cell-autonomous signaling defects within cerebellar projection neurons, abnormal development of the surrounding brain tissue, or both.

The characteristic MTS is formed in part by anatomical abnormalities in the SCPs, which are composed of axons from neurons in the deep cerebellar nuclei (DCN) projecting to targets elsewhere in the brain. The brains of some JS patients show abnormal morphology of the nuclei themselves (Juric-Sekhar et al., 2012), and previous work from the Caspary and Anton labs has shown that Arl13b mutations can affect neuronal migration (although this effect was seen only in interneurons; Higginbotham et al., 2012). If these processes are disrupted in JS, DCN neurons may fail to differentiate properly and/or to reach the appropriate niche in JS brains, which could explain why their axon guidance is impaired. It is not yet known whether cilia-associated proteins such as Arl13b act through Shh or other developmental signaling pathways to regulate DCN neuronal differentiation and/or migration.

Glutamatergic DCN projection neurons in the mouse are derived from Math1-expressing progenitors at the cerebellar rhombic lip between e10.5 and e12.5 (Wang et al., 2005; Machold and Fishell, 2005). (Approximately 40% of neurons in the DCN are GABAergic projection neurons or GABAergic interneurons; less is known about the development of these cells, but they are derived from the same pool of GABAergic precursors in the ventricular zone as Purkinje cells; reviewed in Elsen et al., 2013.) After DCN neurons are born, they migrate rostrally to the nuclear transitory zone (NTZ), where they begin to form three distinct nuclei: medial, interposed, and lateral. In the NTZ, the cells assume either a longitudinal or transverse orientation, which determines whether they will send their axons through the SCP or the uncinate fasciculus, respectively, during axonogenesis. The DCN neurons then descend to their eventual home in the deepest layers of the cerebellum (Altman and Bayer, 1985). These stages in the development of the DCN can also be tracked through expression of molecular markers. En route to the NTZ, subpopulations of DCN neurons express the transcription factors Pax6 and/or reelin. Upon entering the NTZ, these neurons begin to express the marker Tbr1. Later, the interposed and lateral nuclei cease to express Tbr1 and begin to express Brn2 (Fink et al., 2006).

Though many questions remained unanswered about the differentiation and migration of DCN projection neurons, even less is known about the development of the major cerebellar white matter tracts formed by their axons. Robo proteins have been implicated in guiding axons from the lateral and interposed DCN (Tamada et al., 2008). In addition, early work in rat embryos showed that axons from the developing cerebellar plate are attracted to Netrin at the midline, then elongate along the longitudinal axis after crossing the midline (Shirasaki et al., 1995). A more recent study demonstrated that DCN axons may receive additional cues by examining the effects of disrupted Netrin signaling on DCN neurons. Although some DCN neurons null for the repulsive Netrin receptor Unc5c were misguided, the SCP was intact in Unc5c null mice, suggesting that Netrin chemorepulsion is not required for the formation of this tract. Meanwhile, some aberrantly projecting DCN neurons in the *Unc5c* null mice seemed to be attracted to the

floor plate, which is a source of both Netrin and Shh ligand (Kim and Ackerman, 2011). Commissural neurons of the spinal cord display a similar developmental trajectory to DCN neurons in which they are first attracted to the midline, then project longitudinally after midline crossing. Spinal commissural neurons are competent to respond to both Netrin and Shh, among other cues (reviewed in Evans and Bashaw, 2010). Thus, it is possible that DCN neurons use a similar molecular program combining signals from Robo proteins, Netrin, and Shh to guide their axons to distal targets.

Other traditional morphogens can also play a role in axon guidance (reviewed in Sánchez-Camacho and Bovolenta, 2009) and multiple morphogen pathways have been shown to experience disruptions in JS. A study in *Ahi1* null mice used as a model for JS revealed abnormal Wnt signaling along with some cerebellar abnormalities. However, Shh signaling is intact in the absence of Ahi1, and the *Ahi1* null mice did not show midline crossing defects in the SCPs (Lancaster et al., 2011). These data therefore suggest that a non-Wnt factor, possibly Shh, is responsible for regulating cerebellofugal axon guidance.

1.4.2 Non-ciliary roles of ciliopathy proteins

Ciliopathies are defined by their fundamental connection to cilia. Indeed, the gene products of all ciliopathy-associated genes are found in or near cilia. What is less clear is whether these proteins have functions elsewhere in the cell and whether disruption of such non-ciliary functions contributes at all to disease phenotypes.

Arl13b, in particular, is primarily known for its role in ciliogenesis and the regulation of cilia-associated Shh signaling. However, this primarily ciliary protein has been linked to functions in other cellular compartments. For example, Arl13b associates with components of early endosomes and regulates endocytic recycling traffic (Barral et al., 2012). Arl13b has also been found to interact with the actin cytoskeleton and to drive the formation of circular dorsal membrane ruffles that occur during macropinocytosis and cell migration (Casalou et al., 2014).

Previous research has shown that Arl13b's localization to cilia seems crucial for its function, in that non-ciliary forms of Arl13b are unable to rescue phenotypes associated with loss of Arl13b (Cevik et al., 2013; Duldulao et al., 2009). It is not clear whether non-ciliary Arl13b may retain functions associated with other cellular compartments or whether Arl13b must be capable of cilia localization in order to function at all. The latter implies that Arl13b must travel through cilia in order to be fully activated, perhaps by some binding partner that is enriched in cilia. Alternatively, perhaps the same protein domains that promote Arl13b's cilia localization are also essential for its signaling functions. Further exploration of these non-exclusive models to explain Arl13b's extraciliary functions will reveal important information about the role of cilia as a cellular signaling hub as well as the etiology of ciliopathy phenotypes.

Given that cilia-associated proteins are capable of mediating functions outside the cilium, it is conceivable that Arl13b is involved in axonal non-canonical Shh signaling. Recent evidence has shown that numerous ciliopathy-associated gene products are required for many distinct steps of neuronal development in the cerebral cortex, including axon guidance (Guo et al., 2015; Magnani et al., 2015). Furthermore, Arl13b is clearly involved with both interneuron migration, through an apparently cilia-dependent mechanism, and projection neuron axon guidance, through a mechanism that is less clear (Higginbotham et al., 2012). In this way, Arl13b's function may be similar to that of the Shh pathway protein Kif7. Kif7 plays important roles both within and outside of cilia in regulating Shh signaling (Maurya et al., 2013), and Kif7 mutations can cause JS as well as acrocallosal syndrome, another disorder of axon guidance (Dafinger et al., 2011; Putoux et al., 2011; Putoux et al., 2012). Arl13b may interact with Kif7 and/or other Shh pathway proteins to regulate Shh-dependent signal transduction events required for cytoskeletal remodeling in developing axons.

1.5 Summary and objectives

The experiments outlined in this dissertation suggest a possible mechanism for the hallmark anatomical defect in JS by asking whether Arl13b regulates non-canonical Shh signaling important for hindbrain axon guidance. *ARL13B* mutations lead to a range of JS symptoms, including the hindbrain white matter defects that form the MTS (Cantagrel et al., 2008). Previous work by the Caspary lab and our collaborators has shown that null mutations of *Arl13b* or conditional deletion of *Arl13b* using an $Arl13b^{floxed}$ allele with different *Cre* alleles leads to defects in cerebellar development and/or axon guidance reminiscent of JS. $Arl13b^{floxed}$;*Brn4-Cre* mice, which lack Arl13b in all neurons, display gross cerebellar hypoplasia (Nicole Umberger and Sarah Bay, unpublished). This phenotype is likely due to abnormal Shh signaling, as granule neuron precursors in the developing cerebellum require Shh as a proliferative cue (Corrales et al., 2004; Hatten and Roussel, 2011). As part of an ongoing collaboration with Eva Anton (UNC Chapel Hill), the Caspary lab has observed abnormal white matter tracts in $Arl13b^{floxed}$;*NEX-Cre* mice (Higginbotham et al., 2012), which lack Arl13b specifically in projection neurons (Goebbels et al., 2006). Furthermore, mouse embryos that lack Arl13b altogether show abnormalities of the commissural neurons in the developing spinal cord, as shown by experiments done in collaboration with Frédéric Charron (IRCM/McGill University). These studies indicate that some projection neurons require Arl13b for proper axon guidance. The mechanism by which Arl13b affects axon guidance is unknown, however, and no one has examined the effect of *Arl13b* mutations in the projection neurons affected in JS. My dissertation research has focused on answering these questions.

Chapter 2

Materials and Methods

2.1 Mouse embryonic fibroblast protocols and assays

2.1.1 Mouse lines and genotyping

Arl13b^{hnn} mice were generated in an N-ethyl, N-nitrosourea screen (Caspary et al., 2007) on a C57/Bl6 background and maintained on a C3H background. Genotyping for the *Arl13b*^{hnn} allele uses strain-specific markers and detects whether mice are Bl6 or C3H on either side of the *Arl13b* locus. *Arl13b*^{hnn} genotyping primers:

hnn147 Forward	AAT GCC TCA AGT GCC TCT TT
hnn147 Reverse	GGG ACT CAT CTT TGG GAA CA
hnn174 Forward	TGT GGG TGG CAT ATG TAG GA
hnn174 Reverse	GCT AGC TAT TTT CTG TTG CTG GA

Arl13b^{flox} mice were generated by the Caspary lab (Su et al., 2012). Genotyping for the *Arl13b*^{flox} allele involves a size shift in the PCR product based on the addition of a loxP site. *Arl13b*^{flox} genotyping primers:

ConF Forward	AGG ACG GTT GAG AAC CAC TG
Cond200R Reverse	CGA CCA TCA CAA GTG TCA CC

CAGG-Cre^{ERt2} mice were obtained from the Jackson Laboratory (JAX 004682). Generic Cre genotyping primers:

“Tom Cre” Forward	TGA CCC GGC AAA ACA GGT AGT TA
“Tom Cre” Reverse	TTC CCG CAG AAC CTG AAG ATG TT

2.1.2 Generating primary MEFs

Pregnant dams at e12.5 (determined by presence of a vaginal plug at e0.5) were sacrificed by cervical dislocation. The uterus was dissected into cold PBS and individual embryos were isolated. After removing the head and visceral organs, individual embryos were collected in 1 mL

syringes and kept on ice until dissociation. Yolk sacs from each embryo were kept for later genotyping. Embryos were mechanically dissociated by passing several times through an 18g needle in warm MEF media (DMEM containing 10% FBS and 1X penicillin/streptomycin). Dissociated cells were cultured in gelatin-coated 60 mm tissue culture dishes (0.1% gelatin in water, autoclaved and filtered, was placed on dishes for at least one hour before use, then aspirated off before plating MEFs).

For mutant lines lethal before e12.5, embryos as early as e9.5 were used. To make MEFs from e9.5 embryos, the entire embryo was dissociated and cultured in one well of a 12-well plate. For e10.5 or e11.5 embryos, the head was removed before dissociation and cells from individual embryos were cultured in one well of a 6-well plate.

Primary MEFs were maintained in MEF media and passaged every 3-5 days (after they became 90-100% confluent). Passage number for MEFs was tracked from 0 (original plating after dissociation) to 4. Primary MEFs after passage 4 typically become senescent and/or start to differentiate, and should not be used.

2.1.3 Immortalizing MEFs

Primary MEFs at passage 2 or 3 were cultured until 50-75% confluent, then transfected with SV40 T antigen construct to induce immortalization (for Lipofectamine 2000 transfection information, see 2.1.6). Early passage MEFs should not be used for immortalization as these are more likely to contain contaminating cells such as macrophages. After transfection, MEFs were cultured until 90-100% confluent and then split 1:4 and 1:10 into fresh gelatinized tissue culture dishes. Immortalizing MEFs were cultured until confluent and split 1:10 six times (a final dilution factor of 1:1,000,000 from the original primary culture) before being considered fully immortalized. Early in the immortalization process, 1:10 splits may grow very slowly or not at all, therefore 1:4 splits were done to ensure that some cells survived at each passage.

Immortalizing MEFs that took more than 14 days to become confluent after a 1:10 split were discarded.

2.1.4 Site-directed mutagenesis

Early work to generate Arl13b variants was done using site-directed mutagenesis performed in the Caspary lab using the QuikChange Lightning Site-Directed Mutagenesis Kit (Agilent Technologies, 210518). Mutagenesis was performed on the Arl13b cDNA in a Gateway entry vector (Caspary lab plasmid #2) according to the manufacturer's protocols, using the following mutagenic primers (and their reverse complements):

Mutation	**Primer**	**Restriction Site**
V358A	GA ATG AAA AGG AGT CAT CGG GCA GAA CCA GTC AAT ACA GAC G	creates HincII site
KKKTKK→KAATAK	GG TCA GAG TCC GGG GAA AAC AGT AAG GCG GCA ACC GCG AAA CTA AGA ATG AAA AG	creates TauI site
ALEEQ→FLEEF	CCA GAA AGA CAC AAC TGA ACA GCG ATT TCT TGA GGA ATT CGA GAA ACG TGA G	creates EcoRI site
RVRKLRE→AAAALRE	CAA GAG AAA CGT GAG AGG GCT GAA GCA GCC GCG GCG TTA AGG GAA GAA AGA G	creates SacII site

Mutagenesis was confirmed using restriction digests and the mutated Arl13b cDNA was cloned into a mammalian expression vector (Gateway pcDNA-DEST47, ThermoFisher Scientific, 12281-010) via attL/attR site recombination (using LR clonase). As all of these mutations were designed to disrupt candidate cilia localization signals in Arl13b, validation was performed according to the method outlined in section 2.1.6 to determine whether the mutant protein localized to cilia. Only Arl13b^{V358A}-GFP showed disruption of cilia localization; other mutants were not used for further experiments.

Subsequent mutagenesis was done by Oskar Laur at the Emory University Custom Cloning Core Facility. Mutations produced by the Custom Cloning Core include: C8S,C9S; T35N; R79Q; G75Q; Y86C; R200C. All constructs were verified by sequencing of the entire open reading frames.

2.1.5 Generating lentivirus

Arl13b^{WT}-GFP and Arl13b^{V358A}-GFP lentiviral constructs were produced by the Emory University Center for Neurodegenerative Disease Viral Vector Core. All other lentiviral constructs used were generated in the Caspary lab by co-transfecting HEK293FT cells with envelope, packaging, and lentiviral vectors and collecting virus-containing supernatant from the cells.

To generate lentivirus, HEK293FT cells were seeded in 15 cm dishes and cultured in DMEM + 10% FBS and 1X penicillin/streptomycin until 90% confluent. On the day of transfection, media was changed to 18 mL of DMEM + 2% FBS. A transfection solution was prepared using 2 mL serum-free DMEM, 6 µg lentiviral vector, 4.5 µg PAX2 packaging vector, 1.5 µg pMD2.G envelope vector, and 36 µg polyethylenimine (PEI, from 1 mg/mL working stock). The transfection solution was incubated at room temperature for 10 minutes before being added dropwise to the cells. Medium was changed to 10 mL of DMEM + 10% FBS 24 hours after transfection. This medium was left on the virus-producing transfected cells for 24 hours, then passed through a 0.45 µm filter and stored at 4°C. Another 10 mL of DMEM + 1% FBS was added to the cells and the collection procedure was repeated the following day to produce a total of 20 mL of lentivirus-containing supernatant from each 15 cm dish of transfected cells. Lentiviral supernatant was stored at 4°C for several weeks during validation and/or titering, then aliquotted and stored at -20°C.

2.1.6 Expression validation of Arl13b mutations

Before producing lentivirus to drive expression of Ar13b variants it was necessary to validate that these variants can be expressed at detectable levels and visualized in the cilium and/or other cellular compartments. This was done using transient transfections into WT immortalized MEFs using Lipofectamine 2000 followed by immunofluorescence staining for GFP and fluorescent imaging.

For transfections, immortalized MEFs were cultured on glass coverslips coated with 0.1% gelatin in 6-well plates until 50-75% confluent. MEFs were washed with PBS and changed to 1.5 mL of serum-free DMEM per well. For each well, a transfection solution of 5 µg DNA (either the Arl13b variant cDNA expressed in GFP-containing Gateway mammalian expression vector pDEST47, or the Arl13b-GFP variant lentiviral construct) and 10 µL Lipofectamine 2000 was prepared in 500 µL of serum-free DMEM and incubated at room temperature for 30 minutes. The transfection solution was added dropwise to wells and incubated at 37°C for 4-8 hours. Cells were cultured in serum-free DMEM (to induce cilia formation) and coverslips were collected for staining and imaging 24-48 hours post-transfection.

For immunofluorescence staining, coverslips were washed in PBS and fixed in 4% paraformaldehyde for 10 minutes at room temperature. Fixed coverslips were washed with PBS and incubated in antibody wash buffer (PBS + 1% goat serum + 0.1% Triton X-100) for 15 minutes, then placed in a staining chamber and incubated with primary antibodies against GFP (Abcam, ab13970, 1:1000) and acetylated α-tubulin (Sigma, T6793, 1:2500) in antibody wash at 4ºC overnight. The following day, coverslips were washed 3 times for 10-20 minutes in antibody wash and incubated with fluorescent secondary antibodies (Life Technologies Alexa Fluor 488 or 568 against the appropriate species, 1:500) and Hoechst nuclear stain (1:3000) for 1 hour at room temperature. Stained coverslips were then washed 2 times in PBS for 20-30 minutes and dipped briefly in water before mounting in ProLong Gold Antifade Reagent (ThermoFisher, P36934).

2.1.7 FACS purification of lentiviral MEF lines

To establish pure populations of cells expressing wild-type or mutant Arl13b-GFP constructs, fluorescence assisted cell sorting (FACS) was used. Immortalized MEFs were plated at low density (1:10 split from a confluent plate) in 50% MEF medium + 50% lentiviral supernatant (4 mL of each in a 10 cm dish). MEFs were cultured for 48-72 hours to allow time for lentiviral infection and protein expression before FACS. On the day of sorting, MEFs were washed twice in sterile PBS, detached using 0.25% trypsin, and resuspended in sort buffer ($Ca^{2+/}Mg^{2+}$-free PBS with 1% FBS, 1 mM EDTA, 25 mM HEPES pH 7.0, sterilized through a 0.22 μm filter). The cell suspension was centrifuged at 1000 rpm for 5 minutes and the supernatant was removed. Cell pellets were resuspended in 500 μL of sort buffer and placed on ice.

Sorting was performed by the Emory University School of Medicine Core Facility for Flow Cytometry or the Emory+Children's Pediatric Research Center Flow Cytometry Core using a BD FACS Aria II Cell Sorter. A 100 μm nozzle was used for sorting to accommodate the relatively large size of the MEFs. Before sorting lentivirus-infected MEFs for GFP, an uninfected negative control was used to define gates for single cells using forward scatter and side scatter. GFP-positive cells were purified through a two-step process: 1) pre-sort enrichment to isolate GFP-positive MEFs, 2) single-cell sort of the GFP-enriched population into a 24-well plate containing enriched MEF medium (DMEM with 20% FBS and 1X penicillin/streptomycin). Depending on the number of infected cells in a given sample, anywhere from 1-4 wells were filled with 750-5000 GFP-positive MEFs per well. This process creates a genetically heterogeneous cell line produced from multiple founder cells representing a variety of genomic insertion sites for the lentiviral construct and a variety of GFP expression levels.

After FACS, MEFs were maintained in enriched MEF medium for approximately 10 days until wells were 90-100% confluent and could be split. After this point, MEFs were

maintained in standard MEF medium. If more than one well was produced during sorting of a given sample, the individual wells were maintained as separate cell populations.

FACS-purified cell populations were validated by immunofluorescence to check for the presence and localization pattern of Arl13b-GFP fusion proteins. In some cases, GFP expression was no longer detectable by immunofluorescence as cells continued to be passaged after sorting; cell populations in which this occurred were discarded. If sorted cells displayed a mixed phenotype wherein some cells recapitulated the expected phenotype but others did not (for example: if some cells still expressed GFP but others seemed to have lost GFP expression), limiting dilutions were used to subclone individual cells from the line. These subcloned lines were screened for GFP expression and lines that passed screening were subsequently pooled, producing a cell line with genetic heterogeneity similar to the other lentiviral lines used in these experiments.

2.1.8 Stereological analysis of fluorescent micrographs

To quantify ciliogenesis, cilia length, Arl13b-GFP localization, and Shh-dependent enrichment of Smo in cilia, Arl13b-GFP MEF lines were labeled with primary antibodies for acetylated α-tubulin (Sigma, T6793, 1:2500), GFP (Abcam, ab13970, 1:1000), and/or Smo (from Kathryn Anderson, 1:500), fluorescent secondary antibodies (Life Technologies Alexa Fluor 488 or 568 for the appropriate species, 1:500), and Hoechst nuclear stain (1:3000) according to protocols outlined in section 2.1.6. Fluorescent micrographs were acquired with a 40X objective on a Leica CTR6000 microscope using SimplePCI software. For each experiment, microscope settings for a given staining condition were optimized on Arl13b^{WT}-GFP samples and used consistently for imaging all other samples. Slides from a given experiment were all imaged on a single day whenever possible. For experiments quantifying the number and length of cilia, microscopy fields for imaging were chosen based only on the Hoechst staining to ensure unbiased sampling of ciliated versus non-ciliated cells. For experiments quantifying the number of GFP- or

Smo-postitive cilia, microscopy fields for imaging were chosen based on the acetylated α-tubulin staining to ensure that an appreciable number of cilia were present in each image.

Before analysis, images were coded using blindanalysis (Salter, 2016), a script that replaces the original filenames with a random alphanumeric string and creates a .csv keyfile pairing original and coded filenames to be used for later decoding. All image analysis was done while blinded to Arl13b genotype and (where applicable) control vs. Shh treatment conditions.

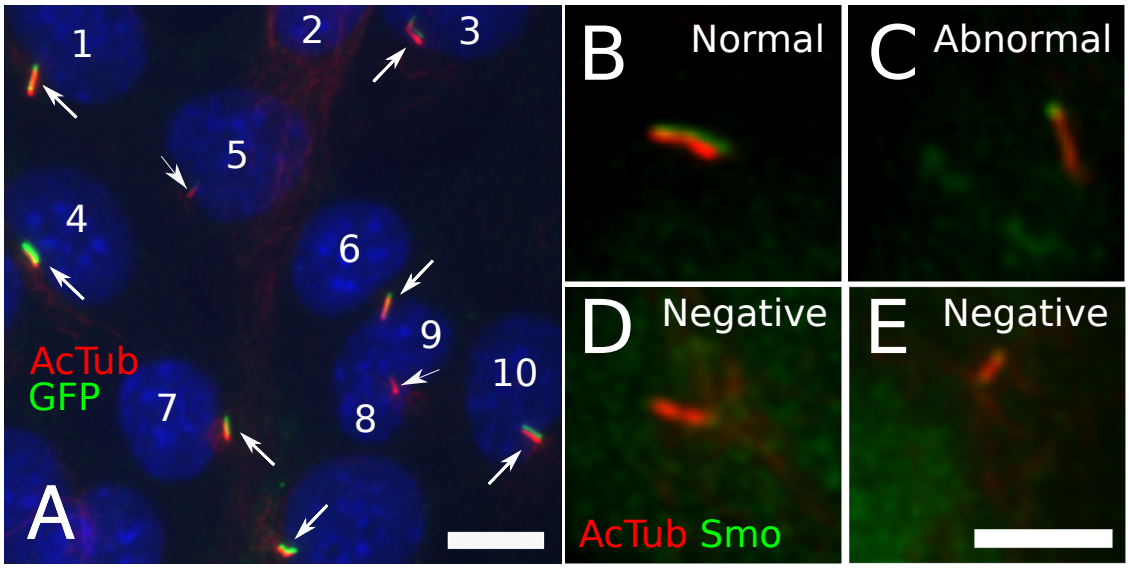

Figure 2.1. Quantifying cells, cilia, and protein localization. **A** Nuclei (Hoeschst, blue) were counted (1-10) if they overlapped with the top or right side of the image field, but not the bottom or left sides. Cilia were counted using acetylated α tubulin (AcTub) staining and categorized as GFP-negative (arrowheads) or GFP-positive (arrows) after observing GFP staining. All cilia were counted, even if belonging to a cell whose nucleus was not counted. Scale bar, 10 µm. **B-E** Smo staining was quantified based on colocalization of AcTub and Smo. Smo-enriched cilia could be either normal (Smo present along the entire length of cilium, B) or abnormal (punctate, C). Cilia where colocalization occurred but Smo fluorescence did not appear significantly brighter than background were labeled Smo-negative (D-E). Scale bar, 5 µm.

Images were analyzed using the FIJI distribution of NIH ImageJ software (Schindelin et al., 2012). For experiments testing the ciliogenesis rate of different MEF lines, nuclei were counted based on Hoescht staining and cilia were counted based on acetylated α-tubulin staining (see Figure 2.1A). All other stereology experiments only analyzed ciliated cells. For experiments measuring cilia length, acetylated α-tubulin staining was used to visualize cilia, which were

traced using the freehand line tool in FIJI and measured using Analyze→Measure. Using 2D images to measure cilia length can underestimate their true length, especially for longer cilia (Saggese et al., 2012). Still, while my absolute measurements of cilia length may be less accurate than those derived from 3D images, this method can be used to compare relative cilia lengths from one cell line to another. For experiments measuring the presence or enrichment of GFP or Smo in cilia, cilia were defined using acetylated α-tubulin staining in one color channel, then the color channel representing GFP or Smo was examined to see whether staining co-localized with acetylated α-tubulin (see Figure 2.1B-E). Data were recorded in spreadsheets showing only the coded filename for each image; all images were quantified before filenames in the spreadsheet were decoded.

2.1.9 Western blots

MEFs were washed in PBS, detached with 0.25% trypsin, resuspended in MEF media, and centrifuged to form pellets. Cell pellets were either lysed immediately or frozen at -80°C until lysis. Lysis was performed using modified RIPA buffer plus SigmaFast protease inhibitors (S8820). Modified RIPA buffer is 50 mM sodium-Tris pH 7.4, 150 mM NaCl, 2% (v/v) NP-40, 0.5% (w/v) deoxycholate, 0.1% (w/v) SDS, and 1 mM DTT. Volumes of 100-200 µL of lysis buffer were used depending on pellet size. Pellets were vortexed vigorously (~30 seconds) in lysis buffer and subjected to end-over-end agitation at 4ºC for one hour. Lysates were clarified by centrifugation at 20,000 x *g* at 4ºC for 45 minutes. Supernatants were saved and concentrations were determined by the Pierce BCA Protein Assay Kit (23227).

Proteins (20 µg) were resolved on Bio-Rad Mini-PROTEAN TGX Stain-Free Precast Gels (4568023, 4568034). Gels were imaged using the Bio-Rad ChemiDoc Touch Imaging System and transferred to a 0.2µm nitrocellulose membrane using the Bio-Rad TransBlot Turbo Transfer System with the Bio-Rad defined "High Molecular Weight" setting. Blots were imaged again to ensure proper transfer before being blocked for ~30 minutes with Pierce Superblock T20

(PBS) (37516). Primary antibodies were diluted in T20 and blots were incubated in primary overnight at 4ºC.

Blots were rinsed 3X 5 minutes in TBST before incubation in secondary antibody. Secondary antibodies were diluted in 5% (w/v) milk in TBST and blots were incubated with secondary for 1 hour at RT. Blots were rinsed 3X 10 minutes in TBST before a 5 minute incubation in Amersham ECL Prime Western Blotting Detection Reagent (RPN2232V1). Blots were then imaged for chemiluminescence using the ChemiDoc.

All analyses of western blots were done using Bio-Rad ImageLab software. Protein bands of interest were normalized to a loading control protein as measured on the stain-free gel.

2.1.10 Quantitative real-time PCR

MEFs were plated in 6-well plates at a density of 3 x 10^5 cells/well. For experiments involving Cre-lox recombination, cells were rinsed and treated with either no virus or AAV-Cre in 0.5% serum medium 24 hours after plating and incubated with control or AAV-Cre medium for 72 hours before treatment with control or Shh conditioned medium. In all other experiments, cells were treated with 0.5% serum control medium or Shh conditioned medium 24 hours after plating. After 24 hours of treatment, cells were harvested by trypsinization, spun down, and flash frozen.

RNA was extracted from cell pellets using the QIAGEN RNeasy kit (74104) after lysis with QIAGEN RLT lysis buffer and QIAShredder (79656) homogenizer columns. RNA concentration was determined by Nanodrop and 200 ng of RNA per reaction was used to synthesize cDNA. cDNA was synthesized using BioRad's iScript Reverse Transcription Supermix (1708840). To generate sufficient quantities of cDNA, 5 reactions from each sample were run in parallel and combined. Pooled cDNA from each sample was diluted 1:5 with water (to reduce any inhibitory effects of residual cDNA synthesis reagents on qPCR).

Stock primers were made at 50 mM in 1X TE and diluted 1:100 in water before use. Primers used were:

Ptch1	Fwd 5'- TGCTGTGCCTGTGGTCATCCTGATT-3' Rev 5'- CAGAGCGAGCATAGCCCTGTGGTTC-3'
Gli1	Fwd 5'-CTTCACCCTGCCATGAAACT-3' Rev 5'-TCCAGCTGAGTGTTGTCCAG-3'
Pold3	Fwd 5'-ACGCTTGACAGGAGGGGGCT-3' Rev 5'- AGGAGAAAAGCAGGGGCAAGCG-3'

Samples were run in technical triplicate. Each reaction contained 2 µL diluted cDNA, 10µL Bio-Rad Sso Advanced Universal SYBR Supermix (1725270; contains Sso7d fusion polymerase), 3 µL 1:100 forward primer, 3 µL 1:100 reverse primer, and 2 µL water. A standard curve of a 1:5 dilution series of cDNA from Shh-treated SmoA1-GFP MEFs (generated by Sarah Bay; chosen because these cells express very high levels of Shh target genes and thus can be diluted to capture a large dynamic range of transcript levels) was run on each plate.

Each plate was run on a Bio-Rad CFX96 Touch Real Time PCR Detection System and data were collected and analyzed using Bio-Rad CFX Manager 3.1. The program conditions were: 95ºC for 5 min; 45 cycles of 95ºC for 15 seconds, 57ºC for 30 seconds, plate read; and generation of a melt curve beginning at 65ºC and ending at 95ºC.

Starting quantities (in arbitrary units) were determined from comparison to the standard curve. Each triplicate set of technical replicates was averaged to give a value for a single biological replicate. Gli1 and Ptch1 expression levels were then normalized to the corresponding Pold3 levels for each replicate of a given sample.

2.1.11 Migration assays

MEF migration assays were performed by Maarten Bijlsma at the Laboratory for Experimental Oncology and Radiobiology, Academic Medical Center, University of Amsterdam, using the HTW FluoroBlok Transwell system (BD Falcon).

Before beginning the migration assay, MEFs were washed with PBS and incubated with 10 μM CellTracker Green in serum-free DMEM for 1 hour. Cells were detached using 5 mM EDTA in PBS, resuspended in serum-free DMEM, and transferred to a Transwell insert (8 μm pore size) in 100 μL of media at a concentration of 50,000 cells/well. The lower portion of the Transwell plate contained 600 μL of control or attractant (1 μg/mL rShhN or 2 μM purmorphamine) medium. During migration, the plate reader measured fluorescence in the lower portion of the Transwell plate once every 2-3 minutes for ~3 hours.

To analyze migration data, several normalization factors were used. Background fluorescence was controlled by subtracting the average value read from a blank well (containing media but no cells) from each individual plate read for the cell-containing wells. Non-specific migration of each cell line was controlled by subtracting the average fluorescence of cells migrating toward control media from each individual plate read for the corresponding cells in the attractant condition. Finally, migration curves for each cell line were made more directly comparable by setting the starting point of each normalized migration curve to zero. This was done by adding or subtracting a normalizing value from every point on the modified migration curve such that the value of the first point on the curve was equal to zero.

2.1.12 Statistical analyses

Data were analyzed for statistical significance using Prism 6 (GraphPad Software). One-way ANOVA or two-way ANOVA (factors: Arl13b genotype; control/Shh treatment) was performed using Dunnett's multiple comparison test for simple effects of Arl13b genotype, wherein the mean of each Arl13b variant was compared to a control mean (usually WT-GFP) with an overall alpha level of 0.05.

2.2 Axon guidance protocols and assays

2.2.1 Mouse lines and genotyping

Arl13b^{flox} mice were generated by the Caspary lab (Su et al., 2012). Genotyping for the *Arl13b*^{flox} allele involves a size shift in the PCR product based on the addition of a loxP site. *Arl13b*^{flox} genotyping primers:

ConF Forward	AGG ACG GTT GAG AAC CAC TG
Cond200R Reverse	CGA CCA TCA CAA GTG TCA CC

Smo^{flox} mice were obtained from the Jackson Laboratory (JAX 004526). Genotyping for the *Smo*^{flox} allele involves a size shift in the PCR product based on the addition of a loxP site. *Smo*^{flox} genotyping primers:

Smo-For Forward	GTT CCC AGG GTT GAA GAC AG
Smo-Rev-WT Reverse	ACA GCC AAC TCA GCA AAA GC

NEX-Cre mice were obtained from Dr. Eva Anton (Goebbels et al., 2006). *Math1-Cre*^{ERt2} mice were obtained from Dr. Ping Chen and are available from the Jackson Laboratory (JAX 007684). All Cre lines were genotyped using generic Cre primers:

"Tom Cre" Forward	TGA CCC GGC AAA ACA GGT AGT TA
"Tom Cre" Reverse	TTC CCG CAG AAC CTG AAG ATG TT

2.2.2 In vivo *tamoxifen-induced recombination*

A 10 mg/mL stock of tamoxifen (Sigma, T5648) was prepared in ethanol and stored at −20°C for up to one month. Immediately before use, a volume of tamoxifen stock solution equivalent to a 0.75 mg/g dose was mixed with 300 µL of corn oil, and the ethanol was removed by vacuum centrifugation at 37°C for approximately 15 minutes. Two doses of tamoxifen in corn oil were given i.p. to each pregnant dam: one at e8.75 (at ~6:00 PM) and one at e9.5 (at ~12:00 PM).

2.2.3 Mouse embryo histology

Embryos were dissected at e11.5 and fixed for 90 minutes in 4% paraformaldehyde at 4°C. Fixed embryos were washed 3 times in PBS for 15-20 minutes and transferred to 30% sucrose overnight at 4°C. The next day, embryos were blotted on a KimWipe to remove excess sucrose, washed 2 times in Optimal Cutting Temperature compound (OCT, Tissue-Tek 4583), embedded in OCT in a histology mold and frozen on dry ice. Frozen blocks were stored at -20°C until sectioning.

Sectioning, staining, and imaging of embryos analyzed for spinal commissural neuron axon guidance was performed by Julien Ferent in the laboratory of Frédéric Charron at IRCM, Montréal, Canada. Blocks were sectioned on a cryostat and sections were mounted on coated glass slides for immunostaining. For staining, slides were washed in PBS 2 times and blocked for 1 hour in PBS containing 10% donkey serum and 0.1% Triton X-100. Slides were incubated overnight at 4°C with primary antibodies diluted in blocking buffer: TAG1 (R&D, af4439) at 1:500, L1 (Chemicon, MAB5272) at 1:500. The following day, slides were washed 3 times in PBS and incubated with secondary antibodies (Alexa Fluor 488 or 568 for the corresponding species of the primary antibody, diluted 1:1000 in PBS). Slides were washed 3 more times in PBS and mounted in Mowiol before imaging.

2.2.4 Mouse brain histology

Mice were perfused with PBS and 4% paraformaldehyde. Whole brains were dissected out and post-fixed overnight in 4% paraformaldehyde, washed in PBS, and embedded in 4% low-melt agarose (Research Products International, A20070) dissolved in PBS. (Low-melt agarose solution was cooled to 37°C before embedding to prevent heat damage to brains.) Brains were cut into 50 μm horizontal sections on a Vibratome and sections were transferred into a 24 well mesh-bottom dish for staining. Sections were blocked at room temperature for 1 hour in blocking buffer (PBS + 5% heat-inactivated goat serum + 3% bovine serum albumin + 0.2% Triton X-100, filter

sterilized) and stained using a primary antibody for GFP (Abcam, ab13970, 1:1000) diluted in blocking buffer overnight at 4°C. The next day, sections were washed 3 times in blocking buffer for 20 minutes, then incubated with secondary antibody (Life Technologies, anti-chicken Alexa Fluor 488, 1:500) and Hoechst nuclear stain (1:3000) diluted in blocking buffer for 1 hour at room temperature. Sections were washed 3 times in PBS, then mounted in ProLong Gold Antifade Reagent (ThermoFisher, P36934).

2.2.5 Mouse ex vivo *DTI*

Adult mice (p60 or older) were perfused with PBS followed by 4% paraformaldehyde. Whole brains were removed and post-fixed overnight in 4% paraformaldehyde at 4°C. Brains were washed in several changes of PBS at 4°C for a total of 24 hours before embedding.

Ex vivo DTI sample preparation, image acquisition, and initial data analysis was performed by Jaekeun Park at the Emory Biomedical Imaging Technology Center core facility. On the day of imaging, brains were carefully embedded in PBS containing 2% agarose and 2mM Gd(III) oxide, taking care to avoid any bubbles. Embedded brains were scanned using 3D DTI acquisition with DTIStandard sequence on a Bruker BioSpec® 94/20, 9.4 Tesla MRI. Acquisition parameters were as follows: TR/TE = 1600/22.6 ms; Average = 1; FOV = 25.6 x 11.8 x 9 mm^3; matrix = 256 x 118 x 90; diffusion gradient duration (δ) = 4 ms; diffusion time (Δ) = 12 ms; b value = 800 s/mm^2; 6 diffusion gradient directions. Initial analysis of DTI data was done using FSLview version 3.2.0 and involved the following steps: 1) Conversion from Bruker image format (2dseq) to nifti image file (ex:data.nii.gz), 2) Creation of masks to extract brain image data from the nifti data image file using fslmaths, 3) Preliminary analysis of DTI data from the extracted brain image file using dtifit.

Additional analysis of DTI data was done by Sarah Suciu in the Caspary lab. Regions of interest (ROIs) were defined on the T1 anatomical scan of each brain using the create mask option's pencil tool. Voxels at the midline of the SCP in all relevant Z planes were selected for

the mask. After the mask was defined, it was applied to the fractional anisotropy (FA) file for the same brain and the getMeanValueMask command was used to determine mean FA values in the ROI. Because the process of creating masks is somewhat subjective, FA values were determined using three separate masks created for each brain on separate occasions, which serve as technical replicates of the ROI definition process. The mean FA for each brain ROI used for subsequent statistical analysis was determined by taking the average of three technical replicates for each brain.

2.2.6 Arl13b knockdown in vitro

Arl13b shRNA knockdown sequences were generated against the rat *Arl13b* gene using the Life Technologies/ThermoFisher Scientific BLOCK-iT RNAi Designer. Three sequences were identified as promising targets, two of which are unique to the rat *Arl13b* gene while one is also a match with mouse *Arl13b*:

shRNA Number	Forward Sequence	Homologous to mouse?
366	TGTGATGGTCGGACTTGATAA	No
785	CTTGTTCAGCAGTCTTGGGAT	Yes
1067	CCATAGCAGCTGTCATCATTG	No

Each Arl13b shRNA oligo was individually cloned into the BLOCK-iT™ Pol II miR RNAi Expression Vector with EmGFP (ThermoFisher Scientific, K4936-00). The shRNA/miR/EmGFP sequence was then cloned via attB/attP site recombination (using BP clonase) into the pDONR221 backbone (ThermoFisher, 12536-017), and via attL/attR site recombination (using LR clonase) into a custom expression vector (Caspary lab plasmid #164) derived from Gateway pcDNA-DEST47 (ThermoFisher Scientific, 12281-010). Plasmid #164 replaced the promoter and polyA regions of Gateway pcDNA-DEST47 with the promoter and polyA from the pCAGGS/ES vector (Stuhmer et al., 2002) to improve its expression in mammalian neurons. The resulting shRNA expression vectors are Caspary lab plasmid #226 (shRNA 366), #227 (shRNA 785), and #228 (shRNA 1067).

Chapter 3

Role of Arl13b in Shh signaling in mouse embryonic fibroblasts

3.1 Introduction

The Shh signaling pathway regulates a wide variety of cellular processes. Shh acts as a morphogen and a mitogen in different cell types at different stages of embryonic development, regulating the transcription of its target genes through the balance of activator (GliA) and repressor (GliR) activity of the Gli family of transcription factors. In vertebrates, this transcriptional signaling requires proteins dynamically trafficking in and out of the primary cilium, and in the absence of cilia, transcriptional Shh signaling does not occur. In addition, non-transcriptional Shh signaling regulates cytoskeletal rearrangements involved in fibroblast migration and axon guidance. Unlike transcriptional Shh signaling, these processes can occur even in vertebrate cells lacking cilia.

The putative small GTPase Arl13b plays a unique role in the regulation of Shh signaling. Wild-type Arl13b protein localizes robustly to cilia, leaving it poised to interact with Shh pathway components during transcriptional signaling. Previous experiments show that Arl13b null *hennin (hnn)* mouse embryos have abnormal neural tube patterning caused by misregulation of Gli proteins (Caspary et al., 2007; Su et al., 2012). Specifically, these data suggest that GliR is relatively normal in Arl13b mutants, but Arl13b is required to properly regulate GliA. Cell biology studies have shown that Arl13b regulates multiple components of the Shh signaling pathway in cilia. *Arl13b*^{hnn} cells have short cilia with defects in the microtubule ultrastructure of the ciliary axoneme (Caspary et al., 2007). The abnormal structure of primary cilia could contribute to misregulation of the Shh pathway in cells lacking Arl13b. Furthermore, many of the proteins that make up the Shh signaling pathway show abnormal localization patterns in *Arl13b*^{hnn} cells (Larkins et al., 2011). Specifically, the Shh receptor Ptch1 and the Shh transducer Smo, normally trafficked out of and into cilia in response to Shh ligand, respectively, are constitutively present in cilia. Meanwhile, Gli proteins fail to display the normal enrichment at the tip of the

cilium upon Shh stimulation. Because Gli activation requires its transport to the tip of the cilium (Liu et al., 2015; Santos and Reiter, 2014), the disrupted ligand-dependent trafficking of Shh pathway proteins may explain why GliA is abnormal in *Arl13b*^{hnn} mutants. The Shh pathway is not the only one affected by *Arl13b* mutations: a large number of ciliary GPCRs are misregulated in neurons that lack Arl13b, leading to abnormal neuronal migration (Higginbotham et al., 2012). It is not yet clear whether the abnormal transport of cilia proteins in *Arl13b*^{hnn} cells arises purely from structural defects in mutant cilia or whether Arl13b has a specific function in regulating protein trafficking.

Most previous studies have used null or conditionally deleted alleles to interrogate Arl13b's function. Total loss of Arl13b is embryonic lethal and pan-neuronal deletion results in early death (p21 in mice). Some point mutations in *Arl13b*, however, are compatible with life and have been linked to the human ciliopathy Joubert Syndrome (JS; Cantagrel et al., 2008). My goal was to analyze the effects of JS-causing and other point mutations on Shh signaling, with the hope of better understanding Arl13b's role in regulating Shh signaling in normal and disease states. Previous studies have identified JS patients with homozygous R79Q and Y86C mutations in ARL13B, as well as an R200C mutation in combination with a truncated protein (Cantagrel et al., 2008; Thomas et al., 2015). I therefore tested these mutations in a mouse embryonic fibroblast (MEF) experimental system to assess their effects on Shh signaling in a variety of assays.

In addition to JS-causing Arl13b variants, I engineered several other mutations in Arl13b that are conserved across species and predicted to affect its function (Figure 3.2A). Arl13b is so named because of its sequence homology to the Arf and Arf-like (Arl) family of small GTPases, but it departs from the typical Arf sequence in several ways that are likely to have functional significance. Arl13b's N-terminal Arf domain includes four consensus nucleotide-binding motifs as well as the switch 1 and switch 2 loops that typically mediate GTPase interactions with effectors and modulators (Joneson et al., 1996; Kuai and Kahn, 2000). However, Arl13b lacks a conserved glutamine in the second nucleotide-binding motif: the sequence is WDVGG**Q** in Arfs

and FDLGG**G** in Arl13b. This motif regulates GTP hydrolysis and mutation of this glutamine in other GTPases leads to a dominant-activating protein that cannot hydrolyze GTP. To determine the significance of Arl13b's departure from other Arf/Arl proteins at this residue, I generated a G75Q mutation that restores the typical Q. To further examine the functional consequences of changes to Arl13b's GTPase domain, I also generated a predicted dominant negative T35N mutation, which is homologous to the Ras^{S17N} and $Arf1^{T31N}$ mutations that disrupt GTP binding (Dascher and Balch, 1994; Feig and Cooper, 1988). $Arl13b^{T35N}$ has been analyzed in other studies but its effect on Shh signaling has not been measured (Duldulao et al., 2009; Hori et al., 2008; Humbert et al., 2012).

Arfs typically contain a myristoylation site which facilitates their association with membranes. Several Arls, including Arl13b, are not myristoylated, but Arl13b does contain a palmitoylation motif that is essential for its membrane association and cilia localization (Cevik et al., 2013). To study the functional consequences of Arl13b palmitoylation, I examined the same C8S,C9S mutation shown by Cevik and colleagues to affect cilia/membrane localization of Arl13b.

To study the possible cilia-independent effects of Arl13b, it was necessary to design a mutation that would disrupt its cilia localization. The cilia localization signal (CiLS) of Arl13b was not known at the time of my initial experiments but was assumed to reside in the protein's C-terminus because Arl13b's N-terminal Arf domain is so similar to other Arf/Arl proteins that do not localize to cilia. Therefore, I identified four motifs in the amino acid sequence of Arl13b's C-terminus that resemble previously-characterized CiLSes (Figure 3.1). The first candidate CiLS, ALEEQ, resembles a motif shown to regulate cilia localization of G protein-coupled receptors (Berbari et al., 2008). The RVRKLRE motif is homologous to a "ciliary targeting sequence" in the ciliary protein fibrocystin (Follit et al., 2010). The KKKTKK sequence resembles a classical basic nuclear localization signal (Dingwall and Laskey, 1991; Nigg, 1997). Studies have shown that such lysine/arginine-rich motifs can serve as CiLSes, with the same signal regulating both

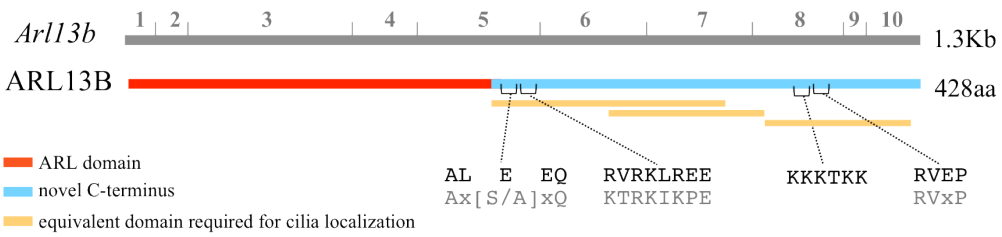

Figure 3.1 Schematic of potential cilia localization signals in mouse Arl13b. Putative CiLSes show the Arl13b amino acid sequence in black, published CiLS consensus sequences in grey. Yellow boxes indicate mouse homologs of regions known to eliminate cilia localization of Arl13b when deleted in zebrafish (c.f. Duldulao et al., 2009).

ciliary and nuclear import of a protein through similar mechanisms (Dishinger et al., 2010; Kee et al., 2012). The remaining sequence, RVEP, was chosen because it is consistent with the known VxP-containing CiLS motifs in rhodopsin, polycystin-1, and polycystin-2 (Deretic et al., 2005; Geng et al., 2006; Ward et al., 2011). All of these motifs are conserved between vertebrate species, and previous experiments showed that when domains homologous to those containing any of these CiLSes were deleted from zebrafish Arl13b, cilia localization of the protein was lost (Duldulao et al., 2009). After performing site-directed mutagenesis in each candidate CiLS (ALEEQ → FLEEF; KKKTKK → KAATAK; RVRKLRE → AAAALRE; RVEP → RAEP), I found that only the mutation in the RVEP sequence (V358A) affected Arl13b's cilia localization. Since then, other studies have confirmed that this motif in Arl13b is required for its cilia localization (Cevik et al., 2013; Higginbotham et al., 2012).

3.2 Results

3.2.1 Mutations in Arl13b affect its cilia localization and have dominant effects on cilia length

I first tested the effects of expressing mutant Arl13b proteins in phenotypically wild-type mouse embryonic fibroblasts (MEFs). I infected *Arl13b*$^{flox/flox}$*;CAGG-Cre*^{ERt2} MEFs (which express wild-type Arl13b unless Cre recombination is induced with tamoxifen; called *Arl13b*^{cond}

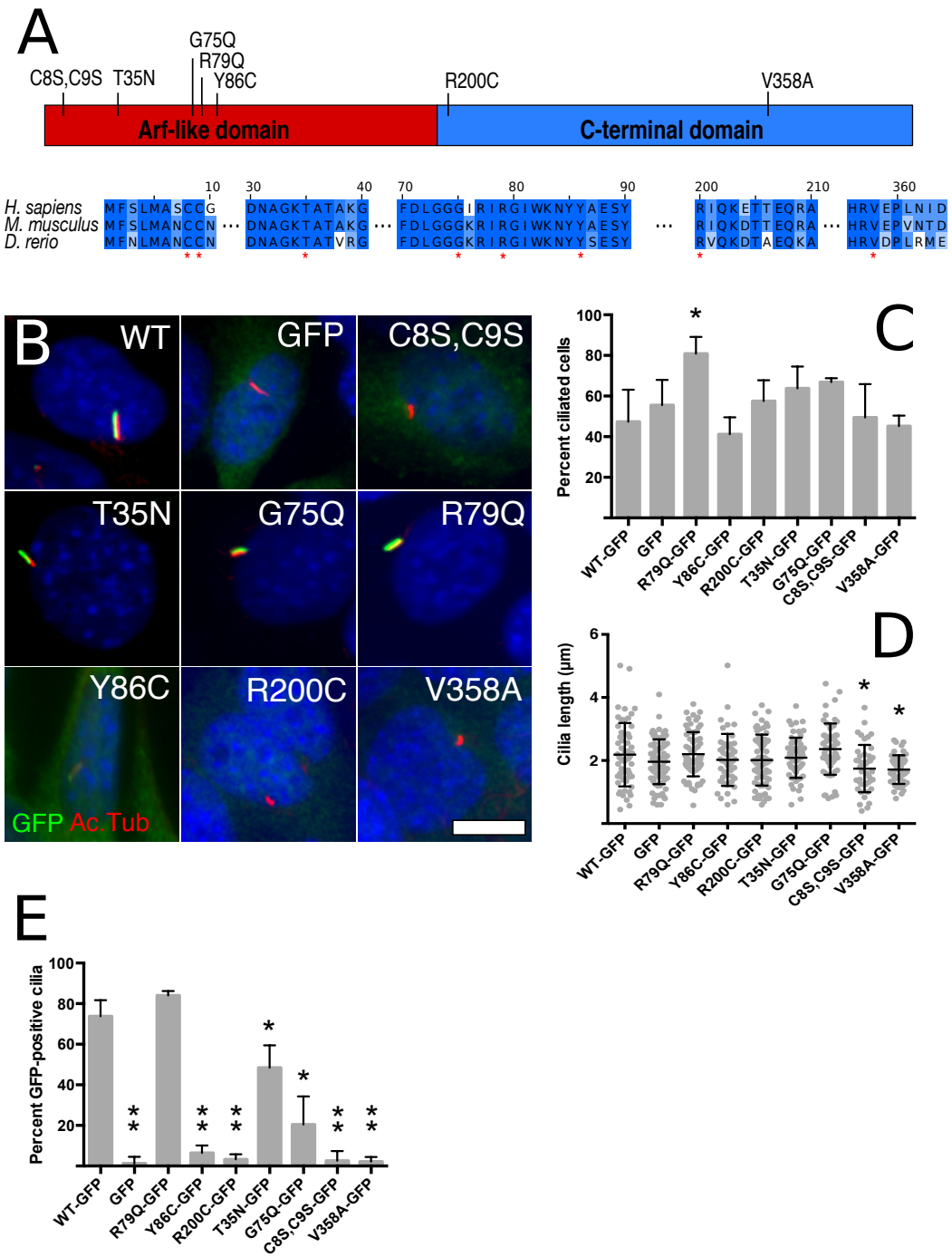

Figure 3.2 Characterizing Arl13b-GFP variants in *Arl13b*^{cond} MEFS. **A** Mutations were generated at conserved residues in Arl13b's Arf and C-terminal domains (red asterisks). **B** Representative images showing localization of Arl13b-GFP (GFP, green) relative to cilia (acetylated α-tubulin, red). Scale bar, 10 µm. **C** Percentage of MEFs with cilia (based on acetylated α-tubulin staining). Asterisk, significant difference from Arl13b^{WT}-GFP. **D** Quantification of cilia length (in µm). Askerisk, significant difference from Arl13b^{WT}-GFP. **E** Percentage of cilia showing GFP. Because only cells with cilia were analyzed, these data do not capture variations in the ciliation rate of different cell lines. Asterisk, significant difference from Arl13b^{WT}-GFP. Double asterisk, no significant difference from GFP-only.

hereafter) with lentiviruses driving the expression of wild-type or mutant Arl13b-GFP fusion proteins or a GFP-only negative control. I used FACS to purify GFP-positive cells and performed all assays on these hetereogeneous lines, which are composed of cells with different insertion sites for the lentiviral vector and variable Arl13b-GFP expression levels.

I observed that several mutants (Arl13b^{C8S,C9S}-GFP, Arl13b^{Y86C}-GFP, Arl13b^{R200C}-GFP, and Arl13b^{V358A}-GFP) fail to localize to cilia in most cells (Figure 3.2B,E). The mutations disrupting Arl13b's palmitoylation site and CiLS have previously been shown to affect its cilia localization (Cevik et al., 2013; Higginbotham et al., 2012), as has the JS-causing Arl13b^{Y86C} mutation (Thomas et al., 2015), but the Arl13b^{R200C}-GFP result conflicts with a previous report that showed normal cilia localization of Arl13b^{R200C}-FLAG in IMCD3 cells (Humbert et al., 2012). It is likely that transient transfection produces higher levels of Arl13b^{R200C} than I was able to achieve through stable lentiviral expression in this cell line, which may allow Arl13b^{R200C} to better compete with wild-type Arl13b for space on the ciliary membrane. Western blot analysis showed significant variability in Arl13b expression (Figure 3.3), with Arl13b^{R200C}-GFP and Arl13b^{Y86C}-GFP displaying the lowest levels of the 87 kDa Arl13b-GFP fusion protein (less than the expression level of 60 kDa endogenous Arl13b). This may also explain why Arl13b^{Y86C}-GFP showed so few GFP-positive cilia: in *Arl13b^{hnn}* cell lines achieving higher Arl13b^{Y86C}-GFP expression, the fraction of GFP-positive cilia was higher (Figure 3.2E). Still, even the low level of expression of Arl13b^{R200C}-GFP was sufficient to alter the transcriptional response to Shh (Figure 3.4), so I conclude that these small amounts of Arl13b-GFP can have biologically significant effects.

I quantified the number of cilia, length of cilia, and percentage of GFP-positive cilia for each line using the fluorescent imaging and stereology methods described in 2.1.8. I found that all of the cell lines were ciliated at rates comparable to Arl13b^{WT}-GFP (mean = 48% ± 6%), with the exception of Arl13b^{R79Q}-GFP, which actually showed an increase in the percentage of ciliated

cells (mean = 80% ± 3%). This suggests that Arl13b^{R79Q} may have direct dominant effects on ciliogenesis, but this phenotype may also result from an indirect effect, such as slowing the cell cycle.

In addition, I found a significant decrease in cilia length in Arl13b^{C8S,C9S}-GFP (mean = 1.7 ± 0.11 μm) and Arl13b^{V358A}-GFP (mean = 1.7 ± 0.06 μm) compared to Arl13b^{WT}-GFP (mean = 2.2 ± 0.13 μm). This suggests that mutations in Arl13b's palmitoylation site or CiLS that keep Arl13b out of the cilium have a dominant negative effect on cilia length. Analysis of GFP staining revealed that all Arl13b-GFP variants except for Arl13b^{R79Q}-GFP showed significant cilia localization defects when compared to Arl13b^{WT}-GFP (mean = 74% ± 3%). In terms of ciliary localization of GFP, Arl13b^{Y86C}-GFP, Arl13b^{R200C}-GFP, Arl13b^{C8S,C9S}-GFP and Arl13b^{V358A}-GFP were statistically indistinguishable from the GFP-only negative control (mean = 1% ± 1%). Although low expression of the Arl13b-GFP fusion protein may contribute to this finding in the Arl13b^{Y86C}-GFP and Arl13b^{R200C}-GFP lines, Arl13b^{C8S,C9S}-GFP and Arl13b^{V358A}-GFP exhibited fairly robust expression (Figure 3.3) indicating that they truly disrupt cilia localization.

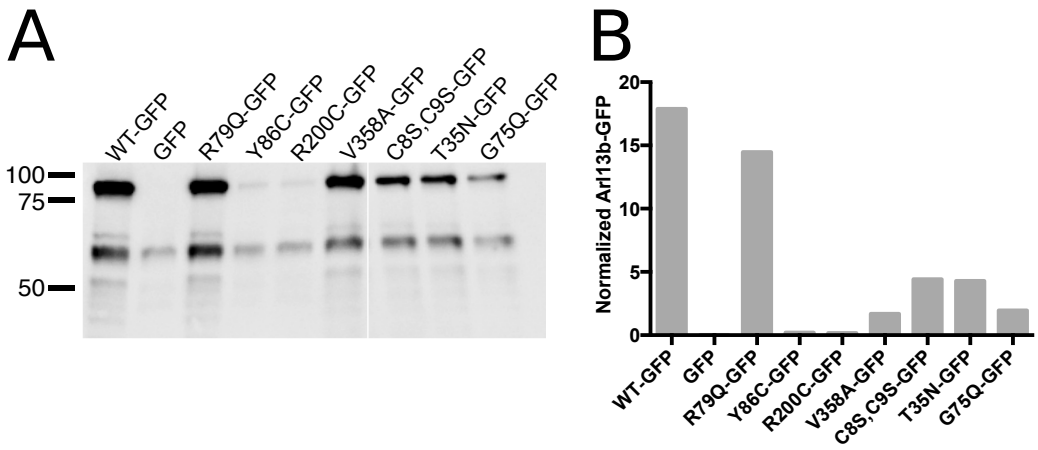

Figure 3.3 Arl13b protein levels in *Arl13b^{cond}* MEFs. **A** Western blot for Arl13b shows 60 kDa endogenous and 87 kDa Arl13b-GFP fusion protein bands. (Some 60 kDa protein may include Arl13b produced from cleavage of the GFP tag from Arl13b-GFP.) **B** Quantification of blot in A. Densities of Arl13b-GFP 87 kDa bands were normalized to total protein in their lane based on stain-free gel imaging (full protocol described in 2.1.9), then presented in quantities relative to endogenous Arl13b levels (as defined by the normalized density of the 60 kDa endogenous Arl13b band in the GFP-only negative control. (Western blot and quantification by Sarah Suciu)

3.2.2 Arl13b mutations have dominant effects on transcriptional Shh signaling

I used quantitative real-time PCR (qPCR) for the Shh target genes *Gli1* and *Ptch1* to measure transcriptional Shh signaling in the Arl13b-GFP conditional MEF lines. (All gene expression values are given as fold change relative to the unstimulated baseline level of expression in the Arl13b^{WT}-GFP cell line.) *Gli1* is not expressed unless transcriptional Shh signaling is active (Bai et al., 2002), whereas *Ptch1* is expressed at baseline to serve its function as a Shh receptor but becomes upregulated upon Shh stimulation in a form of negative feedback (Goodrich et al., 1997; Marigo et al., 1996). Therefore, the magnitude of fold change upon Shh treatment is expected to be much higher for *Gli1* than *Ptch1*, and this is what I consistently observed.

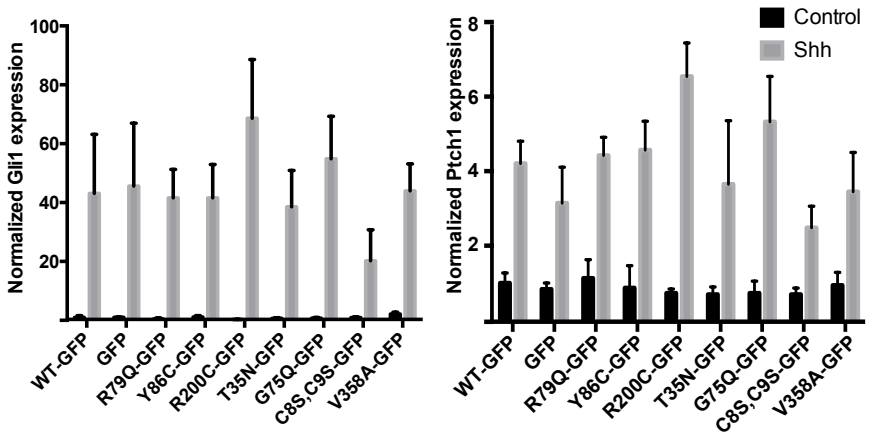

Figure 3.4 Transcriptional response to Shh stimulation in *Arl13b^{cond}* MEFs. All data are shown as fold change relative to the baseline expression level of each target gene in the Arl13b^{WT}-GFP cell line.

Because JS-causing mutations in Arl13b are recessive, I did not predict any effect of these mutations in MEFs that co-express wild-type Arl13b, and did not detect any dominant effects of Arl13b^{R79Q}-GFP or Arl13b^{Y86C}-GFP compared to Arl13b^{WT}-GFP (mean *Gli1* fold change after Shh treatment = 43 ± 10; mean *Ptch1* = 4.2 ± 0.29). Interestingly, Arl13b^{R200C}-GFP appeared to potentiate the Shh response (mean *Gli1* = 69 ± 10; mean *Ptch1* = 6.5 ± 0.45), suggesting that this JS-causing variant may be capable of producing an additive effect on

transcriptional Shh signaling when acting in concert with wild-type Arl13b. In addition, Arl13b^{C8S,C9S}-GFP (mean *Gli1* = 20 ± 5.2; mean *Ptch1* = 2.5 ± 0.29) produced a significant negative effect on signaling, reducing the transcriptional response to Shh ligand (Figure 3.4). Because cilia are so integral to transcriptional Shh signaling, this effect may be due in part to a structural defect in Arl13b^{C8S,C9S}-GFP cilia that also leads to their decreased length (Figure 3.2D). However, Arl13b^{V358A}-GFP cells also had shorter cilia, but their transcriptional response to Shh was normal. Interestingly, though, *Gli1* expression appeared slightly elevated at baseline in the Arl13b^{V358A}-GFP line. This difference was not statistically significant, but it was consistently observed in both *Arl13b^{cond}* and *Arl13b^{hnn}* MEF lines (Figure 3.6). Taken together, these data suggest that Arl13b plays distinct roles in regulating cilia structure and Shh signaling, and that different mutations may affect these functions individually or in combination.

3.2.2.1 Tamoxifen-induced recombination

I next wanted to test the effects of Arl13b mutations in the absence of wild-type Arl13b. To do this, I attempted to delete the endogenous *Arl13b* gene from *Arl13b^{cond}* MEFs. *Arl13b^{cond}* MEFs made from mice carrying the *CAGG-Cre^{ERt2}* transgene undergo Cre-lox recombination after treatment with tamoxifen *in vitro* and exhibit reduced Arl13b protein 42 hours later (Su et al., 2012). However, in subsequent experiments I observed significant variability in the response to tamoxifen in both primary and immortalized *Arl13b^{cond}* MEFs. 48 hours after treatment with 2 μM tamoxifen, 20-30% of cells retained Arl13b in the cilium. To determine whether this was due to the heterogeneous nature of the MEFs, I tested the hypothesis that some cells are more responsive to tamoxifen than others by subcloning lines of immortalized *Arl13b^{cond}* MEFs from the parental population. The results remained variable even in clonal lines, indicating that non-genetic factors play a role in the induction of recombination by tamoxifen. I was hesitant to

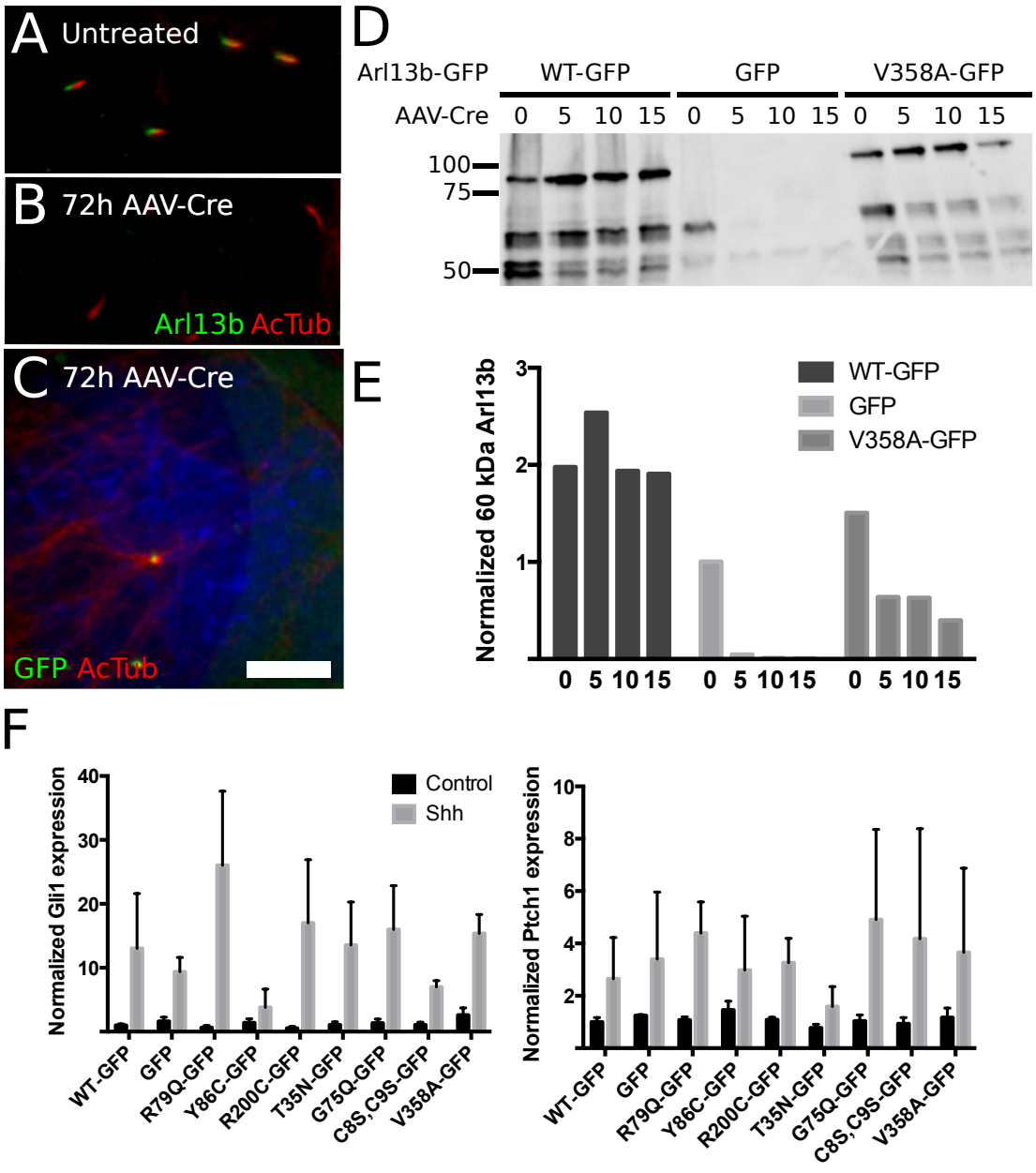

Figure 3.5 Effects of *Arl13b* deletion via AAV-Cre on *Arl13b*^{cond} MEFs. **A-B** Comparison of Arl13b (green) levels in cilia (acetylated α-tubulin, red) of *Arl13b*^{cond} MEFs cultured in the absence or presence of 10 µL AAV-Cre supernatant for 72 hours. **C** Abnormal multinucleated cell seen after AAV-Cre treatment. Scale bar, 10 µm. **D** Western blot for Arl13b showing 60 kDa endogenous and 87 kDa Arl13b-GFP fusion protein bands after 72 hours of treatment with 0, 5, 10, or 15 µL AAV-Cre supernatant. **E** Quantification of blot in D. Densities of Arl13b 60 kDa bands were normalized to total protein in their lane based on stain-free gel imaging (full protocol described in 2.1.9), then presented in quantities relative to endogenous Arl13b levels (as defined by the normalized density of the 60 kDa endogenous Arl13b band in the GFP-only negative control with 0 AAV-Cre). (Western blot and quantification by Sarah Suciu) **F** Transcriptional response to Shh stimulation as measured by qPCR. All data are shown as fold change relative to the baseline expression level of each target gene in the Arl13b^{WT}-GFP cell line.

conduct population-level assays such as qPCR on cells that might retain endogenous wild-type Arl13b, and therefore moved to using viral-mediated Cre expression to drive recombination in hopes that it would produce greater efficacy.

3.2.2.2 AAV-Cre recombination

I treated immortalized *Arl13b*^{cond} MEFs with AAV-Cre and observed loss of Arl13b protein as measured by immunofluorescence and western blotting (Figure 3.5A-E). However, the viral infection caused significant toxicity and cell death in the Arl13b-GFP mutant MEFs, and seemed particularly severe in the Arl13b^{WT}-GFP cell line. Analysis of Shh target genes by qPCR after cells had been treated with AAV-Cre showed an abnormally low response in the Arl13b^{WT}-GFP line (mean *Gli1* fold change after Shh treatment = 13 ± 4.3; mean *Ptch1* = 2.6 ± 0.79; Figure 3.5F). Because of this confounding factor, I decided to abandon Cre-lox recombination in the *Arl13b*^{cond} MEFs and conduct all subsequent experiments in immortalized *Arl13b*^{hnn} MEFs.

3.2.3 Arl13b mutations affect cilia in an Arl13b-null background

After I generated *Arl13b*^{hnn} MEFs expressing Arl13b-GFP through the same method of lentiviral infection and FACS purification used in the *Arl13b*^{cond} MEFs, I characterized them by immunofluorescence and western blotting. As expected, *Arl13b*^{hnn} MEFs revealed more significant effects than the *Arl13b*^{cond} experiments, where the presence of wild-type endogenous Arl13b preserved more Arl13b functions. Although I found no significant differences in the number of *Arl13b*^{hnn} MEF cilia, I noted a high degree of variability in the Arl13b^{R79Q}-GFP cell line (Figure 3.6A). In some experiments, Arl13b^{R79Q}-GFP did appear to be ciliated at a greater frequency than Arl13b^{WT}-GFP cells, similar to the result observed in *Arl13b*^{cond} MEFs (Figure

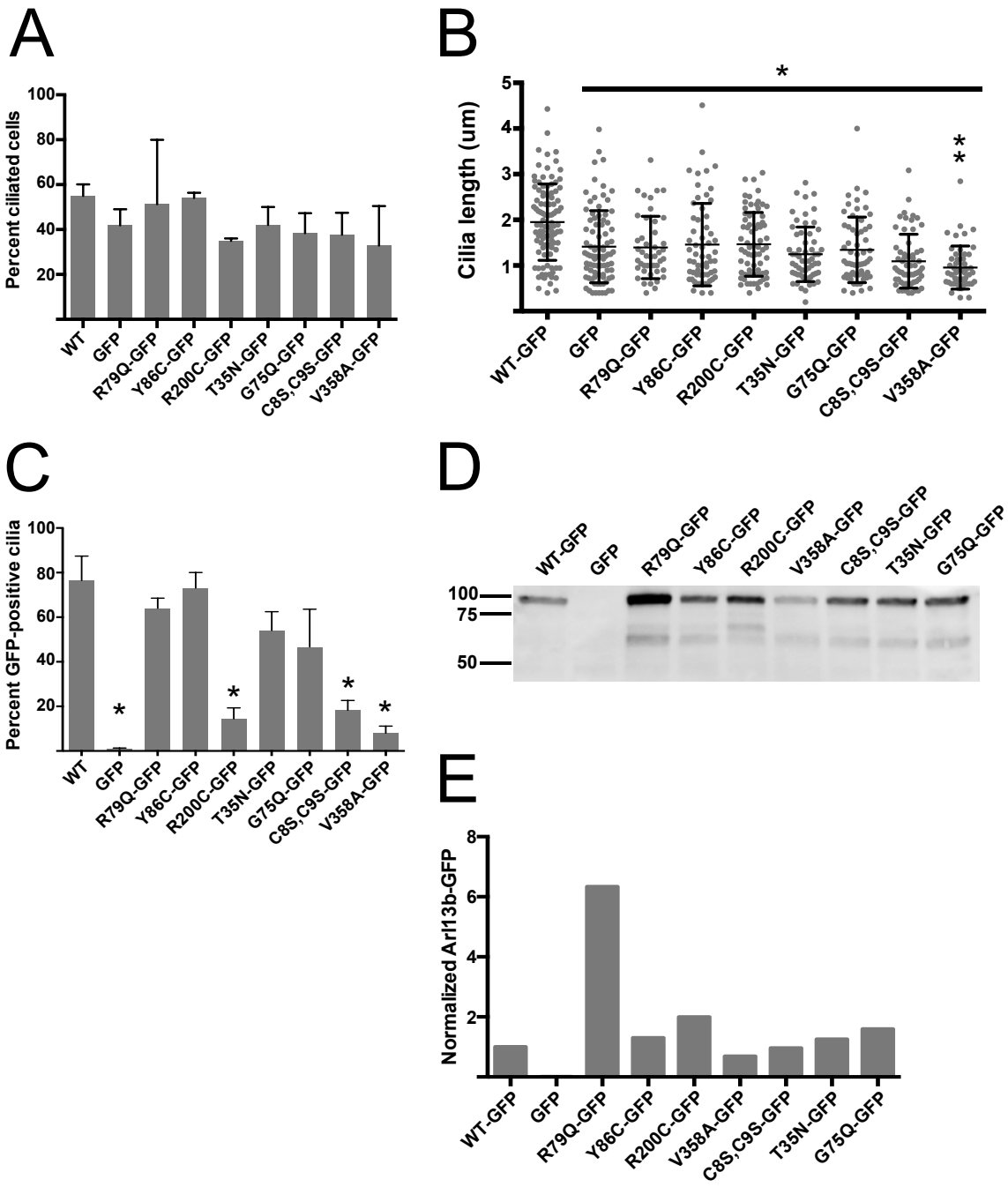

Figure 3.6 Characterizing Arl13b-GFP variants in *Arl13b*^{hnn} MEFs. **A** Percentage of MEFs with cilia (based on acetylated α-tubulin staining). **B** Quantification of cilia length (in μm). Asterisk, significant different from Arl13b^{WT}-GFP; double asterisk, significant difference from GFP-only. **C** Percentage of cilia showing GFP. Asterisk, significant difference from Arl13b^{WT}-GFP. Because only cells with cilia were analyzed, these data do not capture variations in the ciliation rate of different cell lines. **D** Western blot for Arl13b showing 87 kDa Arl13b-GFP fusion protein band. **E** Quantification of blot in D. Densities of Arl13b 87 kDa bands were normalized to total protein in their lane based on stain-free gel imaging (full protocol described in 2.1.9), then presented in quantities relative to Arl13b^{WT}-GFP levels (as defined by the normalized density of the 87 kDa Arl13b-GFP band in the Arl13b^{WT}-GFP lane).

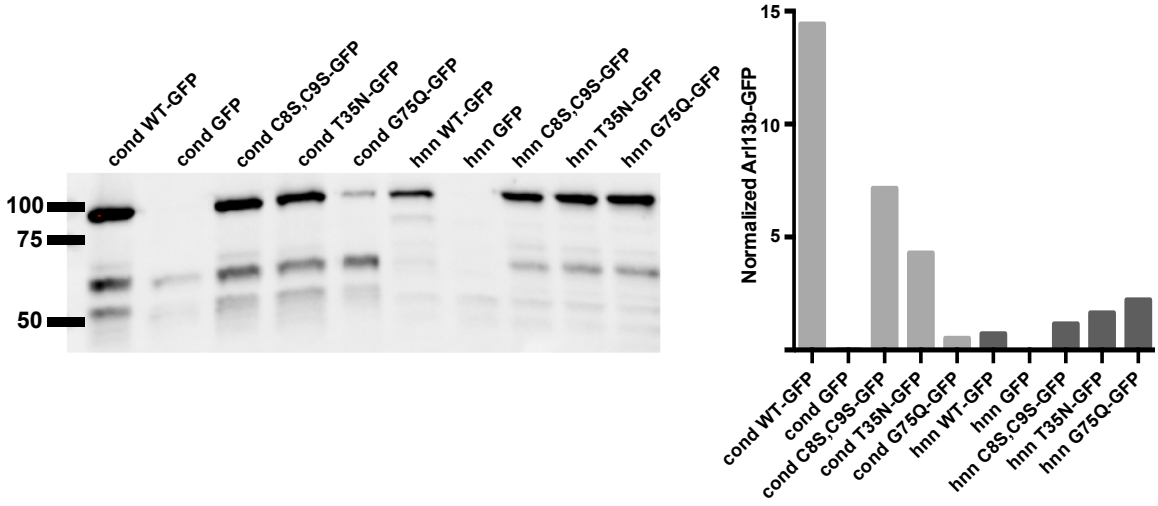

Figure 3.7 Relative Arl13b-GFP expression in *Arl13b*^{cond} and *Arl13b*^{hnn} cell lines. **A** Western blot for Arl13b showing 87 kDa Arl13b-GFP fusion protein and 60 kDa endogenous Arl13b. **B** Quantification of blot in A. Densities of Arl13b 87 kDa bands were normalized to total protein in their lane based on stain-free gel imaging (full protocol described in 2.1.9), then presented in quantities relative to endogenous Arl13b levels (as defined by the normalized density of the 60 kDa Arl13b band in the *Arl13b*^{cond} GFP lane).

3.2C). Furthermore, loss of Arl13b produces a significant decrease in cilia length in GFP-only MEFs (mean = 1.4 ± 0.08 μm) relative to WT MEFs (mean = 1.9 ± 0.08 μm) that could not be rescued by any other variant (Figure 3.6B). In fact, Arl13b^{V358A}-GFP produced cells with cilia significantly *shorter* than the GFP-only negative controls (mean = 0.96 ± 0.07 μm).

When I analyzed the percentage of GFP-positive cilia in each cell line, I found results similar to what I observed in *Arl13b*^{cond} MEFs, with the notable exception of Arl13b^{Y86C}-GFP. In the absence of endogenous wild-type Arl13b, Arl13b^{Y86C}-GFP localizes to 73% ± 7.0% of cilia, indistinguishable from Arl13b^{V358A}-GFP (76% ± 11%), which is in stark contrast to the 6.5% ± 1.5% of GFP-positive cilia observed in Arl13b^{Y86C}-GFP *Arl13b*^{cond} MEFs. In a previous analysis of this variant using transient transfections in *Arl13b*^{hnn} MEFs, I observed Arl13b^{Y86C} in the cilia of transfected cells only about half as often as in cells transfected with wild-type Arl13b (Thomas et al., 2015). In all cases, *Arl13b*^{hnn} MEFs appear to show more GFP-positive cilia than the corresponding variant expressed in *Arl13b*^{cond} MEFs. While for some constructs this may be due

in part to higher expression levels of the fusion protein (Arl13b^{Y86C}-GFP and Arl13b^{R200C}-GFP were more highly expressed in *Arl13b^{hnn}* MEFs than *Arl13b^{cond}* MEFs, compare Figure 3.3 and Figure 3.6D-E), Arl13b^{V358A}-GFP was expressed at higher levels in *Arl13b^{cond}* MEFs but localizes to cilia more often in *Arl13b^{hnn}* MEFs. For other variants, the difference in relative expression levels between cell lines was more difficult to determine, so I compared them directly in another western blot (Figure 3.7). I saw that in Arl13b^{C8S,C9S}-GFP and Arl13b^{T35N}-GFP, relative expression levels are higher in *Arl13b^{cond}* than *Arl13b^{hnn}*, but both variants show more robust cilia localization in *Arl13b^{hnn}* MEFs. This suggests that Arl13b-GFP variants may compete with endogenous wild-type Arl13b for space in the cilium, facilitating the cilia localization of Arl13b variants in an *Arl13b^{hnn}* background.

3.2.4 Arl13b mutations affect Shh signaling in an Arl13b^{hnn} background

Analysis of transcriptional Shh signaling by qPCR showed significant effects for several Arl13b-GFP variants in *Arl13b^{hnn}* MEFs (Figure 3.8). However, these effects were observed only in *Gli1* expression; differences in *Ptch1* did not reach statistical significance. This is likely because *Ptch1* upregulation upon Shh treatment is much more modest than *Gli1* upregulation, so the difference between a response and a failure to respond to Shh is more subtle. For all

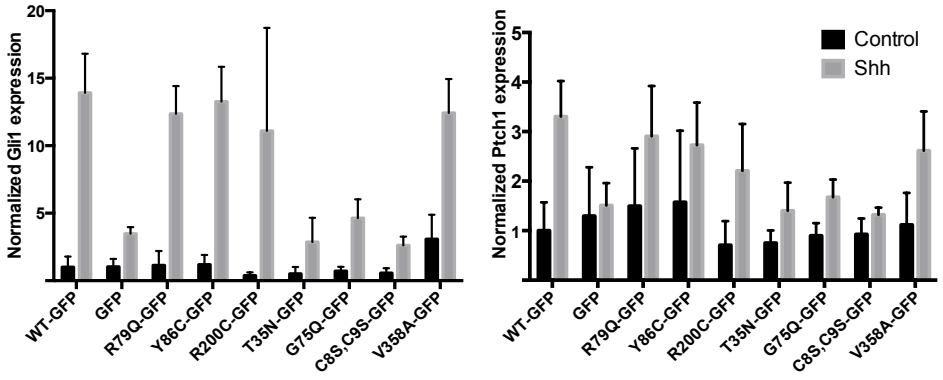

Figure 3.8 Transcriptional response to Shh stimulation in *Arl13b^{hnn}* MEFs. All data are shown as fold change relative to the baseline expression level of each target gene in the Arl13b^{WT}-GFP cell line.

Arl13b^{cond} and *Arl13b*^{hnn} cell lines, *Ptch1* expression mirrored the trends seen in *Gli1* expression, but with smaller changes in the magnitude of fold-change upon Shh treatment.

Consistent with my previous studies using primary MEFs (Su et al., 2012), the GFP-only *Arl13b*^{hnn} MEFs exhibited a very limited Shh response (mean *Gli1* fold change upon Shh treatment = 3.5 ± 0.50) when compared to Arl13b^{WT}-GFP (mean = 14 ± 2.9). Meanwhile, Arl13b^{C8S,C9S}-GFP (mean = 2.6 ± 0.64), Arl13b^{T35N}-GFP (mean = 2.9 ± 1.8), and Arl13b^{G75Q}-GFP (mean = 4.6 ± 1.4) all showed a significantly decreased response to Shh. The result for Arl13b^{C8S,C9S}-GFP was expected, given its effect on transcriptional response in *Arl13b*^{cond} MEFs, but the effect is even more pronounced in *Arl13b*^{hnn} MEFs: Arl13b^{C8S,C9S}-GFP achieves only 19% of the Arl13b^{WT}-GFP response in *Arl13b*^{hnn} MEFs, while it reaches 47% of the Arl13b^{WT}-GFP response in *Arl13*^{cond} MEFs. In addition, Arl13b^{T35N}-GFP and Arl13b^{G75Q}-GFP had no significant effect on transcriptional response in cells that also express wild-type Arl13b, but they were unable to rescue the loss of Arl13b function in *Arl13b*^{hnn} MEFs. These results suggest that GTP binding at Arl13b's Arf-like domain is critical for regulation of the Shh transcriptional response.

3.2.5 Variability in the transcriptional response to Shh

In performing analyses of transcriptional Shh signaling by qPCR, I noticed a surprising degree of variability in the Shh response within cell lines. As an example, I have reproduced the normalized values of *Gli1* and *Ptch1* expression measured in the *Arl13b*^{hnn} cell lines from six independent biological replicates (Table 3.1 and Table 3.2).

Variability in the transcriptional response to Shh may be partially explained by differences in experimental conditions between replicates. Biological replicate #2, for example, produced unusually low Shh-induced *Ptch1* and *Gli1* expression in almost all cell lines, suggesting that some factor acted uniformly on all cell lines to limit Shh induction – perhaps the

***Gli1* Expression Values in *Arl13b^{hnn}* MEFs**									
Ctrl	**WT-GFP**	**GFP**	**R79Q-GFP**	**Y86C-GFP**	**R200C-GFP**	**V358A-GFP**	**C8S,C9S-GFP**	**T35N-GFP**	**G75Q-GFP**
1	0.19	0.39	0.27	0.36	0.19	0.98	0.15	0.17	0.23
2	0.66	1.67	0.81	2.07	0.31	4.46	1.10	0.39	0.68
3	0.39	1.40	0.97	1.57	0.15	5.54	0.43	0.20	0.81
4	0.94	0.55	0.77	0.61	0.31	1.57	0.27	0.16	0.54
5	2.29	0.55	0.69	0.75	0.59	2.01	0.82	1.47	1.20
6	1.53	1.60	3.27	1.81	0.74	3.88	0.63	0.67	0.81
Avg	**1.00**	**1.03**	**1.13**	**1.19**	**0.38**	**3.07**	**0.57**	**0.51**	**0.71**
SEM	0.32	0.24	0.44	0.29	0.09	0.74	0.14	0.21	0.13
Shh	**WT-GFP**	**GFP**	**R79Q-GFP**	**Y86C-GFP**	**R200C-GFP**	**V358A-GFP**	**C8S,C9S-GFP**	**T35N-GFP**	**G75Q-GFP**
1	10.28	2.02	10.47	9.02	5.83	1.79	1.02	0.88	1.49
2	6.29	5.23	5.43	9.19	0.33	20.25	2.26	1.47	3.53
3	9.56	3.95	15.96	17.12	1.60	12.16	3.27	0.78	10.32
4	25.42	2.68	12.69	23.64	6.92	13.49	2.25	0.83	7.20
5	12.84	4.28	19.88	13.84	48.96	10.88	5.42	11.87	3.42
6	19.14	2.66	9.69	6.81	2.91	15.99	1.47	1.32	1.82
Avg	**13.92**	**3.47**	**12.35**	**13.27**	**11.09**	**12.42**	**2.61**	**2.86**	**4.63**
SEM	2.89	0.50	2.07	2.58	7.64	2.52	0.64	1.81	1.41

Table 3.1 *Gli1* expression values measured by qPCR in *Arl13b^{hnn}* MEFs expressing Arl13b-GFP under control (Ctrl) or Shh-stimulated (Shh) conditions in 6 different experiments. Each *Gli1* value was normalized to *Pold3* expression within the same sample. Data are shown as fold change relative to the average *Gli1* level at baseline in Arl13b^{WT}-GFP.

batch of Shh-conditioned media used for treatment that day was not very potent, or fluctuations in the environment inside the incubator stressed the cells. In contrast, replicate #5 produced unusually high *Ptch1* expression in all cell lines. In the same replicate, *Gli1* expression was also quite high in Arl13b^{R79Q}-GFP, Arl13b^{R200C}-GFP, Arl13b^{C8S,C9S}-GFP, and Arl13b^{T35N}-GFP, but fairly average *Gli1* expression in Arl13b^{WT}-GFP, GFP-only, Arl13b^{Y86C}-GFP, Arl13b^{V358A}-GFP, and Arl13b^{G75Q}-GFP. This suggests that some experimental factor in replicate #5 had a differential effect on *Ptch1* versus *Gli1* in the same cells. It may be that after 24 hours of Shh treatment, uniformly upregulated *Ptch1* caused by some common experimental factor was beginning to induce negative feedback on the Shh pathway, thereby inhibiting Shh-mediated transcription of *Gli1* by the time samples were collected in some of the cell lines.

Ptch1 Expression Values in *Arl13b*^{hnn} MEFs									
Ctrl	**WT-GFP**	**GFP**	**R79Q-GFP**	**Y86C-GFP**	**R200C-GFP**	**V358A-GFP**	**C8S,C9S-GFP**	**T35N-GFP**	**G75Q-GFP**
1	0.37	0.57	0.48	1.10	0.48	0.56	0.40	0.36	0.54
2	0.69	1.00	0.75	0.84	0.00	0.72	0.81	0.63	0.69
3	0.56	0.87	1.45	0.87	0.71	1.49	1.28	0.84	1.23
4	1.02	0.69	0.95	0.60	0.53	0.66	0.83	0.66	0.93
5	1.60	3.21	3.70	4.45	1.29	2.24	1.04	0.93	1.11
6	1.76	1.43	1.66	1.58	1.22	1.05	1.19	1.07	0.88
Avg	**1.00**	**1.29**	**1.50**	**1.57**	**0.71**	**1.12**	**0.93**	**0.75**	**0.90**
SEM	0.23	0.40	0.48	0.59	0.20	0.26	0.13	0.10	0.10
Shh	**WT**	**GFP**	**R79Q-GFP**	**Y86C-GFP**	**R200C-GFP**	**V358A-GFP**	**C8S,C9S-GFP**	**T35N-GFP**	**G75Q-GFP**
1	2.17	0.69	2.01	1.11	1.08	0.45	0.89	0.64	0.81
2	1.25	1.05	0.21	1.14	0.43	2.10	1.24	0.73	0.84
3	2.44	1.31	2.35	2.00	1.40	N/A	1.80	1.02	2.92
4	3.57	0.90	2.34	2.85	1.76	2.05	1.34	0.78	1.56
5	6.19	3.72	7.61	6.78	6.84	5.25	N/A	4.23	2.54
6	4.20	1.37	2.92	2.48	1.72	3.21	1.33	1.01	1.37
Avg	**3.30**	**1.51**	**2.91**	**2.73**	**2.21**	**2.61**	**1.32**	**1.40**	**1.67**
SEM	0.72	0.45	1.01	0.86	0.95	0.79	0.15	0.57	0.36

Table 3.2 *Ptch1* expression values measured by qPCR in *Arl13b*^{hnn} MEFs expressing Arl13b-GFP under control (Ctrl) or Shh-stimulated (Shh) conditions in 6 different experiments. Each *Ptch1* value was normalized to *Pold3* expression within the same sample. Data are shown as fold change relative to the average *Ptch1* level at baseline in Arl13b^{WT}-GFP. Cells marked "N/A" indicate samples that were lost or degraded.

3.2.6 Arl13b mutations affect Shh-dependent Smo enrichment in cilia

After observing the effects of Arl13b variants on transcriptional Shh signaling, I investigated whether any of these effects were occurring at the level of Smo trafficking. Previous studies from the Caspary lab showed that *Arl13b*^{hnn} MEFs exhibit abnormal Shh-dependent trafficking of Shh pathway components, including Smo (Larkins et al., 2011), but Arl13b clearly also acts downstream of Smo to regulate Shh signaling (Caspary et al., 2007). Therefore I measured whether Smo was enriched in the cilia of *Arl13b*^{hnn} MEFs expressing Arl13b-GFP variants at baseline and in Shh-stimulated conditions. Because a small amount of Smo is present in cilia even in the absence of Shh signaling (Milenkovic et al., 2015; Ocbina and Anderson, 2008) and immunofluorescence reveals low-level Smo staining in almost all cilia, I will refer to

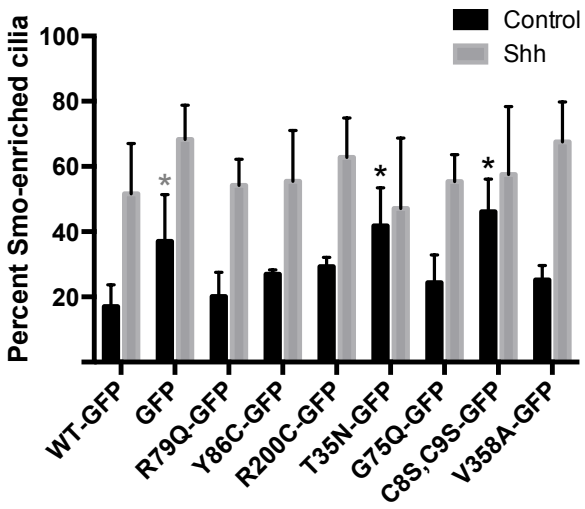

Figure 3.9 Shh-dependent ciliary enrichment of Smo in response to Shh stimulation in *Arl13b*^{hnn} MEFs. Smo enrichment was quantified based on amount of Smo staining colocalized with acetylated α-tubulin according to methods described in 2.1.8. Because only cells with cilia were analyzed, these data do not capture variations in the ciliation rate of different cell lines. Black asterisks, significantly different from Arl13b^{WT}-GFP with multiple comparison adjusted p-value < 0.05. Gray asterisk, adjusted p-value = 0.0500 (95% confidence interval of difference in means = -0.4010 to 1.866×10^{-6}).

"Smo-enriched" cilia rather than "Smo-positive" cilia when describing the accumulation of ciliary Smo that normally reflects active Shh signaling.

Consistent with previous reports, in *Arl13b*^{hnn} MEFs expressing only GFP, Smo is inappropriately enriched in cilia under control conditions (37% ± 14%; Figure 3.9) compared to cells expressing Arl13b^{WT}-GFP (17% ± 6.7%). Similar elevated baseline Smo enrichment occurs in Arl13b^{T35N}-GFP (42% ± 13%) and Arl13b^{C8S,C9S}-GFP (46% ± 10%). Even in cell lines with abnormal ciliary enrichment of Smo at baseline, a trend toward further Smo accumulation in cilia upon Shh stimulation was present, suggesting that Arl13b is not the sole determinant of proper regulation of Smo's enrichment in cilia. However, these mutant lines suggest that Arl13b plays a role in regulating Smo trafficking that requires its presence on the cell membrane and GTP-binding. Interestingly, this regulation of Smo does not explicitly require Arl13b to be present in cilia (since Arl13b^{R200C}-GFP and Arl13b^{V358A}-GFP, both of which fail to localize to cilia, show normal patterns of Smo localization under control and Shh-stimulated conditions).

3.2.7 Arl13b mutations affect non-transcriptional Shh signaling in MEF migration

After characterizing the effects of Arl13b mutations on cilia number and length, Arl13b localization, and transcriptional Shh response, I wanted to test their effects on non-transcriptional Shh signaling. I first became interested in possible effects of Arl13b on non-transcriptional Shh signaling in the context of JS, because JS has been characterized as a human genetic disorder of axon guidance (Engle, 2010), and non-transcriptional Shh signaling can serve as an axon guidance cue (Charron et al., 2003; Fabre et al., 2010; Okada et al., 2006; Yam et al., 2009). However, non-transcriptional Shh signaling can also be studied in MEFs through assays that measure Shh-dependent chemotaxis (Bijlsma et al., 2007; Bijlsma et al., 2012). I therefore initiated a collaboration with Maarten Bijlsma's lab to study Shh-mediated chemotaxis in *Arl13b*^{hnn} MEFs expressing different Arl13b-GFP variants. All chemotaxis assays were performed by Maarten Bijlsma.

In an initial pilot experiment, we showed that *Arl13b*^{hnn} MEFs expressing either GFP-only or Arl13b^{WT}-GFP can both migrate toward FCS, a nonspecific chemoattractant (Figure 3.10C). However, when the MEFs were exposed to either rShhN ligand or the Smo agonist purmorphamine, Arl13b^{WT}-GFP MEFs responded much more strongly to the attractive cues than the GFP-only controls. This suggests that Arl13b does indeed play a role in mediating Shh-mediated chemotaxis in MEFs.

We next chose candidate Arl13b-GFP variants to test in the same assay. Because non-transcriptional Shh signaling does not require a primary cilium, I predicted that mutations disrupting Arl13b's ciliary localization would have less of an effect on migration than they did on Shh-mediated gene transcription – it seems that while the cilium is the locus of transcriptional Shh signal transduction, Arl13b should be able to serve its function regulating chemotaxis from outside of the cilium. I also wanted to test JS-causing variants, given the axon guidance defects in

JS and their possible connection to non- transcriptional Shh signaling. Therefore, we chose to analyze Arl13b^{R79Q}-GFP, Arl13b^{Y86C}-GFP, Arl13b^{R200C}-GFP, and Arl13b^{V358A}-GFP.

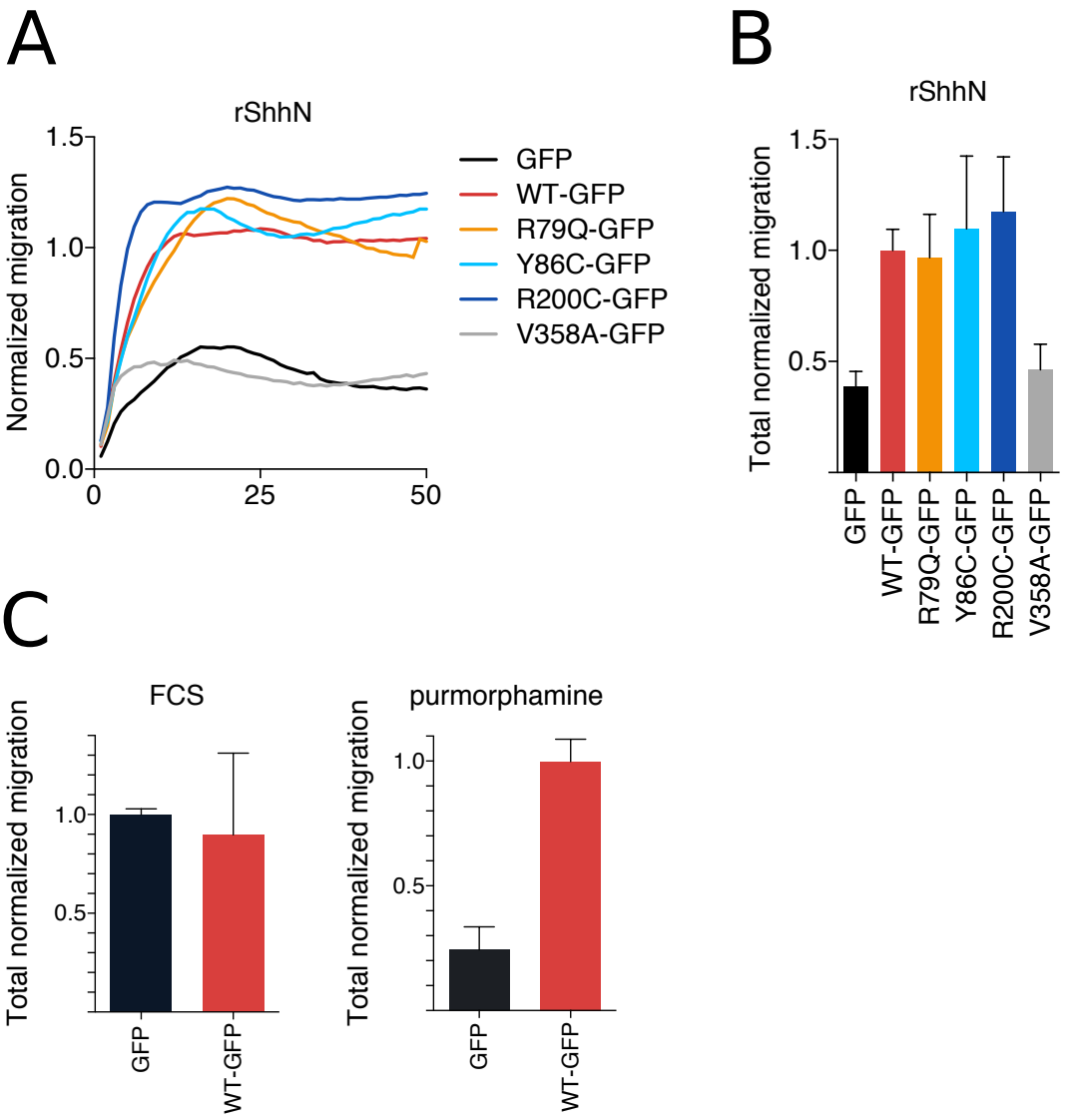

Figure 3.10 Migration of *Arl13b^{hnn}* MEFs expressing Arl13b-GFP variants. All migration assays were performed by Maarten Bijlsma. **A** Average normalized migration curves for *Arl13b^{hnn}* MEFs expressing Arl13b variants migrating toward rShhN, n = 12. **B** Quantification of total migration from experiments shown in A. **C** *Arl13b^{hnn}* MEFs expressing GFP or Arl13b^{WT}-GFP migrate similarly toward FCS, but show significant differences in migration toward the Smo agonist purmorphamine.

Contrary to my prediction, we observed that, compared to Arl13b^{WT}-GFP (mean total normalized migration set to 1.0 ± 0.09 arbitrary units), Arl13b^{V358A}-GFP displays significantly reduced migration and behaved similarly to *Arl13b^{hnn}* MEFs expressing only GFP (mean = 0.39 ± 0.07; Figure 2A-B). This suggests that while the cilium itself is dispensable for non-transcriptional Shh signaling, the CiLS of Arl13b is required for it to transduce this form of signaling. Meanwhile, JS-causing variants of Arl13b were not significantly different from Arl13b^{WT}-GFP in this assay. This suggests that while Arl13b is required for Shh-dependent fibroblast migration, the JS-causing alleles known to disrupt other functions of Arl13b are not implicated in this process.

3.3 Discussion

In this chapter, I used a variety of MEF-based assays to examine the effects of mutations in Arl13b on cilia formation, the regulation of Arl13b and Smo localization in cilia, transcriptional Shh signaling, and non-transcriptional Shh signaling. (Results summarized in Table 3.3 and Table 3.4.) I showed that mutating Arl13b's palmitoylation site was particularly disruptive, indicating that membrane association of Arl13b is critical for its functions. I also showed that mutating Arl13b's GTP-binding domain or its CiLS leads to significant loss of

Arl13b variant (cond MEFs)	Mutation type	GFP in cilia	Cilia number	Cilia length	qPCR Shh response
WT-GFP		Yes	Normal	Normal	Normal
GFP only		**No**	Normal	Normal	Normal
R79Q-GFP	JS	Yes	**More**	Normal	Normal
Y86C-GFP	JS	**No**	Normal	Normal	Normal
R200C-GFP	JS	**No**	Normal	Normal	**Increased**
T35N-GFP	GTPase	**Less**	Normal	Normal	Normal
G75Q-GFP	GTPase	**Less**	Normal	Normal	Normal
V358A-GFP	CiLS	**No**	Normal	**Short**	Normal
C8S,C9S-GFP	Palm.	**No**	Normal	**Short**	**Reduced**

Table 3.3 Summary of results from *Arl13b^{cond}* MEFs. Results of experiments testing the effects of expressing Arl13b variants in *Arl13b^{cond}* MEFs. Statistically significant differences between Arl13b^{WT}-GFP and other variants shown in bold.

function. JS-causing mutations in Arl13b also produced some effects on cilia and Shh signaling, but these were much more modest. The results from the JS-causing variants are perhaps not surprising, given that loss of Arl13b is incompatible with life – any disease-causing mutation is expected be less severe than a total loss-of-function mutation. Meanwhile, the variants that produced defects in transcriptional signaling, Shh-dependent Smo enrichment, and/or migration all tended to phenocopy *Arl13b*^{hnn} MEFs expressing GFP only, suggesting that these mutations, like null mutations of *Arl13b*, would be incompatible with life. Overall, my data represent a step forward in understanding the relationship between Arl13b's structure and function, and how unique protein domains individually regulate multiple functions in protein localization, ciliogenesis, and Shh signaling.

Arl13b variant (hnn MEFs)	Mutation type	GFP in cilia	Cilia number	Cilia length	Smo in cilia	qPCR Shh response	Shh migration
WT-GFP		Yes	Normal	Normal	Normal	Normal	Normal
GFP only	Null	**No**	Normal	**Short**	**Abnormal**	**Reduced**	**Impaired**
R79Q-GFP	JS	Yes	Varied	**Short**	Normal	Normal	Normal
Y86C-GFP	JS	Yes	Normal	**Short**	Normal	Normal	Normal
R200C-GFP	JS	**No**	Normal	**Short**	Normal	Normal	Normal
T35N-GFP	GTPase	Yes	Normal	**Short**	**Abnormal**	**Reduced**	?
G75Q-GFP	GTPase	Yes	Normal	**Short**	Normal	**Reduced**	?
V358A-GFP	CiLS	**No**	Normal	**Shorter**	Normal	Normal	**Impaired**
C8S,C9S-GFP	Palm.	**No**	Normal	**Short**	**Abnormal**	**Reduced**	?

Table 3.4 Summary of results from *Arl13b*^{hnn} MEFs. Results of experiments testing the effects of expressing Arl13b variants in *Arl13hnn*^{d} MEFs. Statistically significant differences between Arl13b^{WT}-GFP and other variants shown in bold.

3.3.1 Dominant effects of Arl13b mutations

This is the first study, to my knowledge, to show dominant effects of Arl13b mutations. JS-causing mutations are recessive and no significant effects have been observed in heterozygous carriers of JS alleles. Other studies that have explored functional consequences of Arl13b variants

have done so in an Arl13b null background (Duldulao et al., 2009) or after knocking down endogenous Arl13b via siRNA (Humbert et al., 2012).

My results from *Arl13b*^{cond} MEFs showed that mutations in Arl13b's palmitoylation site or CiLS had dominant negative effects on cilia length. Arl13b^{C8S,C9S}-GFP also reduced the transcriptional response to Shh in a dominant fashion, but qPCR results were normal for Arl13b^{V358A}-GFP. This suggests that restricting Arl13b from its usual location on the membrane not only prevents it from executing its functions there, but actively inhibits cilia outgrowth and Shh transcriptional induction. The most likely mechanism through which this might occur is competition by mutant Arl13b for binding with Arl13b's typical interaction partners. If mislocalized Arl13b binds and sequesters effectors away from the ciliary membrane, they can no longer perform their functions, even if wild-type Arl13b is still present in the cilium.

Not much is known about Arl13b's effectors or binding partners, but previous work has shown that mutations in Arl13b, including Arl13b^{T35N}, Arl13b^{R79Q} and Arl13b^{R200C}, can alter the cilia localization of INPP5E, a phosphatase that regulates the phosphatidylinositol composition of the cilia membrane (Humbert et al., 2012). A recent study has also shown evidence that Arl13b can act as a guanine nucleotide exchange factor (GEF) for Arl3, a GTPase specifically involved in the trafficking of cargoes like INPP5E to the cilium, and that Arl13b^{R79Q} and Arl13b^{R200C} mutations impair the activation of Arl3 (Gotthardt et al., 2015). It will be interesting to investigate the effects of Arl13b^{C8S,C9S} and Arl13b^{V358A} mutations on INPP5E targeting, although it is likely that these mutants are acting through separate/additional mechanisms than the one described by Humbert and colleagues, as the Arl13b^{T35N} and Arl13b^{R79Q} variants did not produce dominant effects in my assays. In a similar vein, my data showing differential effects of Arl13b mutations across a variety of functional assays suggest that Arl13b – like other GTPases – has multiple independently-regulated functions, including some that may be separate from Arl3 GEF activity.

Arl13b^{R200C}-GFP also produced a dominant effect in *Arl13b*^{cond} MEFs, potentiating the transcriptional response to Shh. Like Arl13b^{C8S,C9S}-GFP and Arl13b^{V358A}-GFP, Arl13b^{R200C}-GFP

fails to localize to cilia in my assays, but it does not have the same effects on cilia length and transcriptional Shh signaling as these other non-ciliary variants. Further complicating the interpretation of this result is the fact that the potentiation of the Shh response seen in Arl13b^{R200C}-GFP *Arl13b^{cond}* MEFs was not observed in *Arl13b^{hnn}* MEFs, although if Arl13b^{R200C}-GFP is working to potentiate the Shh response in a manner independent from wild-type Arl13b, this is perhaps to be expected. Intriguingly, western blotting of lysates from Arl13b^{R200C}-GFP *Arl13b^{hnn}* MEFs (Figure 3.6D) showed a band between 60 and 75 kDa that was much more prominent in this variant than any other cell line. (This band was not observed in Arl13b^{R200C}-GFP *Arl13b^{cond}* MEFs, but Arl13b^{R200C}-GFP was expressed at very low overall levels in this line.) Assuming that the 60 kDa band represents Arl13b from which the GFP tag has been cleaved, this larger Arl13b-reactive band might indicate a unique post-translational modification of Arl13b that is favored by the R200C mutation. If Arl13b^{R200C}-GFP does indeed have some gain-of-function effect on Shh signaling, it may be associated with this apparent size shift.

3.3.2 Variability in transcriptional Shh response may indicate differences in negative feedback

My qPCR experiments showed considerable variability in the Shh response within cell lines from replicate to replicate (Table 1 and Table 2), most of which can likely be attributed to minor differences in experimental conditions from day to day. In replicates in which *Ptch1* showed a particularly robust Shh response across all cell lines, it appeared that elevated *Ptch1* expression after Shh stimulation was causing negative feedback on *Gli1* induction, and that this effect was more pronounced for some Arl13b variants than others. It is not clear why Ptch1-mediated feedback would occur non-uniformly, but it is interesting to note that the apparent negative feedback effect was less pronounced in Arl13b^{C8S,C9S}-GFP and Arl13b^{T35N}-GFP, which also show inappropriately high levels of Smo in cilia even under unstimulated conditions (Figure 3.8). If these Arl13b mutations cause misregulation of the Shh pathway at the level of Smo, it is not surprising that *Ptch1*-mediated feedback, which acts upstream of Smo, would have a

dampened effect. It is less clear why Arl13b^{R79Q}-GFP and Arl13b^{R200C}-GFP would fail to experience feedback. Arl13b^{R200C}-GFP showed an elevated Shh response in *Arl13*^{cond} MEFs, suggesting that it may be capable of stimulating the Shh pathway at higher-than-usual levels, perhaps by reducing the effect of negative feedback. Arl13b^{R79Q}-GFP, meanwhile, appeared relatively normal in all assays of transcriptional Shh signaling, but it is still a disease-causing mutation. Perhaps the R79Q mutation alters the time course of the Shh response in a manner that produces deleterious effects in the integration of Shh signaling over time – temporal components of Shh signaling are critical for normal development (Balaskas et al., 2012; Dessaud et al., 2007; Dessaud et al., 2008), but more difficult to capture when analyzing a single time point after *in vitro* Shh stimulation.

The issue of Shh signaling over time is an important one to consider in interpreting all of my assays. All of my measurements of gene transcription and Smo localization were taken 24 hours after Shh stimulation. Exposure to Shh for as little as 1 hour is sufficient to induce Smo enrichment in cilia, which then continues to accumulate for at least 24 hours (Corbit et al., 2005; Rohatgi et al., 2007). However, as Shh signaling induces negative feedback through the inhibitory proteins Ptch1 and Hhip1 (Ribes and Briscoe, 2009), these factors serve to inhibit Smo and to sequester Shh ligand, both of which over time result in decreased active signaling and thus, less ciliary Smo enrichment. Activated Smo is targeted by β-arrestins for clathrin-mediated endocytosis into recycling endosomes (Chen et al., 2004; Kovacs et al., 2008), a process which facilitates Smo's association with the motor protein Kif3a and potentiates – but is not explicitly required for (Milenkovic et al., 2009) – its cilia localization. It is not clear how Arl13b works to regulate Shh-dependent enrichment of Smo in the cilium. Given the intricate balance of various factors that act in concert to integrate Shh signaling over time, it is not surprising that mutations in Arl13b seem capable of disrupting this balance and perturbing the normal pattern of negative feedback.

3.3.3 Cilia localization of Arl13b is required for only a subset of its functions

One of the more surprising results of this study was the fact that Arl13b variants that do not localize to cilia are still competent to perform many of Arl13b's functions. Arl13b is primarily considered to be a cilia protein, and JS, like other diseases resulting from cilia-related genetic mutations, is considered a ciliopathy. Transcriptional Shh signaling is tightly linked to cilia. And yet, non-ciliary Arl13b^{V358A}-GFP exhibits a normal Shh transcriptional response in both *Arl13b^{cond}* and *Arl13b^{hnn}* MEFs. Meanwhile, in assays of non-transcriptional Shh signaling, Arl13b^{V358A}-GFP MEFs show significant impairment in their Shh response, despite the fact that the cilium itself is not necessary for Shh-dependent cell migration. This suggests distinct roles for Arl13b in transcriptional versus non-transcriptional Shh signaling, one of which requires its CiLS motif and one of which does not. Since the cilium itself is not required for non-transcriptional signaling, it is difficult to understand why Arl13b's CiLS would be required for this process. Perhaps Arl13b must interact with a binding partner that is found only in cilia in order to potentiate non-transcriptional Shh signaling, and Arl13b^{V358A} and this binding partner never encounter each other in ciliated cells. Alternatively, the CiLS in Arl13b may regulate more than just cilia localization: this motif may help Arl13b associate with specialized membrane microdomains, only some of which are found in the cilium. Other signaling domains on the membrane may occur at the leading edge of a fibroblast, where non-transcriptional Shh signals are transduced to produce migration.

Experiments on non-ciliary Arl13b produced other surprising results as well: Arl13b^{V358A}-GFP MEFs showed slightly elevated transcriptional Shh signaling at baseline. These results were not statistically significant after correction for multiple comparisons between many Arl13b variants, but they seem to describe a real trend that is consistent across *Arl13b^{cond}* and *Arl13b^{hnn}* MEFs. These results suggest that Arl13b^{V358A}-GFP may disrupt processes outside of cilia that normally inhibit the production of GliA in the absence of Shh. Alternatively, the CiLS mutation may interfere with the production of GliR. This elevated baseline signaling was not seen

in GFP-only *Arl13b*^{hnn} MEFs, implying that it arises from a gain of function in Arl13b^{V358A}-GFP. However, *Arl13b*^{hnn} embryos show an expansion of ventrolateral cell fates in the caudal neural tube, consistent with low-level ligand-independent activation of transcriptional Shh signaling (Caspary et al., 2007). It may be that low-level activation of the Shh pathway at baseline also occurs in *Arl13b*^{hnn} MEFs, but some compensatory mechanism adjusts the balance of signaling, leaving me unable to detect it in qPCR assays. (It is clear that not all *Arl13b* null cells experience severe signs of misregulated basal Shh signaling, because the rostral neural tube of *Arl13b*^{hnn} embryos appears relatively normal in terms of patterning.) If Arl13b^{V358A}-GFP cells are particularly impaired in their ability to compensate for misregulated ligand-independent signaling, that would explain their behavior in my qPCR assays.

The interpretation of the results of my experiments on Arl13b^{V358A}-GFP are complicated by the fact that the exact mechanism of Arl13b's ciliary targeting is not known. The RVxPx CiLS motif in Arl13b is similar to motifs used by other proteins, including rhodopsin, polycystin-1, and polycystin-2, for ciliary targeting (Deretic et al., 1998; Geng et al., 2006). In these proteins, the CiLS motif is required for the formation of a protein complex at the trans-Golgi network (TGN) destined for traffic to cilia. The VxPx motifs of rhodopsin and polycystin-1 are required for their association with Arf4, which in the case of rhodopsin and polycystin-1 forms a complex along with Rab11 and the Arf GAP ASAP1 at the TGN (Mazelova et al., 2009; Wang et al., 2012; Ward et al. 2011). Polycystin-2 is thought to traffic to cilia by a different route, but its VxPx motif is still capable of binding Arf4, and in most cases it traffics in a complex with polycystin-1 (Geng et al., 2006; Köttgen and Walz, 2005). It will be interesting to test whether Arl13b uses a similar mechanism for targeting to cilia from the TGN, and whether binding partners specific to the Arl13b CiLS are also involved in its noncanical Shh signaling functions.

3.3.4 Summary and Future Directions

Taken together, my experiments on the functional consequences of Arl13b mutations in different protein domains lay an important foundation for testing hypotheses about the overall mechanism of Arl13b's regulation of cilia formation and Shh signaling. Arl13b mutations in different domains affect different subsets of functions: Arl13b^{V358A} disrupts non-transcriptional Shh signaling, elevates baseline transcriptional Shh signaling, and leaves the transcriptional response to Shh ligand intact; both Arl13b^{T35N} and Arl13b^{G75Q} reduce the transcriptional response to Shh but only Arl13b^{T35N} affects Shh-dependent enrichment of Smo in cilia; Arl13b^{C8S,C9S} produces dominant effects on both cilia length and Shh signaling; no Arl13b variant examined in my studies was able to rescue the cilia length defect in *Arl13b^{hnn}* MEFs. Thus, each mutant cell line that I created represents a new tool to better understand the mechanisms through which Arl13b regulates these distinct cellular processes.

A logical next step in this research is to continue the analysis of non-transcriptional Shh signaling by testing Shh-dependent migration in the rest of my Arl13b variants, and we have plans to do so. Also, in addition to the cell lines analyzed here, I have already generated more cell lines in which MEFs of varying genetic backgrounds express wild-type or mutant Arl13b-GFP. *Arl13b^{hnn};Ift172^{wimple}* MEFs, which lack cilia altogether, can be used to test whether cells without cilia, which normally are capable of Shh-dependent migration, can still respond to this cue if Arl13b is disrupted. I also generated cell lines expressing a mutant Smo protein that cannot localize to cilia, to test whether Arl13b plays a role in regulating Smo trafficking and/or activation outside of the cilium. Ongoing work in the Caspary lab and through collaborations that I established will use these tools to further investigate the discrete functions of Arl13b in Shh signaling.

Chapter 4

Arl13b and Shh-dependent axon guidance: a model for Joubert Syndrome

4.1 Introduction

In addition to its well-defined roles as a mitogen and a morphogen, Shh can act through non-transcriptional pathways to regulate the cytoskeletal remodeling that occurs during axon guidance. Shh was first shown to function as an axon guidance cue in commissural neurons of the developing spinal cord (Charron et al., 2003), where it has chemoattractive and chemorepulsive effects at different developmental time points (Bourikas et al., 2005; Wilson and Stoeckli, 2013). Shh also serves as an axon guidance cue at the optic chiasm (Fabre et al., 2010) and in the enteric nervous system (Jin et al., 2015). With the exception of post-crossing commissural neurons, which cease to express Smo, studies of Shh-dependent axon guidance all confirm that Smo is essential for this process. Downstream of Smo, Src family kinases are responsible for mediating cytoskeletal rearrangements required for growth cone turning in commissural neurons (Yam et al., 2009). In the enteric nervous system, Shh-dependent chemorepulsion downstream of Gas1 signals through the Smo-coupled Gαi protein Gnaz (Jin et al., 2015). While all of these data emphasize the importance of Smo signaling locally at the growth cone, the mechanism regulating the trafficking and activation of Smo in axons is not yet known.

The human ciliopathy Joubert Syndrome (JS) is defined by a constellation of neuroanatomical features called the molar tooth sign (MTS) that includes axon guidance defects. Currently, little is known about the molecular etiology of axon guidance defects in JS. It is not known whether Shh-dependent axon guidance regulates development of the affected white matter tracts, but several lines of evidence suggest that Shh may contribute to the characteristic hindbrain malformations in JS. Other JS phenotypes, including cerebellar hypoplasia, craniofacial abnormalities, and polydactyly, are related to abnormal Shh signaling. Furthermore, the products of many JS-associated genes, including *ARL13B*, *KIF7*, *RPGRIPL1*, *TCTN1*, and *TCTN2*,

regulate Shh signaling (Caspary et al., 2007; Cheung et al., 2009; Endoh-Yamagami et al., 2009; Liem et al., 2009; Reiter and Skarnes, 2006; Vierkotten et al., 2007).

Because Arl13b has been established as a regulator of Shh signaling, I was interested in whether it might play a role in regulating Shh-dependent axon guidance, and whether disruption of Arl13b-dependent Shh signal transduction in axons might explain the axon guidance phenotypes in JS patients. I tested whether loss of Arl13b in hindbrain projection neurons produces axon guidance phenotypes consistent with JS, and whether these phenotypes can be recapitulated by deleting *Smo* in the same cells. Working in collaboration with the Charron lab, I also tested whether perturbing Arl13b in neurons known to use Shh as a guidance cue produced axonal defects comparable to those caused by mutations in Shh pathway components.

4.2 Results

4.2.1 Arl13b regulates axon guidance in neurons associated with JS phenotypes

4.2.1.1 Loss of Arl13b causes abnormal hindbrain development

When I began my investigation of Arl13b's role as a potential axon guidance cue, preliminary data had already suggested *Arl13b* mutant mice could serve as a model for JS. The Caspary lab previously showed that pan-neuronal loss of Arl13b early in brain development in *Arl13b*$^{flox/flox}$*;Brn4-Cre* (*Arl13b*$^{\Delta Brn4}$) mice causes cerebellar hypoplasia, a key feature of the MTS (Figure 4.1A-B). This likely occurs through misregulation of Shh-dependent proliferation in the developing cerebellum. Furthermore, a previous study focusing on neuronal migration (Higginbotham et al., 2012) done in collaboration with Eva Anton's lab had indicated some abnormalities in axon guidance in *Arl13b*$^{flox/flox}$*;NEX-Cre* (*Arl13b*$^{\Delta NEX}$) mice, which lose Arl13b in all projection neurons.

I continued to collaborate with the Anton lab to investigate Arl13b-dependent axon guidance in hindbrain white matter tracts. To test whether Arl13b regulates normal hindbrain

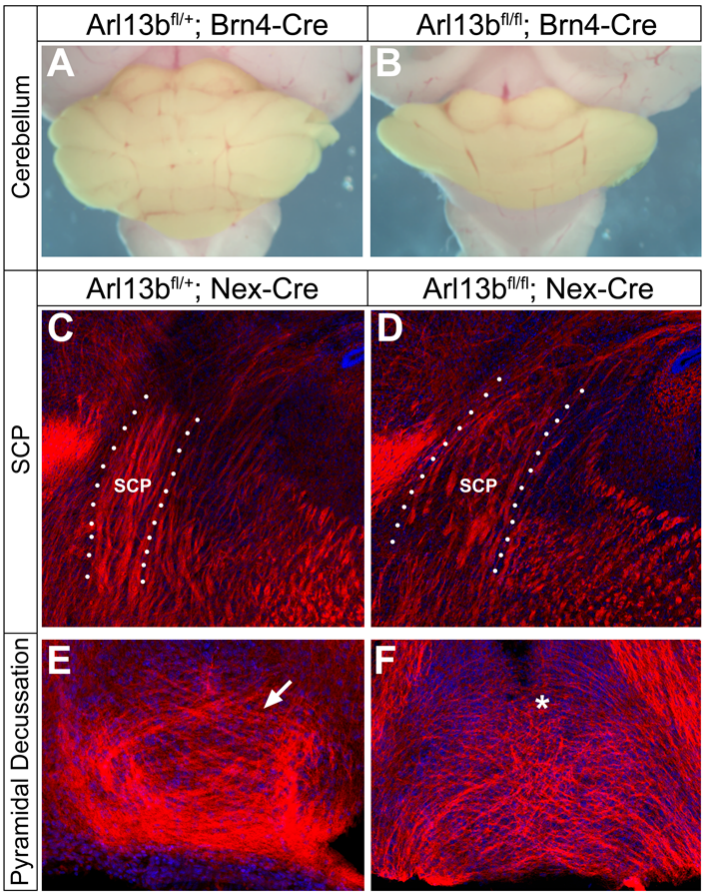

Figure 4.1 Deletion of Arl13b causes hindbrain phenotypes consistent with JS. **A-B** Pan-neuronal deletion of *Arl13b* by Brn4-Cre causes cerebellar hypoplasia relative to control brain at p21. Yellow highlights cerebellar tissue**. C-F** Effects of deletion of *Arl13b* in projection neurons by NEX-Cre on the superior cerebellar peduncle (SCP) and corticospinal tract at the pyramidal decussation (arrow, asterisk) at p7. Red, L1 antibody; blue, DAPI.

development, we analyzed hindbrain white matter tracts in *Arl13b*$^{\Delta NEX}$ mice at several developmental stages. At p7, *Arl13b*$^{\Delta NEX}$ mice compared to *Arl13b*$^{flox/+}$*;NEX-Cre* controls showed abnormal thickening and disorganization of the superior cerebellar peduncle (SCP; Figure 4.1C-D) and disorganization of midline crossing fibers at the pyramidal decussation of the corticospinal tract (Figure 4.1E-F). These phenotypes are consistent with the MTS and other axon guidance defects previously reported in JS patients.

I next analyzed the same tracts adult *Arl13b*$^{\Delta NEX}$ mice. For ease of histological imaging, I also crossed the *Arl13b*$^{\Delta NEX}$ mice with mice carrying *mTau-GFP* Cre reporter allele, which drives

the expression of GFP specifically in the axons of cells that have undergone Cre-lox recombination. In adult *Arl13b*$^{\Delta NEX}$; *mTau-GFP* mice and *Arl13b*$^{flox/+;}$*NEX-Cre;mTau-GFP* controls, the SCP appears as a somewhat darker axon tract against a background of bright green. (Although neurons in the DCN whose axons form the SCP should be Cre-positive in these mice, axons from other cells also expressing NEX-Cre, such as cortical projection neurons, seem to create high GFP background signal in the hindbrain.) Anecdotally, controls seemed to show higher GFP background fluorescence in the hindbrain than *Arl13b*$^{\Delta NEX}$ animals. However,

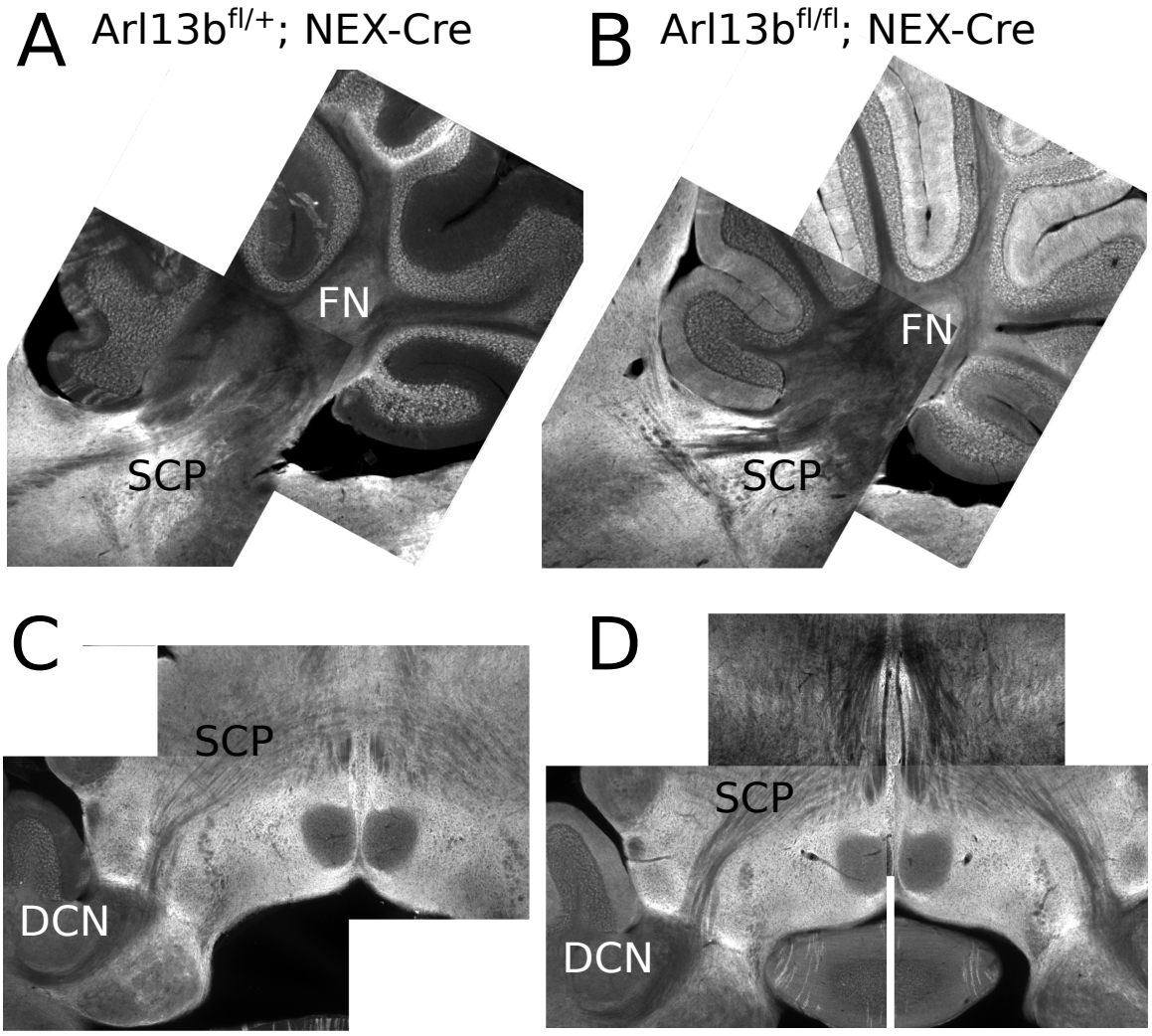

Figure 4.2 Histological staining of control and *Arl13b*$^{\Delta NEX}$ brains. A-B Sagittal and C-D horizontal sections through control (left) and *Arl13b*$^{\Delta NEX}$ brains expression mTau-GFP in Cre-positive axons. SCP, superior cerebellar peduncle; DCN, deep cerebellar nuclei; FN, fastigial nucleus (of DCN).

anatomical differences in the SCPs between the two groups were not readily apparent by histological staining, and did not seem to recapitulate the phenotypes observed in p7 pups. From this I concluded that, unlike human JS, in which the MTS persists throughout life, *Arl13b*$^{\Delta NEX}$ seems to cause a developmental delay or temporary abnormality in the anatomy of large hindbrain white matter tracts that is largely rectified by adulthood. Still, I was curious whether any abnormalities in the SCP might persist in *Arl13b*$^{\Delta NEX}$ mice, and moved on to other methods of analysis to determine whether these tracts contained finer anatomical abnormalities that are more difficult to detect by histology.

4.2.1.2 Loss of Arl13b or Smo causes anatomical changes in the SCP as measured by DTI

To determine whether the SCP might exhibit more subtle anatomical changes in adult *Arl13b*$^{\Delta NEX}$ mice, I developed an *ex vivo* mouse brain imaging protocol in collaboration with Sarah Suciu and the Emory/Georgia Tech Biomedical Imaging Technology Center. After some optimization, we were able to resolve voxels of approximately 0.16 × 0.16 × 0.16 mm in size using T1-weighted magnetic resonance imaging (MRI) as well as diffusion tensor imaging (DTI) with 6 diffusion gradient directions. MRI produces images of anatomical structure, while DTI allows us to determine the principal diffusion direction in which white matter tracts travel and to use fractional anisotropy (FA) to roughly estimate their integrity. Use of DTI in JS patients has revealed a complete loss of midline crossing fibers in the SCP and corticospinal tract (Hsu et al., 2015; Poretti et al., 2007; Poretti et al., 2013). Therefore, we investigated midline crossing in the SCPs of *Arl13b*$^{\Delta NEX}$ mice and controls to see whether their phenotypes mirrored those seen in humans with *ARL13B* mutations. We also looked at *Smo*$^{\Delta NEX}$ mice to see whether specifically ablating Shh signaling in the neurons that give rise to the SCP produced phenotypes consistent with *Arl13b*$^{\Delta NEX}$ mice.

Similar to traditional histological methods, *ex vivo* imaging revealed no obvious differences between control, *Arl13b*$^{\Delta NEX}$, and *Smo*$^{\Delta NEX}$ mice in the T1 anatomical scans (Figure

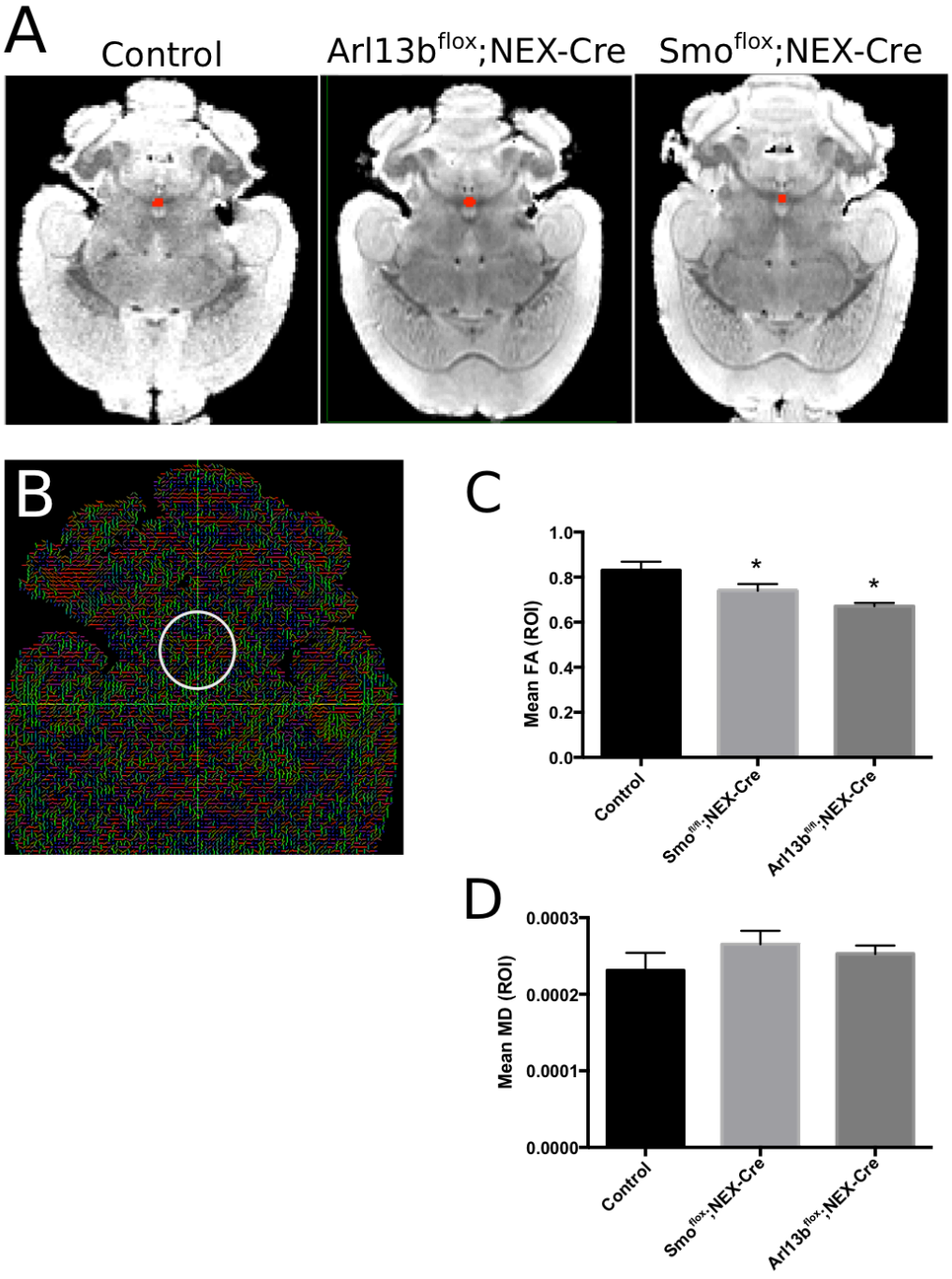

Figure 4.3 Diffusion tensor imaging of SCP. **A** Representative horizontal T1 scans of control, *Arl13b*$^{\Delta NEX}$ and *Smo*$^{\Delta NEX}$ brains. ROI for analysis highlighted in red. **B** Example of DTI data. Lines indicate primary direction determined for each voxel. Red, left-right; green, anterior-posterior; blue, inferior-superior. Left-right voxels within white circle show SCP midline crossing ROI. **C** Mean FA values within the SCP midline crossing ROI; n = 3 for each genotype. Asterisk, significant difference from Control. **D** Mean MD values within the SCP midline crossing ROI; n = 3 for each genotype. (ROI analysis by Sarah Suciu)

4.3A). In all cases, the SCPs were clearly visible and the midline region contained voxels with a left-right principal diffusion direction, consistent with decussating fibers (Figure 4.3B). This type of analysis does not capture all of the DTI information, however. The principal diffusion direction is determined by weighting the degree of diffusivity in each of the directions measured (left-right, anterior-posterior, inferior-superior) and determining which one has the largest FA value. Using this method, any differences in magnitude of the FA value of the principal direction are lost. Because a single voxel contains multiple axons, a voxel may have a very high FA value in its principal direction, indicating that it contains white matter tracts of strong integrity that all travel in a single direction, or a lower FA value, indicating that it may contain tracts traveling in directions other than the primary one and/or tracts of reduced integrity. Therefore, we defined a region of interest (ROI) at the midline of the SCP and measured the average FA values of all voxels in that ROI for each brain. (ROI analysis was done in collaboration with Sarah Suciu, who hand-selected each voxel in the ROIs.)

Analysis of FA in the SCP midline ROI revealed that both $Arl13b^{\Delta NEX}$ (mean = 0.67 ± 0.01) and $Smo^{\Delta NEX}$ mice (mean = 0.74 ± 0.03) have lower average FA values than controls (mean = 0.83 ± 0.02) in this region (Figure 4.3C). The changes in FA in $Arl13b^{\Delta NEX}$ versus $Smo^{\Delta NEX}$ were not significantly different from each other, suggesting that they may arise from a common mechanism. We also analyzed mean diffusivity (MD), a measurement of the free diffusion of water in each voxel. A decrease in FA could arise from two possible mechanisms: increased anisotropy in the non-principal direction (e.g., more axons perpendicular or oblique to the main tract), or 2) decreased anisotropy in the principal direction (e.g., fewer axons and/or less myelin, meaning that water diffusion is overall not as constrained). MD values help differentiate between the two. We found that mean MD in the ROI was not significantly different between $Arl13b^{\Delta NEX}$, $Smo^{\Delta NEX}$, and controls, indicating that the changes in FA we observed are unlikely to arise from changes in the overall number of axons in the ROI, or the myelination or integrity of the axons.

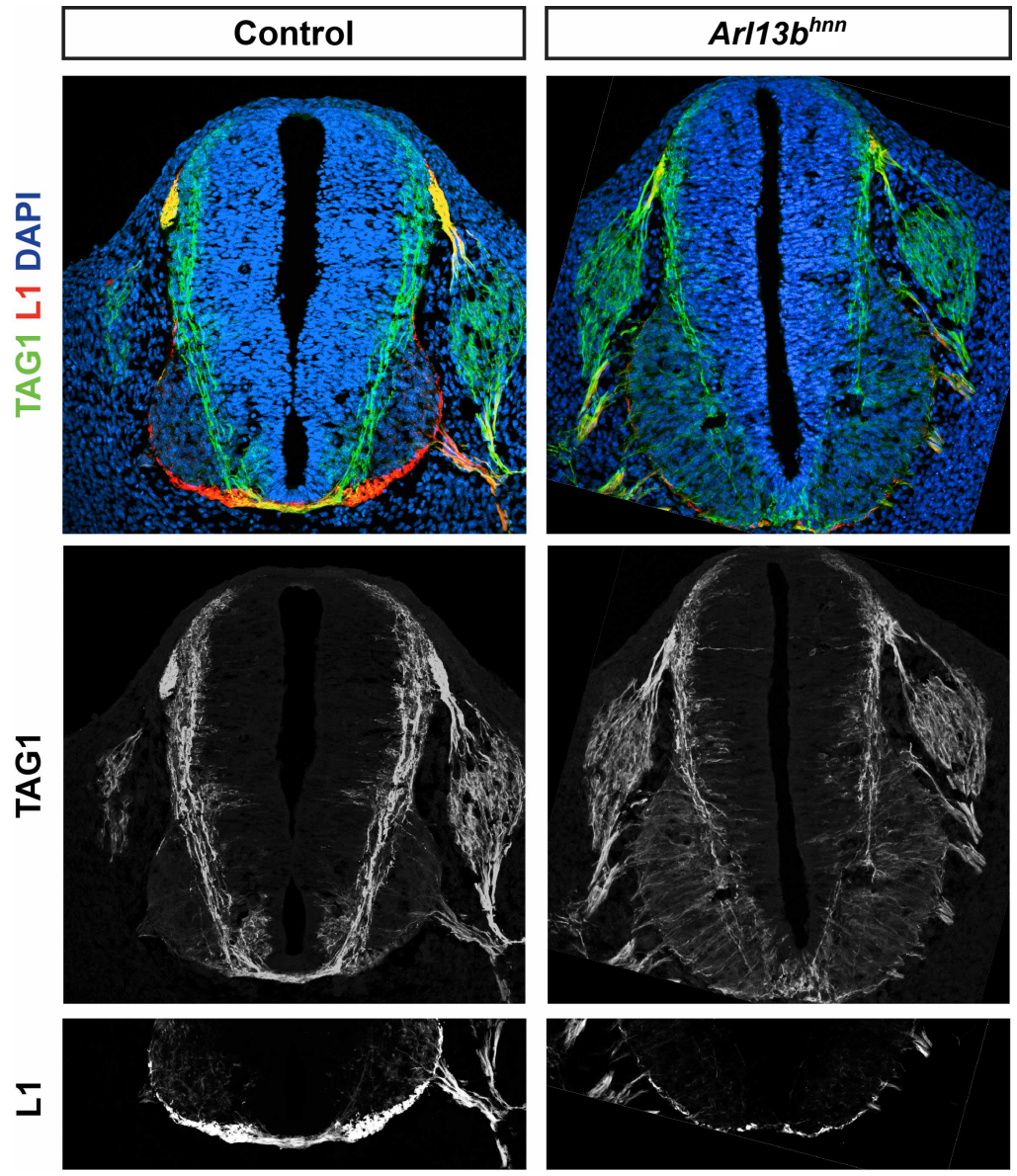

Figure 4.4 Effects of Arl13b mutation on spinal commissural neuron development. Pre-midline-crossing (TAG1) and post-midline-crossing (L1) commissural axons in control (left) or *Arl13b*^{hnn} (right) littermates. (Immunofluorescence staining and fluorescent microscopy by Julien Ferent.)

Instead, it is likely that the mutant mice have more axons that wander from the principal direction of the decussating portion SCP.

4.2.2 Arl13b regulates axon development in neurons that use Shh as a guidance cue

4.2.2.1 Arl13b regulates spinal commissural neuron axon guidance in vivo

Shh regulates the guidance of spinal commissural neuron axons across the midline, which occurs by e11.5 in the mouse. *Arl13b*^{hnn} embryos survive until e13.5, so I worked in collaboration with Julien Ferent from the Charron lab to analyze axon guidance in these neurons. I predicted that if Arl13b regulates Shh-dependent axon guidance, these neurons would show a phenotype reminiscent of the commissural axon guidance defects seen in embryos lacking Smo or the Shh receptors Boc and Cdo (Okada et al., 2006).

Analysis of the *Arl13b*^{hnn} embryos revealed that indeed, there are guidance defects in the commissural axons (Figure 4.4). TAG1-positive pre-crossing fibers fail to form orderly tracts and seem to inappropriately invade the motor neuron domain (a domain which is expanded in *Arl13b*^{hnn}; Caspary et al., 2007). Additionally, we observed very few L1-positive post-crossing axons. Importantly, these axon guidance phenotypes are seen in both the caudal neural tube, where *Arl13b*^{hnn} embryos exhibit the most severe neural patterning defects, and rostral neural tube, where *Arl13b*^{hnn} neural patterning defects are less pronounced.

4.2.2.2 Loss or knockdown of Arl13b potentiates spinal commissural neuron axon outgrowth

Because the complete loss of Arl13b protein in *Arl13b*^{hnn} embryos may have non-cell-autonomous effects on Shh-dependent axon guidance, I wanted to develop an *in vitro* system to look specifically at cell-autonomous effects. Working in collaboration with Julien Ferent, I developed several candidate shRNA constructs (details in 2.2.6) to knock down *Arl13b* in cultured rat spinal commissural neurons. Work to test the effects of Arl13b knockdown on Shh-specific axon turning in these cells is ongoing. In the process of developing the protocols for

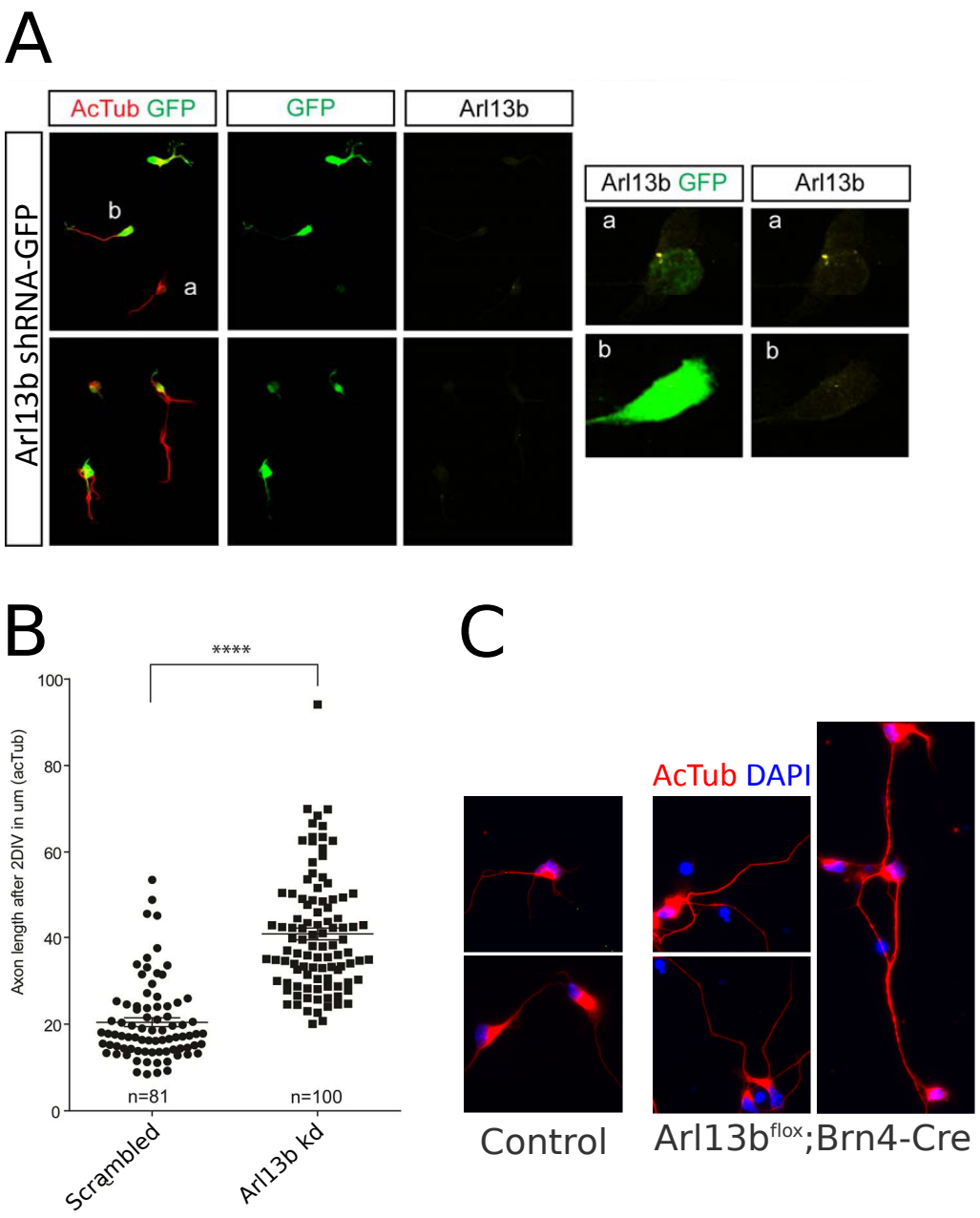

Figure 4.5 Arl13b knockdown or deletion in cultured spinal commissural neurons. **A** Expression of a GFP-tagged construct containing shRNA against rat *Arl13b* in rat spinal commissural neurons. Acetylated α tubulin (AcTub) staining shows neurites and cilia. Staining for Arl13b in cilium of an untransfected neuron (a) and a transfected neuron (b) shows knockdown. **B** Quantification of axon length in rat neurons transfected with scrambled or Arl13b shRNA. (Rat neuron culture experiments by Julien Ferent.) **C** Representative images of dissociated mouse spinal commissural neurons from control or *Arl13b*$^{flox/flox}$*;Brn4-Cre* mice show differences in axon outgrowth. AcTub, acetylated α tubulin (labeling neurites).

these experiments, we noticed that reducing or ablating Arl13b in spinal cord commissural neurons seems to potentiate axon outgrowth. Julien Ferent quantified this effect in rat neurons (Figure 4.5A-B), which I confirmed anecdotally by examining spinal commissural neurons cultured from Arl13b null mouse neurons (*Arl13b*$^{flox/flox}$*;Brn4-Cre*) and their control littermates (Figure 4.5C). In either species, neurons lacking Arl13b grew longer axons (defined at 2DIV as the longest neurite labeled by acetylated α tubulin). These data show that loss of Arl13b does produce cell-autonomous abnormalities in axonal development.

4.3 Discussion

In this chapter, I used a variety of methods to test the effects of Arl13b and/or Smo mutations on Shh-dependent axon guidance, and to determine whether Shh-dependent axon guidance defects may play a role in JS etiology. I found that Arl13b regulates axon guidance in neurons implicated in JS and in neurons known to use Shh as a guidance cue, but the phenotypes I measured do not perfectly recapitulate either human JS features or previously-defined Shh-dependent axon guidance defects. These results are consistent with the hypothesis that Arl13b regulates the development of white matter tracts by affecting non-transcriptional Shh signaling, but they also suggest that Arl13b may regulate axonal development through additional Shh-independent mechanisms.

4.3.1 Abnormal white matter tracts in Arl13b *and* Smo *mutants*

Juvenile *Arl13b*$^{\Delta NEX}$ mice exhibit abnormal development of both the SCP and the corticospinal tract, consistent with phenotypes observed in JS patients (Figure 4.1). However, these phenotypes are much less obvious in adult animals (Figure 4.2). It is unclear why this change over time occurs, but it may be that axons are responding to different guidance cues at different developmental periods, and Shh-dependent guidance and/or other guidance mechanisms perturbed in *Arl13b*$^{\Delta NEX}$ mice are less important later in development.

Analysis of adult mice found significantly lower average FA values in the midline region of the SCP in both *Arl13b*$^{\Delta NEX}$ and *Smo*$^{\Delta NEX}$ mice (Figure 4.3), consistent with the model that Arl13b regulates Shh-dependent axon guidance in these neurons, and that abnormal Shh-dependent axon guidance may contribute to white matter phenotypes in human JS. Future experiments will investigate the same ROI in *Arl13b*$^{\Delta NEX}$*;Smo*$^{\Delta NEX}$ double deletion mice to determine whether the loss of Arl13b and the loss of Shh signaling produce an additive effect on axon guidance defects, or whether these two proteins appear to lie in the same pathway.

A decrease in FA may result from either increased diffusivity perpendicular to the principal direction and/or reduced diffusivity parallel to the principal direction, with a variety of different possible explanations for why these changes have occurred (Alexander et al., 2007). If *Arl13b*$^{\Delta NEX}$ fiber tracts recapitulate the defects seen in JS patients, their midline crossing should be misguided, resulting in more axons traveling diagonal or perpendicular to the left-right direction in each voxel. JS SCPs are also thicker than those of average patients, so the decrease in *Arl13b*$^{\Delta NEX}$ FA value might also be interpreted as an indication that axons are less tightly fasciculated – fewer axons per voxel would reduce FA, even if all axons are traveling in the same direction. However, the same FA phenotype could be explained by other changes, such as defects in myelination. Indeed, while changes in FA affect *Arl13b*$^{\Delta NEX}$ and *Smo*$^{\Delta NEX}$ animals to a similar degree, suggesting that the white matter abnormalities between these groups share a common etiology, it is possible that the observed changes arise through distinct mechanisms in each genotype. However, analysis of MD shows that control, *Arl13b*$^{\Delta NEX}$ and *Smo*$^{\Delta NEX}$ mice all experience roughly the same mean diffusivity in the midline region of the SCP, suggesting that their differences in FA are not likely to arise from a reduction in the overall number of axons or axonal integrity. Future studies will be needed compare FA values from other white matter tracts in these brains to determine whether the defect is specific to midline crossing fibers, to the hindbrain, to regions associated with JS symptoms, or whether it reflects a more general defect in white matter development.

In any case, neither *Arl13b*$^{\Delta NEX}$ nor *Smo*$^{\Delta NEX}$ mice exhibited axon guidance phenotypes as severe as those observed in JS patients. When considering the implication of these results on our understanding of JS axon guidance phenotype etiology, it is important to note that the conditional deletion of *Arl13b* or *Smo* requires the NEX promoter to initiate Cre-lox recombination and for Arl13b or Smo protein to turn over completely in order for neurons to become functionally null for these proteins. The technical limitations of this method may leave residual Arl13b or Smo protein in the projection neurons as they are being guided toward their targets, limiting the effect of the deletion.

Furthermore, even if the conditional deletion works perfectly, *Arl13b*$^{\Delta NEX}$ and *Smo*$^{\Delta NEX}$ mice are only expected to exhibit cell-autonomous axon guidance defects. In JS patients, both the developing axons themselves and the territories through which they project are affected by the JS-causing mutation in *ARL13B* or other cilia genes. Perhaps abnormal development of other cell types in the hindbrain exacerbates the axon guidance phenotype in the projection neurons of JS patients. For example, if JS-causing mutations in humans act similarly to Arl13b mutations in mice, the source of Shh ligand guiding hindbrain axons may be disrupted. *Arl13b*^{hnn} embryos fail to specify the floor plate, which serves as a source of Shh ligand throughout the developing nervous system and is known to be involved in DCN axon guidance (Kim and Ackerman, 2011; Shirasaki et al., 1995). While there's no evidence to suggest that JS patients experience such a severe neural patterning phenotype, they may experience more subtle developmental abnormalities that disrupt important axon guidance cues. For example, mutations in the cilia-associated transcription factor *Rfx3* as well as the JS-causing gene *Inpp5e* cause identical abnormal guidance of thalamocortical axons, suggesting that many cilia gene products may act in concert to regulate neural patterning and axon guidance in a variety of brain regions (Magnani et al., 2015). The degree to which these neurodevelopmental defects may be Shh-dependent remains to be determined.

4.3.2 Loss of Arl13b alters guidance and outgrowth in spinal commissural neuron axons

An interaction between cell-autonomous and non-cell-autonomous mechanisms may also explain why *Arl13b*^{hnn} embryos exhibited more noticeable axon guidance phenotypes than *Arl13b*$^{\Delta NEX}$ mice (Figure 4.4). In *Arl13b*^{hnn} embryos, changes in neural patterning and particularly in the distribution of Shh ligand may contribute to the guidance defect we observed in spinal commissural neuron axons. In the caudal neural tube, *Arl13b*^{hnn} embryos fail to specify the floor plate, a primary source of Shh ligand at the midline. This could certainly cause non-cell-autonomous guidance defects in Shh-sensitive axons. However, a Shh-positive floor plate *is* observed in the rostral neural tube of *Arl13b*^{hnn} embryos, yet commissural axon guidance defects still occur in this region. Therefore, while non-cell-autonomous changes in the surrounding environment may contribute to abnormal axon guidance in *Arl13b*^{hnn} embryos, they do not seem to fully explain the phenotype. To better dissect the cell-autonomous and non-cell-autonomous aspects of abnormal commissural axon guidance *in vivo*, it will be necessary to analyze the effect of conditional deletion of *Arl13b* specifically in the spinal commissural neurons. Experiments using Wnt1-Cre for this purpose are ongoing in the Caspary lab.

In addition to conditional deletion experiments, ongoing *in vitro* studies will better elucidate the relationship between Arl13b and Shh-dependent axon guidance. While those experiments are still in progress, we have already detected axon outgrowth abnormalities in Arl13b-deficient cultured spinal commissural neurons (Figure 4.5). The mechanism underlying this phenotype is not clear, but it seems to exemplify the intricate relationship between developing axons and the centrosome, which serves as the microtubule organizing center of the cell and also happens to be situated at the base of the primary cilium (reviewed in Higginbotham and Gleeson, 2007). Given their defects in cilia, Arl13b-deficient neurons may experience more general misregulation of signaling pathways that regulate cell polarity and axon outgrowth, like the Par3-Par6-APKC pathway (Shi et al., 2004), which has also been implicated in ciliogenesis (Sfakianos et al., 2007).

Alternatively, loss of Arl13b may lead to abnormal regulation of PI3K signaling at the growth cone, thereby potentiating axon outgrowth. It is known that PI3K signaling potentiates axon outgrowth, and a balance between kinase and phosphatase activity at the growth cone regulates neurite outgrowth (Ooms et al., 2006). Arl13b and other cilia proteins have been shown to regulate PP2A, a phosphatase that opposes the activity of PI3K by dephosphorylating Akt at the basal body of the cilium (Umberger and Caspary, 2015). Furthermore, Arl13b regulates INPP5E, a phosphatidyl inositol polyphosphatase that dephosphoylates the $PI(3,4,5)P_3$ produced by PI3K (Gotthardt et al., 2015; Humbert et al., 2012). It may be that loss of Arl13b disrupts these or other phosphatases at the growth cone, thus removing the usual brake on PI3K-mediated axon outgrowth.

4.3.3 Summary and future directions

Taken together, my studies on the role of Arl13b in regulating Shh-dependent axon guidance have identified a novel mechanism through which JS-causing mutations in *ARL13B* may contribute to disease phenotypes. My data are consistent with a model in which Arl13b regulates axon outgrowth and proper guidance of Shh-dependent white matter tracts, and suggest that this process is disrupted in the white matter of JS patients. Ongoing research in the Caspary lab and through collaborations that I established will continue to investigate this model from a variety of angles. For instance, although my data show that $Arl13b^{\Delta NEX}$ and $Smo^{\Delta NEX}$ mice have anatomical abnormalities at the midline region of the SCP, additional experiments using unilateral tract tracing will be performed to test whether these defects truly reflect a reduced number of fibers crossing the midline. Furthermore, while the data presented here have shown that loss of Arl13b produces cell-autonomous defects in spinal commissural neuron axons, future experiments are required to specifically examine the response of these neurons to Shh cues. Finally, although these studies are designed to elucidate the etiology of JS, all experiments thus far have centered on Arl13b null neurons. Future work will investigate axon guidance phenotypes in neurons

expressing Arl13b variants – the Caspary lab has used CRISPR-Cas9 gene targeting to generate mice with the JS-causing Arl13b^{R79Q} mutation, as well as mice with a mutation in the Arl13b CiLS.

Chapter 5

Perspectives

This dissertation has focused on exploring how Arl13b regulates Shh signaling through multiple mechanisms and distinct functional domains, and how *Arl13b* mutations may contribute to the white matter defects in JS through misregulation of Shh signaling. In this chapter, the implications of my results are discussed in context with other research in related fields.

5.1 Ciliary and non-ciliary Arl13b regulates Shh signaling through distinct mechanisms

My experiments in Chapter 3 showed that various mutations in *Arl13b* can disrupt both transcriptional and non-transcriptional Shh signaling, and that some of these mutations restrict Arl13b from localizing to cilia, with variable effects on its function. These data suggest that Arl13b acts to regulate Shh signaling through multiple mechanisms both within and outside of the cilium, but provide little insight into the nature of those mechanisms. My results must therefore be integrated with previous research on Arl13b's functions in cilia and Shh signaling.

Recent studies have shown that Arl13b is involved in the Arl3-dependent ciliary targeting of INPP5E via PDE6D (Gotthardt et al., 2015; Humbert et al., 2012), which in turn controls transcriptional Shh signaling by regulating the recruitment of Tulp3 and Gpr161 to the ciliary membrane (Chávez et al., 2015; Pal et al., 2016). Importantly, mutations in *INPP5E* and *PDE6D* have also been linked to JS (Bielas et al., 2009; Thomas et al., 2014), suggesting that misregulation of any member of this pathway may lead to similar disease phenotypes. My data predict that different Arl13b variants will have distinct effects on this pathway, given the variable effects on Shh signaling I observed in my Arl13b mutant cell lines. Humbert and colleagues previously showed that JS-causing mutations in *Arl13b* disrupt INPP5E trafficking to cilia, but the same Arl13b variants did not produce significant effects on Shh signaling in many of my assays. Future experiments could investigate INPP5E trafficking in my Arl13b variant cell lines

and examine the relationship between the severity of INPP5E-related phenotypes and the disruption of Shh signaling in different experimental systems.

Furthermore, my data suggest that there may be Arl13b functions not described by the Arl13b→Arl3→PDE6D→INPP5E→Tulp3/Gpr161 model. Non-transcriptional Shh signaling, as measured by Shh-dependent fibroblast migration, is disrupted in MEFs expressing Arl13b^{V358A}-GFP, but transcriptional Shh signaling in these cells is relatively intact, albeit slightly elevated at baseline. There is currently no evidence to suggest that Arl3, INPP5E, Tulp3, and/or Gpr161 are involved in non-transcriptional Shh signaling. Importantly, all previous work on the Arl13b→Arl3→PDE6D→INPP5E→Tulp3/Gpr161 model has emphasized the spatially restricted nature of these proteins, most of which are highly enriched in the primary cilium, whereas my data on Arl13b^{V358A} suggest that keeping Arl13b out of cilia spares some of its functions in regulating Shh signaling. Future experiments should explore whether any/all of the proteins implicated in Arl13b's regulating of ciliary protein targeting and transcriptional Shh signaling are acting similarly in the non-transcriptional arm of the pathway, or whether Arl13b acts through an independent mechanism in this process.

Ongoing research in the Caspary lab on INPP5E has produced models in which Arl13b and INPP5E may regulate Shh signaling independently of Tulp3/Gpr161. The Caspary lab generated a novel allele of *INPP5E*, *INPP5E^{M2}*, through a forward genetic screen. *INPP5E^{M2}* embryos, similar to *Arl13b^{hnn}* embryos, show signs of misregulated Shh signaling that fails to reach its highest levels in the most ventral region of the neural tube. This is not only consistent with a model in which INPP5E is an important Arl13b effector for regulating Shh signaling, but is an expected consequence of increased Gpr161 localization to cilia, as Gpr161 normally acts as a negative regulator of Shh signaling. However, just like *Arl13b^{hnn}* embryos, *INPP5E^{M2}* embryos show an expansion of Shh-dependent neuronal precursors in the ventral neural tube that is indicative of constitutively active transcriptional Shh signaling. It is unclear how increased ciliary Gpr161 could explain this phenotype. Future experiments will investigate whether ciliary

membrane proteins that create permissive conditions for Shh signaling are also regulated by INPP5E, thereby providing a model for how Arl13b and its putative effector seem to both upregulate and downregulate transcriptional Shh signaling when perturbed in developing embryos.

Possible Shh-permissive regulatory targets of INPP5E include TRPC1 channels and IP_3 receptors, which are required for the Ca^{2+} signaling that occurs downstream of Shh ligand binding in the neural tube (Belgacem and Borodinsky, 2011). In addition, as a regulator of phosphatidyl inositol polyphosphates in the ciliary membrane, INPP5E may indirectly control the production of IP_3 from $PI(4,5)P_2$ by phospholipase C that potentiates this signaling cascade. It will be interesting to test this model in my Arl13b variant cell lines and compare/contrast with phenotypes seen in *INPP5E*^{M2} cells. Such experiments will show whether abnormal IP_3 and/or Ca^{2+} signaling caused by misregulation of INPP5E or some other mechanism contributes to the decreased transcriptional response to Shh in Arl13b mutant cells.

5.2 Arl13b and receptor traffic

The Caspary lab has previously used *Arl13b* null cells to show that Arl13b regulates the localization of different Shh signaling pathway components in primary cilia (Larkins et al., 2011). My research indicates that point mutations in Arl13b can also disrupt the normal Shh-dependent traffic of Smo – Arl13b^{C8S,C9S}-GFP and Arl13b^{T35N}-GFP cell lines showed baseline ciliary enrichment of Smo comparable to *Arl13b*^{hnn} MEFs expressing GFP only. Arl13b^{C8S,C9S}-GFP was the most severely affected variant in most of my assays, so it is perhaps not surprising that it failed to restore normal Smo traffic. Arl13b^{T35N}-GFP, however, was capable of rescuing some Arl13b functions, but not the regulation of Smo traffic. This suggests that the GTPase domain of Arl13b is specifically required for its function in regulating the proper level of Smo in the cilium. A previous study on which I worked in collaboration with Holden Higginbotham and Eva Anton showed that interneurons lacking Arl13b exhibit atypical cilia localization patterns of many

different guidance cue receptors, which may contribute to the abnormal migration of these interneurons (Higginbotham et al., 2012). In the same study, Arl13b variants including Arl13b^{R200C}, Arl13b^{R79Q}, and Arl13b^{V358A} were unable to rescue interneuron migration. Because all of these variants exhibited Smo localization patterns indistinguishable from cells expressing Arl13b^{WT}-GFP in my experiments, I must conclude that either Smo localization is regulated through a unique mechanism not shared by the guidance cue receptors analyzed in the Anton lab study, or that abnormal cilia localization of these receptors is not what causes the migration defect in Arl13b null interneurons. (Guidance cue receptor localization in cells expressing Arl13b variants was not measured directly in that study.) It would be interesting to test the effects of Arl13b^{T35N} on these guidance cue receptors, to see if they behave differently from Smo in an Arl13b mutant background.

Thus far, work investigating Arl13b's regulation of ciliary protein traffic has been more phenomenological than mechanistic. However, recent studies have begun to suggest possible mechanisms through which Arl13b might regulate both cilia protein traffic and ciliogenesis. Small GTPases in the Rab and Arf/Arl family are involved in many aspects of vesicular formation and trafficking. In particular, Rab8 and Rab11 are integrally involved with the formation of the ciliary vesicle, a structure that forms early in ciliogenesis (Knödler et al., 2010; Nachury et al., 2007; Westlake et al., 2011; Yoshimura et al., 2007). This vesicle consists of a membranous structure that forms around the centriole as the ciliary basal body and axoneme begin to form. The ciliary vesicle later fuses with the plasma membrane to allow the nascent cilium to extend into the extracellular space. Members of the EHD family of recycling endosome proteins were recently shown to serve as essential regulators of ciliary vesicle formation (Lu et al., 2015). Moreover, EHD1 colocalizes with Smo in the cilium only after Shh stimulation in wild-type cells, but Smo is constitutively present in the cilia of *EHD1* null cells (Bhattacharyya et al., 2016). *EHD1* null embryos display abnormally short cilia and elevated baseline transcriptional Shh signaling, similar to *Arl13b*^{hnn} embryos. However, *EHD1* null embryo

phenotypes are more severe than *Arl13b*^{hnn}: they die before e11.5 (*Arl13b*^{hnn} survive until e13.5) and show abnormal processing of Gli3 into its GliR form (GliR is intact in *Arl13b*^{hnn}). Still, given that Arl13b localizes to and regulates recycling endosomes (Barral et al., 2012), these data suggest that it may play a critical role in the function of EHD1-positive vesicles that contribute to both ciliogenesis and ciliary trafficking of Smo.

Through mechanisms shared with or distinct from those involving its regulation of ciliary protein trafficking, Arl13b may also be involved in the regulation of axonal protein trafficking. Shh-dependent axon guidance may depend upon Arl13b directing Smo to the growth cone, which would provide a mechanism to explain why both *Arl13b*$^{\Delta NEX}$ and *Smo*$^{\Delta NEX}$ mice show the same white matter phenotype at the midline of the SCP. Ongoing experiments testing whether knockdown of Arl13b leads to defects in Shh-dependent axon guidance can also investigate whether these neurons also experience Smo trafficking defects. It would also be interesting to test whether mutations in the cilia localization signal of Smo increase its trafficking to axons and/or potentiate the response to attractive or repulsive Shh cues – similar work in migrating fibroblasts showed that overexpression of non-ciliary Smo increased chemotaxis in response to Shh (Bijlsma et al., 2012).

Additionally, future research should investigate whether Arl13b is involved in regulating any of the events downstream of Smo activation that occur in non-transcriptional Shh signaling, such as the activation of Src family kinases (Yam et al., 2009). If Arl13b doesn't directly affect the trafficking of Smo to axons, it may play a role in the activation of Smo or the transduction of the Shh signal to downstream components of the non-canonical Shh pathway.

5.3 Common factors regulating ciliogenesis, migration, and axon guidance

My data and other studies in the field indicate that Arl13b plays a role in regulating multiple cellular processes broadly related to cytoskeletal dynamics: ciliogenesis, fibroblast migration, and axon outgrowth and guidance. In each of these processes, the reorganization of

microtubules and/or actin filaments in the cell allows for changes in cell shape to occur on a variety of timescales in a transient or stable manner. In this dissertation, I have proposed that Arl13b mediates cell migration and axon guidance through the transduction of signals from a shared upstream signal: the Shh-dependent activation of Smo. But changes in cilia number, cilia length, and axon outgrowth mediated by loss or mutation of Arl13b suggest that it also plays a role in shaping the cytoskeleton through mechanisms other than Shh signaling.

Here, again, the putative Arl13b effector INPP5E could explain the phenotypes seen in Arl13b mutant cells. $PI(4,5)P_2$ and PI(4)P, both products of INPP5E dephosphorylation of phosphatidylinositol polyphosphates, serve important functions in cilia, growth cones, and the leading edge of migrating fibroblasts. A recent study showed that INPP5E acts in concert with the phosphatidylinositol phosphate kinase PIPKIγ to coordinate the initiation of ciliogenesis (Xu et al., 2016). In addition, $PI(4,5)P_2$ rafts are found on the membranes of axonal growth cones as well as on the leading edge of migrating cells (Ling et al., 2006). These rafts regulate the dynamics of the actin cytoskeleton involved in cell motility by recruiting Cdc42, WASP, and ERM proteins, and they are required for axon growth and guidance (reviewed in Caroni, 2001; Kamiguchi, 2006). It remains to be determined whether INPP5E has any role in regulating $PI(4,5)P_2$ rafts at the growth cone or fibroblast leading edge. However, another inositol polyphosphate 5-phosphatase, PIPP, has been shown to regulate PI3-kinase-dependent neurite elongation. $PI(3,4,5)P_3$ promotes axon outgrowth by activating Akt, while PIPP serves as a brake on this process by dephosphorylating $PI(3,4,5)P_3$ (Ooms et al., 2006). Arl13b-dependent INPP5E could act through a similar mechanism, which would explain the abnormal axon outgrowth phenotype in Arl13b-deficient commissural neurons showed in Figure 4.5. Alternatively, Arl13b could regulate PIPP or other phosphatases in the growth cone. This model is reminiscent of the Caspary lab's discovery that Arl13b regulates the phosphatase PP2A, which also serves to balance PI3K-dependent phosphorylation of Akt, at the base of the cilium (Umberger and Caspary, 2015). It would be informative to examine phosphatase activity in Arl13b-deficient neurons, as well as

cells expressing Arl13b variants, to test the validity of this model for Arl13b's regulation of cytoskeletal dynamics.

Downstream of phosphatidylinositol polyphosphates, the actin cytoskeleton is integrally involved in axon outgrowth and guidance, as well as cell migration. F-actin polymerization at the leading edge of axonal growth cones determines their rate of outgrowth, while a constant retrograde flow of actin can be regulated independently to fine-tune this growth. Axon turning in response to chemoattractants can be blocked by cytochalasin, which prevents actin polymerization. Meanwhile, chemorepulsive factors that produce growth cone collapse result in a net loss of F-actin at the leading edge (reviewed in Dent and Gertler, 2003; Luo, 2002). Similarly, actin networks at the leading edge of migrating cells control the extension of filopodia and lamellipodia required for migration (reviewed in Mitchison and Cramer, 1996). Intriguingly, ciliogenesis and cilia length also seem connected to actin dynamics. A screen for regulators of ciliogenesis uncovered many proteins associated with actin, leading to the discovery that actin assembly affects the stability of the pericentrosomal preciliary compartment, an essential structure that forms in early ciliogenesis (Kim et al., 2010). Furthermore, some motile cilia are directly anchored to the actin cytoskeleton. The ciliopathy-associated protein NPHP4 interacts through adaptor proteins with the subapical actin web in multiciliated cells, and its depletion results in both decreased motile ciliogenesis and disorganized actin networks (Yasunaga et al., 2015).

Arl13b also regulates actin dynamics, indicating another potential mechanism through which loss or mutation of Arl13b may affect ciliogenesis, cell migration, and axon guidance. Previous studies have shown that Arl13b is found at actin-rich regions of the plasma membrane, that it interacts with actin in a co-immunoprecipitation assay, and that it is involved in the formation of recycling endosome tubular vesicles and circular dorsal membrane ruffles, both of which are actin-dependent structures (Barral et al., 2012; Casalou et al., 2014). These studies compared wild-type and Arl13b null cells, but also examined the effects of an Arl13b$^{1\text{-}193}$

truncated protein in which the GTPase domain is intact but the novel C-terminal domain is absent. This truncated protein was unable to rescue actin-dependent structures in Arl13b null cells and showed a weaker association with actin. Further research investigating the effects of point mutations in Arl13b on these actin-related phenotypes could shed light onto the mechanism through which Arl13b regulates a variety of cytoskeletal processes in the cell.

5.4 Defects in Shh-dependent neural development as a model for Joubert Syndrome

My experiments in Chapter 4 showed that *Arl13b* mutant mice can be used to model some aspects of JS and that these JS-like phenotypes also occur when *Smo* is deleted in the relevant populations of projection neurons. This suggests that there is a Shh-dependent component to hindbrain white matter development. While ongoing research in the Caspary lab will continue to explore the role of Arl13b in Shh-dependent axon guidance, this work has implications beyond those immediate next steps.

By generating an animal model of JS hindbrain malformations, my experiments provide new opportunities for investigating the neuroanatomical and neurophysiological defects in JS. My research thus far has focused on a single hallmark feature of JS: axon guidance defects in the SCP. Future studies can make use of this model to explore other aspects of JS. Experiments with particular relevance to human health will involve the study of hindbrain nuclei and white matter tracts linked to respiratory function in *Arl13b* mutant mice, as it is the respiratory symptoms of JS that are most commonly linked to early mortality.

Intriguingly, Math1-derived populations of neurons seem to be implicated in many JS-related and/or Shh-sensitive aspects of neural development. Math1 is expressed in cerebellar granule neuron precursors, spinal commissural neurons, and the glutamatergic projection neurons of the DCN. This same transcription factor also helps define the fate of neurons from the rhombic lip that go on to form the parafacial respiratory group/retrotrapeziod nucleus in the ventral respiratory column of the medulla (Rose et al 2009). Glutamatergic inputs from these nuclei

regulate respiratory rhythms (reviewed in: Onimaru et al., 2006). JS patients exhibit abnormal respiratory rhythms with episodic apnea and hyperpnea that can be fatal. Furthermore, these abnormal breathing patterns represent a challenge for anesthesiologists when JS patients require surgery for their other symptoms. Conditional deletion of *Arl13b* using a Math1-Cre would allow us to delete a JS-related gene in these hindbrain nuclei and assess the effects on respiration, thereby generating an animal model of one of the most severe disease phenotypes in JS. Ongoing work developing targeted mouse alleles of Arl13b including the JS-causing Arl13b^{R200C} mutation may also produce a good animal model for respiratory disease phenotypes. In either case, use of *Arl13b* mutant mice as an animal model will support future studies on the anatomy and physiology of these hindbrain nuclei in JS and may help to improve treatment of JS patients' respiratory symptoms.

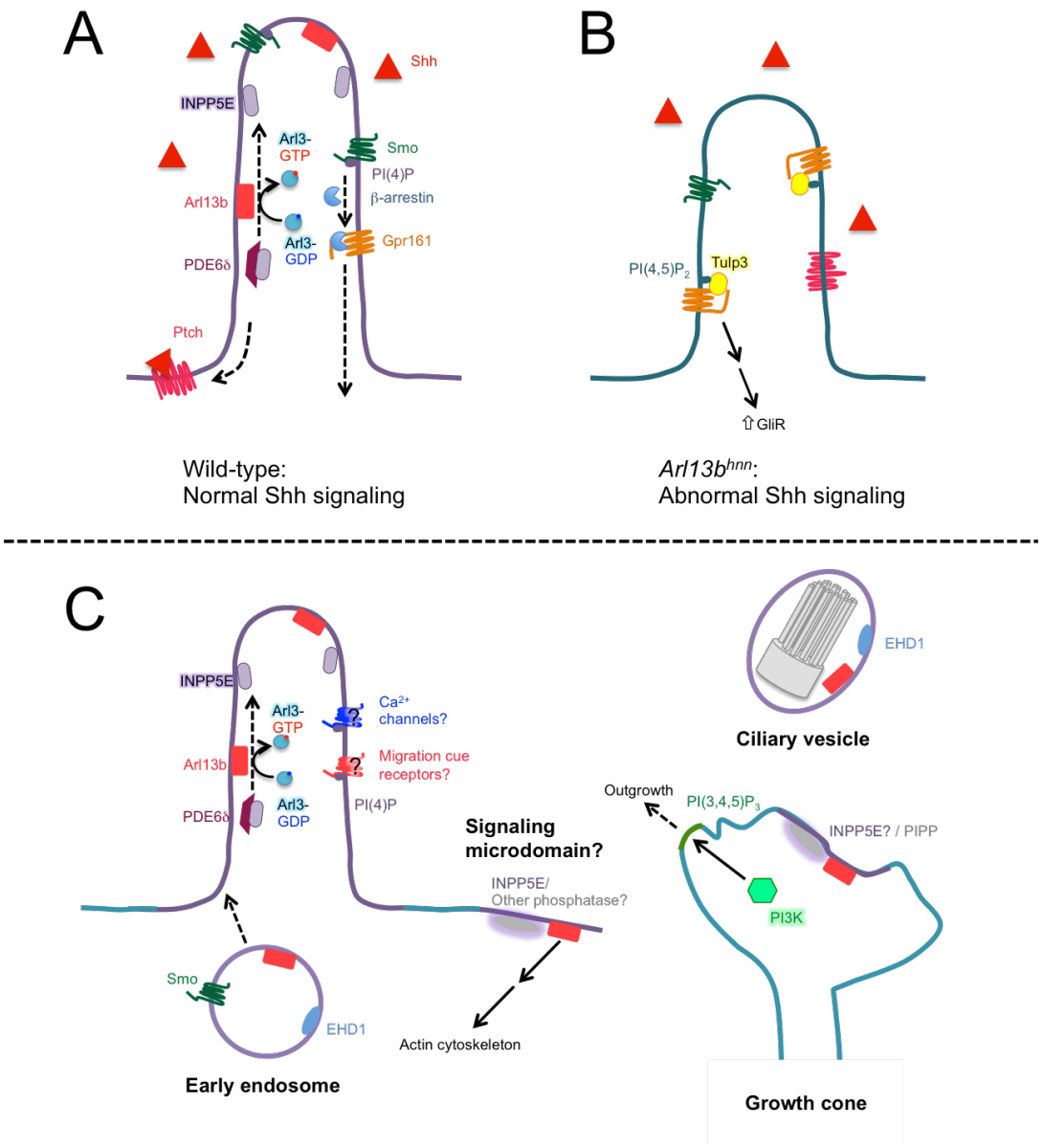

Figure 5.1 Models of Arl13b function. **A** In wild-type cilia, Arl13b GEF activity leads to release of INPP5E from PDE6δ. INPP5E activity causes high levels of PI(4)P in the ciliary membrane. The presence of Shh causes PI(4)P to preferentially bind Smo and promote its activation. Active Smo causes β-arrestin mediated endocytosis of the inhibitory Gpr161, facilitating transcriptional Shh pathway activation. **B** In Arl13b^{hnn} cilia, INPP5E is not targeted to cilia, causing abnormally high PI(4,5)P_2 levels. This stabilizes Gpr161via Tulp3 and inhibits transcriptional Shh signaling. Also, both Ptch and Smo are found in cilia regardless of the presence of Shh ligand. **C** Proposed (speculative) functions of Arl13b based on my experiments. Arl13b's regulation of ciliary INPP5E may affect GPCRs in addition to Smo and Gpr161, such as Ca^{2+} channels permissive for transcriptional Shh signaling, or neuronal migration cue receptors. Arl13b may regulate ciliogenesis in the **ciliary vesicle** and Smo traffic to the cilium through **early endosomes**, along with the EHD1 family of proteins. Arl13b and INPP5E or other phosphatases may also govern the phosphatidyl inositol polyphosphate composition of membrane **signaling microdomains** outside of the cilium that are important for non-transcriptional Shh signaling in fibroblast migration. Arl13b in the **growth cone** may control axon outgrowth and/or turning by regulating the membrane composition through INPP5E or other effectors.

References

Afzelius, B. A. (1976). A human syndrome caused by immotile cilia. *Science* **193**, 317–9.

Alcedo, J., Ayzenzon, M., Von Ohlen, T., Noll, M. and Hooper, J. E. (1996). The Drosophila smoothened gene encodes a seven-pass membrane protein, a putative receptor for the hedgehog signal. *Cell* **86**, 221–32.

Alexander, A. L., Lee, J. E., Lazar, M. and Field, A. S. (2007). Diffusion tensor imaging of the brain. *Neurotherapeutics* **4**, 316–29.

Alfaro, A. C., Roberts, B., Kwong, L., Bijlsma, M. F. and Roelink, H. (2014). Ptch2 mediates the Shh response in Ptch1-/- cells. *Development* **141**, 3331–9.

Altman, J. and Bayer, S. A. (1985). Embryonic development of the rat cerebellum. II. Translocation and regional distribution of the deep neurons. *J. Comp. Neurol.* **231**, 27–41.

Anderson, E., Peluso, S., Lettice, L. A. and Hill, R. E. (2012). Human limb abnormalities caused by disruption of hedgehog signaling. *Trends Genet.* **28**, 364–73.

Ansley, S. J., Badano, J. L., Blacque, O. E., Hill, J., Hoskins, B. E., Leitch, C. C., Kim, J. C., Ross, A. J., Eichers, E. R., Teslovich, T. M., et al. (2003). Basal body dysfunction is a likely cause of pleiotropic Bardet-Biedl syndrome. *Nature* **425**, 628–33.

Ayers, K. L. and Thérond, P. P. (2010). Evaluating Smoothened as a G-protein-coupled receptor for Hedgehog signalling. *Trends Cell Biol.* **20**, 287–98.

Bai, C. B., Auerbach, W., Lee, J. S., Stephen, D. and Joyner, A. L. (2002). Gli2, but not Gli1, is required for initial Shh signaling and ectopic activation of the Shh pathway. *Development* **129**, 4753–4761.

Bai, C. B., Stephen, D. and Joyner, A. L. (2004). All mouse ventral spinal cord patterning by Hedgehog is Gli dependent and involves an activator function of Gli3. *Dev. Cell* **6**, 103–115.

Balaskas, N., Ribeiro, A., Panovska, J., Dessaud, E., Sasai, N., Page, K. M., Briscoe, J. and Ribes, V. (2012). Gene regulatory logic for reading the Sonic Hedgehog signaling gradient in the vertebrate neural tube. *Cell* **148**, 273–284.

Barkovich, A. J., Millen, K. J. and Dobyns, W. B. (2009). A developmental and genetic classification for midbrain-hindbrain malformations. *Brain* 3199–3230.

Barral, D. C., Garg, S., Casalou, C., Watts, G. F. M., Sandoval, J. L., Ramalho, J. S., Hsu, V. W. and Brenner, M. B. (2012). Arl13b regulates endocytic recycling traffic. *Proc. Natl. Acad. Sci. U. S. A.* **109**, 21354–9.

Belgacem, Y. H. and Borodinsky, L. N. (2011). Sonic hedgehog signaling is decoded by calcium spike activity in the developing spinal cord. *Proc. Natl. Acad. Sci. U. S. A.* **108**, 4482–7.

Berbari, N. F., Lewis, J. S., Bishop, G. A., Askwith, C. C. and Mykytyn, K. (2008). Bardet-Biedl syndrome proteins are required for the localization of G protein-coupled receptors to primary cilia. *Proc. Natl. Acad. Sci. U. S. A.* **105**, 4242–6.

Berbari, N. F., O'Connor, A. K., Haycraft, C. J. and Yoder, B. K. (2009). The primary cilium as a complex signaling center. *Curr. Biol.* **19**, R526–35.

Bhattacharyya, S., Rainey, M. A., Arya, P., Dutta, S., George, M., Storck, M. D., McComb, R. D., Muirhead, D., Todd, G. L., Gould, K., et al. (2016). Endocytic recycling protein EHD1 regulates primary cilia morphogenesis and SHH signaling during neural tube

development. *Sci. Rep.* **6**, 20727.

Bielas, S. L., Silhavy, J. L., Brancati, F., Kisseleva, M. V, Al-Gazali, L., Sztriha, L., Bayoumi, R. A., Zaki, M. S., Abdel-Aleem, A., Rosti, R. O., et al. (2009). Mutations in INPP5E, encoding inositol polyphosphate-5-phosphatase E, link phosphatidyl inositol signaling to the ciliopathies. *Nat. Genet.* **41**, 1032–6.

Bijlsma, M. F., Borensztajn, K. S., Roelink, H., Peppelenbosch, M. P. and Spek, C. A. (2007). Sonic hedgehog induces transcription-independent cytoskeletal rearrangement and migration regulated by arachidonate metabolites. *Cell. Signal.* **19**, 2596–604.

Bijlsma, M. F., Damhofer, H. and Roelink, H. (2012). Hedgehog-stimulated chemotaxis is mediated by smoothened located outside the primary cilium. *Sci. Signal.* **5**, ra60.

Bourikas, D., Pekarik, V., Baeriswyl, T., Grunditz, A., Sadhu, R., Nardó, M. and Stoeckli, E. T. (2005). Sonic hedgehog guides commissural axons along the longitudinal axis of the spinal cord. *Nat. Neurosci.* **8**, 297–304.

Braddock, S. R., Henley, K. M. and Maria, B. L. (2007). The face of Joubert syndrome: a study of dysmorphology and anthropometry. *Am. J. Med. Genet. A* **143A**, 3235–42.

Brancati, F., Dallapiccola, B. and Valente, E. M. (2010a). Joubert Syndrome and related disorders. *Orphanet J. Rare Dis.* **5**, 20.

Brancati, F., Dallapiccola, B. and Valente, E. M. (2010b). Joubert Syndrome and related disorders. *Orphanet J. Rare Dis.* **5**, 20.

Brennan, D., Chen, X., Cheng, L., Mahoney, M. and Riobo, N. A. (2012). Noncanonical Hedgehog signaling. *Vitam. Horm.* **88**, 55–72.

Briscoe, J. and Ericson, J. (2001). Specification of neuronal fates in the ventral neural tube. *Curr. Opin. Neurobiol.* **11**, 43–9.

Brown, J. M. and Witman, G. B. (2014). Cilia and Diseases. *Bioscience* **64**, 1126–1137.

Cantagrel, V., Silhavy, J. L., Bielas, S. L., Swistun, D., Marsh, S. E., Bertrand, J. Y., Audollent, S., Attié-Bitach, T., Holden, K. R., Dobyns, W. B., et al. (2008). Mutations in the cilia gene ARL13B lead to the classical form of Joubert syndrome. *Am. J. Hum. Genet.* **83**, 170–9.

Caroni, P. (2001). Actin cytoskeleton regulation through modulation of PI(4,5)P(2) rafts. *EMBO J.* **20**, 4332–6.

Casalou, C., Seixas, C., Portelinha, A., Pintado, P., Barros, M., Ramalho, J. S., Lopes, S. S. and Barral, D. C. (2014). Arl13b and the non-muscle myosin heavy chain IIA are required for circular dorsal ruffle formation and cell migration. *J. Cell Sci.* **127**, 2709–22.

Caspary, T., Larkins, C. E. and Anderson, K. V. (2007). The graded response to Sonic Hedgehog depends on cilia architecture. *Dev. Cell* **12**, 767–78.

Cevik, S., Sanders, A. a W. M., Van Wijk, E., Boldt, K., Clarke, L., van Reeuwijk, J., Hori, Y., Horn, N., Hetterschijt, L., Wdowicz, A., et al. (2013). Active Transport and Diffusion Barriers Restrict Joubert Syndrome-Associated ARL13B/ARL-13 to an Inv-like Ciliary Membrane Subdomain. *PLoS Genet.* **9**, e1003977.

Charron, F., Stein, E., Jeong, J., McMahon, A. P. and Tessier-Lavigne, M. (2003). The Morphogen Sonic Hedgehog Is an Axonal Chemoattractant that Collaborates with Netrin-1 in Midline Axon Guidance. *Cell* **113**, 11–23.

Chávez, M., Ena, S., Van Sande, J., de Kerchove d'Exaerde, A., Schurmans, S. and Schiffmann, S. N. (2015). Modulation of ciliary phosphoinositide content regulates

trafficking and Sonic hedgehog signaling output. *Dev. Cell* **34**, 338–50.

Chen, W., Ren, X.-R., Nelson, C. D., Barak, L. S., Chen, J. K., Beachy, P. A., de Sauvage, F. and Lefkowitz, R. J. (2004). Activity-dependent internalization of smoothened mediated by beta-arrestin 2 and GRK2. *Science* **306**, 2257–60.

Chen, M.-H., Wilson, C. W., Li, Y.-J., Law, K. K. Lo, Lu, C.-S., Gacayan, R., Zhang, X., Hui, C. and Chuang, P.-T. (2009). Cilium-independent regulation of Gli protein function by Sufu in Hedgehog signaling is evolutionarily conserved. *Genes Dev.* **23**, 1910–28.

Chen, Y., Yue, S., Xie, L., Pu, X., Jin, T. and Cheng, S. Y. (2011). Dual Phosphorylation of suppressor of fused (Sufu) by PKA and GSK3beta regulates its stability and localization in the primary cilium. *J. Biol. Chem.* **286**, 13502–11.

Cheung, H. O.-L., Zhang, X., Ribeiro, A., Mo, R., Makino, S., Puviindran, V., Law, K. K. L., Briscoe, J. and Hui, C.-C. (2009). The kinesin protein Kif7 is a critical regulator of Gli transcription factors in mammalian hedgehog signaling. *Sci. Signal.* **2**, ra29.

Chiang, C., Litingtung, Y., Lee, E., Young, K. E., Corden, J. L., Westphal, H. and Beachy, P. A. (1996). Cyclopia and defective axial patterning in mice lacking Sonic hedgehog gene function. *Nature* **383**, 407–13.

Chizhikov, V. V, Davenport, J., Zhang, Q., Shih, E. K., Cabello, O. A., Fuchs, J. L., Yoder, B. K. and Millen, K. J. (2007). Cilia proteins control cerebellar morphogenesis by promoting expansion of the granule progenitor pool. *J. Neurosci.* **27**, 9780–9.

Corbit, K. C., Aanstad, P., Singla, V., Norman, A. R., Stainier, D. Y. R. and Reiter, J. F. (2005). Vertebrate Smoothened functions at the primary cilium. *Nature* **437**, 1018–21.

Corrales, J. D., Rocco, G. L., Blaess, S., Guo, Q. and Joyner, A. L. (2004). Spatial pattern of sonic hedgehog signaling through Gli genes during cerebellum development. *Development* **131**, 5581–90.

Corrales, J. D., Blaess, S., Mahoney, E. M. and Joyner, A. L. (2006). The level of sonic hedgehog signaling regulates the complexity of cerebellar foliation. *Development* **133**, 1811–21.

Dafinger, C., Liebau, M. C., Elsayed, S. M., Hellenbroich, Y., Boltshauser, E., Korenke, G. C., Fabretti, F., Janecke, A. R., Ebermann, I., Nürnberg, G., et al. (2011). Mutations in KIF7 link Joubert syndrome with Sonic Hedgehog signaling and microtubule dynamics. *J. Clin. Invest.* **121**, 2662–7.

Dascher, C. and Balch, W. E. (1994). Dominant inhibitory mutants of ARF1 block endoplasmic reticulum to Golgi transport and trigger disassembly of the Golgi apparatus. *J. Biol. Chem.* **269**, 1437–1448.

Davis, E. E. and Katsanis, N. (2012). The ciliopathies: a transitional model into systems biology of human genetic disease. *Curr. Opin. Genet. Dev.* **22**, 290–303.

Denef, N., Neubuser, D., Perez, L. and Cohen, S. M. (2000). Hedgehog Induces Opposite Changes in Turnover and Subcellular Localization of Patched and Smoothened. *Cell* **102**, 521–531.

Dent, E. W. and Gertler, F. B. (2003). Cytoskeletal Dynamics and Transport in Growth Cone Motility and Axon Guidance. *Neuron* **40**, 209–227.

Deretic, D., Schmerl, S., Hargrave, P. A., Arendt, A. and McDowell, J. H. (1998). Regulation of sorting and post-Golgi trafficking of rhodopsin by its C-terminal sequence QVS(A)PA. *Proc. Natl. Acad. Sci. U. S. A.* **95**, 10620–5.

Deretic, D., Williams, A. H., Ransom, N., Morel, V., Hargrave, P. A. and Arendt, A. (2005). Rhodopsin C terminus, the site of mutations causing retinal disease, regulates trafficking by binding to ADP-ribosylation factor 4 (ARF4). *Proc. Natl. Acad. Sci. U. S. A.* **102**, 3301–6.

Dessaud, E., Yang, L. L., Hill, K., Cox, B., Ulloa, F., Ribeiro, A., Mynett, A., Novitch, B. G. and Briscoe, J. (2007). Interpretation of the sonic hedgehog morphogen gradient by a temporal adaptation mechanism. *Nature* **450**, 717–20.

Dessaud, E., McMahon, A. P. and Briscoe, J. (2008). Pattern formation in the vertebrate neural tube: a sonic hedgehog morphogen-regulated transcriptional network. *Development* **135**, 2489–503.

Ding, Q., Motoyama, J., Gasca, S., Mo, R., Sasaki, H., Rossant, J. and Hui, C. C. (1998). Diminished Sonic hedgehog signaling and lack of floor plate differentiation in Gli2 mutant mice. *Development* **125**, 2533–43.

Ding, Q., Fukami, S. i, Meng, X., Nishizaki, Y., Zhang, X., Sasaki, H., Dlugosz, A., Nakafuku, M. and Hui, C. c (1999). Mouse suppressor of fused is a negative regulator of sonic hedgehog signaling and alters the subcellular distribution of Gli1. *Curr. Biol.* **9**, 1119–22.

Dingwall, C. and Laskey, R. A. (1991). Nuclear targeting sequences--a consensus? *Trends Biochem. Sci.* **16**, 478–81.

Dishinger, J. F., Kee, H. L., Jenkins, P. M., Fan, S., Hurd, T. W., Hammond, J. W., Truong, Y. N.-T., Margolis, B., Martens, J. R. and Verhey, K. J. (2010). Ciliary entry of the kinesin-2 motor KIF17 is regulated by importin-beta2 and RanGTP. *Nat. Cell Biol.* **12**, 703–10.

Dixon-Salazar, T., Silhavy, J. L., Marsh, S. E., Louie, C. M., Scott, L. C., Gururaj, A., Al-Gazali, L., Al-Tawari, A. A., Kayserili, H., Sztriha, L., et al. (2004). Mutations in the AHI1 gene, encoding jouberin, cause Joubert syndrome with cortical polymicrogyria. *Am. J. Hum. Genet.* **75**, 979–87.

Doherty, D. (2009). Joubert syndrome: insights into brain development, cilium biology, and complex disease. *Semin. Pediatr. Neurol.* **16**, 143–54.

Duldulao, N. A., Lee, S. and Sun, Z. (2009). Cilia localization is essential for in vivo functions of the Joubert syndrome protein Arl13b/Scorpion. *Development* **136**, 4033–42.

Echelard, Y., Epstein, D., St. Jacques, B., Shen, L., Mohler, J., McMahon, J. and McMahon, A. (1993). Sonic-hedgehog, a member of a family of putative signaling molecules, is implicated in the regulation of CNS polarity. *Cell* **75**, 1417–1430.

Eggenschwiler, J. T. and Anderson, K. V (2007). Cilia and developmental signaling. *Annu. Rev. Cell Dev. Biol.* **23**, 345–73.

Endoh-Yamagami, S., Evangelista, M., Wilson, D., Wen, X., Theunissen, J.-W., Phamluong, K., Davis, M., Scales, S. J., Solloway, M. J., de Sauvage, F. J., et al. (2009). The mammalian Cos2 homolog Kif7 plays an essential role in modulating Hh signal transduction during development. *Curr. Biol.* **19**, 1320–6.

Engle, E. C. (2010). Human genetic disorders of axon guidance. *Cold Spring Harb. Perspect. Biol.* **2**, a001784.

Epstein, D. J., Marti, E., Scott, M. P. and McMahon, A. P. (1996). Antagonizing cAMP-dependent protein kinase A in the dorsal CNS activates a conserved Sonic hedgehog signaling pathway. *Development* **122**, 2885–94.

Evans, T. A. and Bashaw, G. J. (2010). Axon guidance at the midline: of mice and flies. *Curr.*

Opin. Neurobiol. **20**, 79–85.

Fabre, P. J., Shimogori, T. and Charron, F. (2010). Segregation of ipsilateral retinal ganglion cell axons at the optic chiasm requires the Shh receptor Boc. *J. Neurosci.* **30**, 266–75.

Feig, L. A. and Cooper, G. M. (1988). Inhibition of NIH 3T3 cell proliferation by a mutant ras protein with preferential affinity for GDP. *Mol. Cell. Biol.* **8**, 3235–3243.

Fink, A. J., Englund, C., Daza, R. a M., Pham, D., Lau, C., Nivison, M., Kowalczyk, T. and Hevner, R. F. (2006). Development of the deep cerebellar nuclei: transcription factors and cell migration from the rhombic lip. *J. Neurosci.* **26**, 3066–76.

Follit, J. A., Li, L., Vucica, Y. and Pazour, G. J. (2010). The cytoplasmic tail of fibrocystin contains a ciliary targeting sequence. *J. Cell Biol.* **188**, 21–8.

Geng, L., Okuhara, D., Yu, Z., Tian, X., Cai, Y., Shibazaki, S. and Somlo, S. (2006). Polycystin-2 traffics to cilia independently of polycystin-1 by using an N-terminal RVxP motif. *J. Cell Sci.* **119**, 1383–95.

Gina E. Elsen , Gordana Juric-Sekhar, Ray A. M. Daza, R. F. H. (2013). Development of Cerebellar Nuclei. In *Handbook of the Cerebellum and Cerebellar Disorders* (ed. Manto, M.), Schmahmann, J. D.), Rossi, F.), Gruol, D. L.), and Koibuchi, N.), pp. 179–205. Dordrecht: Springer Netherlands.

Goebbels, S., Bormuth, I., Bode, U., Hermanson, O. and Schwab, M. H. (2006). Genetic Targeting of Principal Neurons in Neocortex and Hippocampus of NEX-Cre Mice. *Genesis* **44**, 611–621.

Goodrich, L. V., Milenkovic, L., Higgins, K. M. and Scott, M. P. (1997). Altered neural cell fates and medulloblastoma in mouse Patched mutants. *Science (80-.).* **277**, 1109–1113.

Gotthardt, K., Lokaj, M., Koerner, C., Falk, N., Gießl, A. and Wittinghofer, A. (2015). A G-protein activation cascade from Arl13B to Arl3 and implications for ciliary targeting of lipidated proteins. *Elife* **4**,.

Guo, J., Higginbotham, H., Li, J., Nichols, J., Hirt, J., Ghukasyan, V. and Anton, E. S. (2015). Developmental disruptions underlying brain abnormalities in ciliopathies. *Nat. Commun.* **6**, 7857.

Hammerschmidt, M., Bitgood, M. J. and McMahon, A. P. (1996). Protein kinase A is a common negative regulator of Hedgehog signaling in the vertebrate embryo. *Genes Dev.* **10**, 647–58.

Hatten, M. E. and Roussel, M. F. (2011). Development and cancer of the cerebellum. *Trends Neurosci.* **34**, 134–42.

Haycraft, C. J., Banizs, B., Aydin-Son, Y., Zhang, Q., Michaud, E. J. and Yoder, B. K. (2005). Gli2 and Gli3 localize to cilia and require the intraflagellar transport protein polaris for processing and function. *PLoS Genet.* **1**, e53.

Higginbotham, H. R. and Gleeson, J. G. (2007). The centrosome in neuronal development. *Trends Neurosci.* **30**, 276–83.

Higginbotham, H., Eom, T.--y., Mariani, L. E., Bachleda, A., Gukassyan, V., Caspary, T. and Anton, E. S. (2012a). Primary cilia regulate the migration and placement of interneurons in the developing cerebral cortex. *Under Revis.*

Higginbotham, H., Eom, T.-Y., Mariani, L. E., Bachleda, A., Hirt, J., Gukassyan, V., Cusack, C. L., Lai, C., Caspary, T. and Anton, E. S. (2012b). Arl13b in primary cilia regulates the migration and placement of interneurons in the developing cerebral cortex.

Dev. Cell **23**, 925–938.

Hori, Y., Kobayashi, T., Kikko, Y., Kontani, K. and Katada, T. (2008). Domain architecture of the atypical Arf-family GTPase Arl13b involved in cilia formation. *Biochem. Biophys. Res. Commun.* **373**, 119–24.

Hsu, C. C.-T., Kwan, G. N. C. and Bhuta, S. (2015). High-Resolution Diffusion Tensor Imaging and Tractography in Joubert Syndrome: Beyond Molar Tooth Sign. *Pediatr. Neurol.*

Hu, D. and Helms, J. A. (1999). The role of sonic hedgehog in normal and abnormal craniofacial morphogenesis. *Development* **126**, 4873–84.

Hu, D., Young, N. M., Li, X., Xu, Y., Hallgrímsson, B. and Marcucio, R. S. (2015). A dynamic Shh expression pattern, regulated by SHH and BMP signaling, coordinates fusion of primordia in the amniote face. *Development* **142**, 567–74.

Huangfu, D. and Anderson, K. V (2005). Cilia and Hedgehog responsiveness in the mouse. *Proc. Natl. Acad. Sci. U. S. A.* **102**, 11325–30.

Huangfu, D. and Anderson, K. V (2006). Signaling from Smo to Ci/Gli: conservation and divergence of Hedgehog pathways from Drosophila to vertebrates. *Development* **133**, 3–14.

Huangfu, D., Liu, A., Rakeman, A. S., Murcia, N. S., Niswander, L. and Anderson, K. V (2003). Hedgehog signalling in the mouse requires intraflagellar transport proteins. *Nature* **426**, 83–7.

Humbert, M. C., Weihbrecht, K., Searby, C. C., Li, Y., Pope, R. M., Sheffield, V. C. and Seo, S. (2012). ARL13B, PDE6D, and CEP164 form a functional network for INPP5E ciliary targeting. *Proc. Natl. Acad. Sci. U. S. A.* **109**, 19691–6.

Humke, E. W., Dorn, K. V, Milenkovic, L., Scott, M. P. and Rohatgi, R. (2010). The output of Hedgehog signaling is controlled by the dynamic association between Suppressor of Fused and the Gli proteins. *Genes Dev.* **24**, 670–82.

Ingham, P. W., Nakano, Y. and Seger, C. (2011). Mechanisms and functions of Hedgehog signalling across the metazoa. *Nat. Rev. Genet.* **12**, 393–406.

Jessell, T. M. (2000). Neuronal specification in the spinal cord: inductive signals and transcriptional codes. *Nat. Rev. Genet.* **1**, 20–9.

Jin, S., Martinelli, D. C., Zheng, X., Tessier-Lavigne, M. and Fan, C.-M. (2015). Gas1 is a receptor for sonic hedgehog to repel enteric axons. *Proc. Natl. Acad. Sci. U. S. A.* **112**, E73–80.

Joneson, T., White, M. A., Wigler, M. H. and Bar-Sagi, D. (1996). Stimulation of membrane ruffling and MAP kinase activation by distinct effectors of RAS. *Science* **271**, 810–2.

Joubert, M., Eisenring, J. J., Robb, J. P. and Andermann, F. (1969). Familial agenesis of the cerebellar vermis. A syndrome of episodic hyperpnea, abnormal eye movements, ataxia, and retardation. *Neurology* **19**, 813–25.

Juric-Sekhar, G., Adkins, J., Doherty, D. and Hevner, R. F. (2012). Joubert syndrome: brain and spinal cord malformations in genotyped cases and implications for neurodevelopmental functions of primary cilia. *Acta Neuropathol.* 695–709.

Kamiguchi, H. (2006). The region-specific activities of lipid rafts during axon growth and guidance. *J. Neurochem.* **98**, 330–5.

Kee, H. L., Dishinger, J. F., Blasius, T. L., Liu, C.-J., Margolis, B. and Verhey, K. J. (2012). A size-exclusion permeability barrier and nucleoporins characterize a ciliary pore complex

that regulates transport into cilia. *Nat. Cell Biol.* **14**, 431–7.

Khan, A. O., Oystreck, D. T., Seidahmed, M. Z., AlDrees, A., Elmalik, S. A., Alorainy, I. A. and Salih, M. A. (2008). Ophthalmic Features of Joubert Syndrome. *Ophthalmology* **115**, 2286–2289.

Kim, D. and Ackerman, S. L. (2011). The UNC5C Netrin Receptor Regulates Dorsal Guidance of Mouse Hindbrain Axons. *J. Neurosci.* **31**, 2167–2179.

Kim, J., Kato, M. and Beachy, P. A. (2009). Gli2 trafficking links Hedgehog-dependent activation of Smoothened in the primary cilium to transcriptional activation in the nucleus. *Proc. Natl. Acad. Sci. U. S. A.* **106**, 21666–71.

Kim, J., Lee, J. E., Heynen-Genel, S., Suyama, E., Ono, K., Lee, K., Ideker, T., Aza-Blanc, P. and Gleeson, J. G. (2010). Functional genomic screen for modulators of ciliogenesis and cilium length. *Nature* **464**, 1048–51.

Kim, J., C Hsia, E. Y., Brigui, A., Plessis, A., Beachy, P. A. and Zheng, X. (2015). The role of ciliary trafficking in Hedgehog receptor signaling. *Sci. Signal.* **8**, ra55.

Knödler, A., Feng, S., Zhang, J., Zhang, X., Das, A., Peränen, J. and Guo, W. (2010). Coordination of Rab8 and Rab11 in primary ciliogenesis. *Proc. Natl. Acad. Sci. U. S. A.* **107**, 6346–51.

Kogerman, P., Grimm, T., Kogerman, L., Krause, D., Unden, A., Sandstedt, B., Toftgard, R. and Zaphiropoulos, P. (1999). Mammalian Suppressor-of-Fused modulates nuclear-cytoplasmic shuttling of GLI-1. *Nat. Cell Biol.* **1**, 312–319.

Köttgen, M. and Walz, G. (2005). Subcellular localization and trafficking of polycystins. *Eur. J. Physiol.* **451**, 286–93.

Kovacs, J. J., Whalen, E. J., Liu, R., Xiao, K., Kim, J., Chen, M., Wang, J., Chen, W. and Lefkowitz, R. J. (2008). Beta-arrestin-mediated localization of smoothened to the primary cilium. *Science (80-.).* **320**, 1777–81.

Kuai, J. and Kahn, R. A. (2000). Residues forming a hydrophobic pocket in ARF3 are determinants of GDP dissociation and effector interactions. *FEBS Lett.* **487**, 252–256.

Lancaster, M. A., Gopal, D. J., Kim, J., Saleem, S. N., Silhavy, J. L., Louie, C. M., Thacker, B. E., Williams, Y., Zaki, M. S. and Gleeson, J. G. (2011). Defective Wnt-dependent cerebellar midline fusion in a mouse model of Joubert syndrome. *Nat. Med.* **17**, 726–31.

Larkins, C. E., Aviles, G. D. G., East, M. P., Kahn, R. A. and Caspary, T. (2011). Arl13b regulates ciliogenesis and the dynamic localization of Shh signaling proteins. *Mol. Biol. Cell* **22**, 4694–703.

Lee, J. E. and Gleeson, J. G. (2011). A systems-biology approach to understanding the ciliopathy disorders. *Genome Med.* **3**, 59.

Lei, Q., Zelman, A. K., Kuang, E., Li, S. and Matise, M. P. (2004). Transduction of graded Hedgehog signaling by a combination of Gli2 and Gli3 activator functions in the developing spinal cord. *Development* **131**, 3593–604.

Liem, K. F., He, M., Ocbina, P. J. R. and Anderson, K. V (2009). Mouse Kif7/Costal2 is a cilia-associated protein that regulates Sonic hedgehog signaling. *Proc. Natl. Acad. Sci. U. S. A.* **106**, 13377–82.

Ling, K., Schill, N. J., Wagoner, M. P., Sun, Y. and Anderson, R. A. (2006). Movin' on up: the role of PtdIns(4,5)P(2) in cell migration. *Trends Cell Biol.* **16**, 276–84.

Litingtung, Y. and Chiang, C. (2000). Specification of ventral neuron types is mediated by an

antagonistic interaction between Shh and Gli3. *Nat. Neurosci.* **3**, 979–85.

Liu, A., Wang, B. and Niswander, L. A. (2005). Mouse intraflagellar transport proteins regulate both the activator and repressor functions of Gli transcription factors. *Development* **132**, 3103–11.

Liu, J., Zeng, H. and Liu, A. (2015). The loss of Hh responsiveness by a non-ciliary Gli2 variant. *Development* **142**, 1651–60.

Lu, H., Toh, M. T., Narasimhan, V., Thamilselvam, S. K., Choksi, S. P. and Roy, S. (2014). A function for the Joubert syndrome protein Arl13b in ciliary membrane extension and ciliary length regulation. *Dev. Biol.* **397**, 225–236.

Lu, Q., Insinna, C., Ott, C., Stauffer, J., Pintado, P. A., Rahajeng, J., Baxa, U., Walia, V., Cuenca, A., Hwang, Y.-S., et al. (2015). Early steps in primary cilium assembly require EHD1/EHD3-dependent ciliary vesicle formation. *Nat. Cell Biol.* **17**, 228–40.

Luo, L. (2002). Actin cytoskeleton regulation in neuronal morphogenesis and structural plasticity. *Annu. Rev. Cell Dev. Biol.* **18**, 601–35.

Lupo, G., Harris, W. A. and Lewis, K. E. (2006). Mechanisms of ventral patterning in the vertebrate nervous system. *Nat. Rev. Neurosci.* **7**, 103–14.

Machold, R. and Fishell, G. (2005). Math1 is expressed in temporally discrete pools of cerebellar rhombic-lip neural progenitors. *Neuron* **48**, 17–24.

Magnani, D., Morlé, L., Hasenpusch-Theil, K., Paschaki, M., Jacoby, M., Schurmans, S., Durand, B. and Theil, T. (2015). The ciliogenic transcription factor Rfx3 is required for the formation of the thalamocortical tract by regulating the patterning of prethalamus and ventral telencephalon. *Hum. Mol. Genet.* **24**, 2578–93.

Maria, B. L., Quisling, R. G., Rosainz, L. C., Yachnis, A. T., Gitten, J., Dede, D. and Fennell, E. (1999). Molar Tooth Sign in Joubert Syndrome: Clinical, Radiologic, and Pathologic Significance. *J. Child Neurol.* **14**, 368–376.

Mariani, L. E. and Caspary, T. (2013). Primary Cilia, Sonic Hedgehog Signaling, and Spinal Cord Development. In *Cilia and Nervous System Development and Function* (ed. Tucker, K. L.) and Caspary, T.), pp. 55–82. Dordrecht: Springer Netherlands.

Marigo, V., Davey, R. A., Zuo, Y., Cunningham, J. M. and Tabin, C. J. (1996). Biochemical evidence that patched is the Hedgehog receptor. *Nature* **384**, 176–9.

Matise, M. P., Epstein, D. J., Park, H. L., Platt, K. A. and Joyner, A. L. (1998). Gli2 is required for induction of floor plate and adjacent cells, but not most ventral neurons in the mouse central nervous system. *Development* **125**, 2759–70.

Maurya, A. K., Ben, J., Zhao, Z., Lee, R. T. H., Niah, W., Ng, A. S. M., Iyu, A., Yu, W., Elworthy, S., van Eeden, F. J. M., et al. (2013). Positive and negative regulation of Gli activity by Kif7 in the zebrafish embryo. *PLoS Genet.* **9**, e1003955.

May, S. R., Ashique, A. M., Karlen, M., Wang, B., Shen, Y., Zarbalis, K., Reiter, J., Ericson, J. and Peterson, A. S. (2005). Loss of the retrograde motor for IFT disrupts localization of Smo to cilia and prevents the expression of both activator and repressor functions of Gli. *Dev. Biol.* **287**, 378–89.

Mazelova, J., Astuto-Gribble, L., Inoue, H., Tam, B. M., Schonteich, E., Prekeris, R., Moritz, O. L., Randazzo, P. A. and Deretic, D. (2009). Ciliary targeting motif VxPx directs assembly of a trafficking module through Arf4. *EMBO J.* **28**, 183–92.

Milenkovic, L., Scott, M. P. and Rohatgi, R. (2009). Lateral transport of Smoothened from the

plasma membrane to the membrane of the cilium. *J. Cell Biol.* **187**, 365–74.

Milenkovic, L., Weiss, L. E., Yoon, J., Roth, T. L., Su, Y. S., Sahl, S. J., Scott, M. P. and Moerner, W. E. (2015). Single-molecule imaging of Hedgehog pathway protein Smoothened in primary cilia reveals binding events regulated by Patched1. *Proc. Natl. Acad. Sci. U. S. A.* **112**, 8320–5.

Mitchison, T. . and Cramer, L. . (1996). Actin-Based Cell Motility and Cell Locomotion. *Cell* **84**, 371–379.

Motoyama, J. (2003). Differential requirement for Gli2 and Gli3 in ventral neural cell fate specification. *Dev. Biol.* **259**, 150–161.

Motoyama, J., Milenkovic, L., Iwama, M., Shikata, Y., Scott, M. P. and Hui, C. (2003). Differential requirement for Gli2 and Gli3 in ventral neural cell fate specification. *Dev. Biol.* **259**, 150–61.

Nachtergaele, S., Mydock, L. K., Krishnan, K., Rammohan, J., Schlesinger, P. H., Covey, D. F. and Rohatgi, R. (2012). Oxysterols are allosteric activators of the oncoprotein Smoothened. *Nat. Chem. Biol.* **8**, 211–20.

Nachury, M. V., Loktev, A. V., Zhang, Q., Westlake, C. J., Peränen, J., Merdes, A., Slusarski, D. C., Scheller, R. H., Bazan, J. F. and Sheffield, V. C. (2007). A Core Complex of BBS Proteins Cooperates with the GTPase Rab8 to Promote Ciliary Membrane Biogenesis. *Cell* **129**, 1201–1213.

Nigg, E. A. (1997). Nucleocytoplasmic transport: signals, mechanisms and regulation. *Nature* **386**, 779–87.

Ocbina, P. J. R. and Anderson, K. V (2008). Intraflagellar transport, cilia, and mammalian Hedgehog signaling: analysis in mouse embryonic fibroblasts. *Dev. Dyn.* **237**, 2030–8.

Okada, A., Charron, F., Morin, S., Shin, D. S., Wong, K., Fabre, P. J., Tessier-Lavigne, M. and McConnell, S. K. (2006). Boc is a receptor for sonic hedgehog in the guidance of commissural axons. *Nature* **444**, 369–73.

Onimaru, H., Homma, I., Feldman, J. L. and Janczewski, W. A. (2006). Point:Counterpoint: The parafacial respiratory group (pFRG)/pre-Bötzinger complex (preBötC) is the primary site of respiratory rhythm generation in the mammal. *J. Appl. Physiol.* **100**, 2094–2098.

Ooms, L. M., Fedele, C. G., Astle, M. V, Ivetac, I., Cheung, V., Pearson, R. B., Layton, M. J., Forrai, A., Nandurkar, H. H. and Mitchell, C. A. (2006). The inositol polyphosphate 5-phosphatase, PIPP, Is a novel regulator of phosphoinositide 3-kinase-dependent neurite elongation. *Mol. Biol. Cell* **17**, 607–22.

Pal, K., Hwang, S.-H., Somatilaka, B., Badgandi, H., Jackson, P. K., DeFea, K. and Mukhopadhyay, S. (2016). Smoothened determines β-arrestin-mediated removal of the G protein-coupled receptor Gpr161 from the primary cilium. *J. Cell Biol.* **212**, 861–75.

Pan, Y., Wang, C. and Wang, B. (2009). Phosphorylation of Gli2 by protein kinase A is required for Gli2 processing and degradation and the Sonic Hedgehog-regulated mouse development. *Dev. Biol.* **326**, 177–89.

Parisi, M. A. and Glass, I. A. (2012). Joubert Syndrome and Related Disorders. In *GeneReviews™* (ed. Pagon, R. A.), Bird, T. D.), Dolan, C. R.), Stephens, K.), and Adam, M. P.), Seattle, WA: University of Washington.

Parisi, M. A., Pinter, J. D., Glass, I. A., Field, K., Maria, B. L., Chance, P. F., Mahurin, R. K. and Cramer, S. C. (2004). Cerebral and cerebellar motor activation abnormalities in a subject with Joubert syndrome: functional magnetic resonance imaging (MRI) study. *J.*

Child Neurol. **19**, 214–8.

Parisi, M. A., Doherty, D., Chance, P. F. and Glass, I. A. (2007). Joubert syndrome (and related disorders) (OMIM 213300). *Eur. J. Hum. Genet.* **15**, 511–21.

Park, H. L., Bai, C., Platt, K. A., Matise, M. P., Beeghly, A., Hui, C. C., Nakashima, M. and Joyner, A. L. (2000). Mouse Gli1 mutants are viable but have defects in SHH signaling in combination with a Gli2 mutation. *Development* **127**, 1593–605.

Pazour, G. J., Dickert, B. L., Vucica, Y., Seeley, E. S., Rosenbaum, J. L., Witman, G. B. and Cole, D. G. (2000). Chlamydomonas IFT88 and its mouse homologue, polycystic kidney disease gene tg737, are required for assembly of cilia and flagella. *J. Cell Biol.* **151**, 709–18.

Persson, M., Stamataki, D., te Welscher, P., Andersson, E., Böse, J., Rüther, U., Ericson, J. and Briscoe, J. (2002). Dorsal-ventral patterning of the spinal cord requires Gli3 transcriptional repressor activity. *Genes Dev.* **16**, 2865–78.

Polizio, A. H., Chinchilla, P., Chen, X., Manning, D. R. and Riobo, N. A. (2011). Sonic Hedgehog activates the GTPases Rac1 and RhoA in a Gli-independent manner through coupling of smoothened to Gi proteins. *Sci. Signal.* **4**, pt7.

Poretti, A., Boltshauser, E., Loenneker, T., Valente, E. M., Brancati, F., Il'yasov, K. and Huisman, T. A. G. M. (2007). Diffusion tensor imaging in Joubert syndrome. *AJNR. Am. J. Neuroradiol.* **28**, 1929–33.

Poretti, A., Meoded, A., Rossi, A., Raybaud, C. and Huisman, T. A. G. M. (2013). Diffusion tensor imaging and fiber tractography in brain malformations. *Pediatr. Radiol.* **43**, 28–54.

Pospisilik, J. A., Schramek, D., Schnidar, H., Cronin, S. J. F., Nehme, N. T., Zhang, X., Knauf, C., Cani, P. D., Aumayr, K., Todoric, J., et al. (2010). Drosophila genome-wide obesity screen reveals hedgehog as a determinant of brown versus white adipose cell fate. *Cell* **140**, 148–60.

Putoux, A., Thomas, S., Coene, K. L. M., Davis, E. E., Alanay, Y., Ogur, G., Uz, E., Buzas, D., Gomes, C., Patrier, S., et al. (2011). KIF7 mutations cause fetal hydrolethalus and acrocallosal syndromes. *Nat. Genet.* **43**, 601–6.

Putoux, A., Nampoothiri, S., Laurent, N., Cormier-Daire, V., Beales, P. L., Schinzel, A., Bartholdi, D., Alby, C., Thomas, S., Elkhartoufi, N., et al. (2012). Novel KIF7 mutations extend the phenotypic spectrum of acrocallosal syndrome. *J. Med. Genet.* **49**, 713–20.

Reiter, J. F. and Skarnes, W. C. (2006). Tectonic, a novel regulator of the Hedgehog pathway required for both activation and inhibition. *Genes Dev.* **20**, 22–7.

Ribes, V. and Briscoe, J. (2009). Establishing and interpreting graded Sonic hedgehog signaling during vertebrate neural tube patterning: the role of negative feedback. *Cold Spring Harb. Perspect. Biol.* **1**, a002014–a002014.

Rohatgi, R., Milenkovic, L. and Scott, M. P. (2007). Patched1 regulates hedgehog signaling at the primary cilium. *Science (80-.).* **317**, 372–6.

Romani, M., Micalizzi, A., Kraoua, I., Dotti, M. T., Cavallin, M., Sztriha, L., Ruta, R., Mancini, F., Mazza, T., Castellana, S., et al. (2014). Mutations in B9D1 and MKS1 cause mild Joubert syndrome: expanding the genetic overlap with the lethal ciliopathy Meckel syndrome. *Orphanet J. Rare Dis.* **9**, 72.

Roussel, M. F. and Hatten, M. E. (2011). Cerebellum development and medulloblastoma. *Curr. Top. Dev. Biol.* **94**, 235–82.

Ruiz-Gómez, A., Molnar, C., Holguín, H., Mayor, F. and de Celis, J. F. (2007). The cell

biology of Smo signalling and its relationships with GPCRs. *Biochim. Biophys. Acta* **1768**, 901–12.

Saggese, T., Young, A. A., Huang, C., Braeckmans, K. and McGlashan, S. R. (2012). Development of a method for the measurement of primary cilia length in 3D. *Cilia* **1**, 11.

Salter, J. (2016). blindanalysis: v1.0.

Sánchez-Camacho, C. and Bovolenta, P. (2008). Autonomous and non-autonomous Shh signalling mediate the in vivo growth and guidance of mouse retinal ganglion cell axons. *Development* **135**, 3531–41.

Sánchez-Camacho, C. and Bovolenta, P. (2009). Emerging mechanisms in morphogen-mediated axon guidance. *BioEssays* **31**, 1013–25.

Santos, N. and Reiter, J. F. (2014). A central region of Gli2 regulates its localization to the primary cilium and transcriptional activity. *J. Cell Sci.* **127**, 1500–10.

Sasaki, H., Nishizaki, Y., Hui, C., Nakafuku, M. and Kondoh, H. (1999). Regulation of Gli2 and Gli3 activities by an amino-terminal repression domain: implication of Gli2 and Gli3 as primary mediators of Shh signaling. *Development* **126**, 3915–3924.

Schindelin, J., Arganda-Carreras, I., Frise, E., Kaynig, V., Longair, M., Pietzsch, T., Preibisch, S., Rueden, C., Saalfeld, S., Schmid, B., et al. (2012). Fiji: an open-source platform for biological-image analysis. *Nat. Methods* **9**, 676–82.

Seo, S., Zhang, Q., Bugge, K., Breslow, D. K., Searby, C. C., Nachury, M. V and Sheffield, V. C. (2011). A novel protein LZTFL1 regulates ciliary trafficking of the BBSome and Smoothened. *PLoS Genet.* **7**, e1002358.

Sfakianos, J., Togawa, A., Maday, S., Hull, M., Pypaert, M., Cantley, L., Toomre, D. and Mellman, I. (2007). Par3 functions in the biogenesis of the primary cilium in polarized epithelial cells. *J. Cell Biol.* **179**, 1133–40.

Shi, S.-H., Cheng, T., Jan, L. Y. and Jan, Y.-N. (2004). APC and GSK-3beta are involved in mPar3 targeting to the nascent axon and establishment of neuronal polarity. *Curr. Biol.* **14**, 2025–32.

Shirasaki, R., Tamada, A., Katsumata, R. and Murakami, F. (1995). Guidance of cerebellofugal axons in the rat embryo: Directed growth toward the floor plate and subsequent elongation along the longitudinal axis. *Neuron* **14**, 961–972.

Stone, D. M., Hynes, M., Armanini, M., Swanson, T. A., Gu, Q., Johnson, R. L., Scott, M. P., Pennica, D., Goddard, A., Phillips, H., et al. (1996). The tumour-suppressor gene patched encodes a candidate receptor for Sonic hedgehog. *Nature* **384**, 129–34.

Stuhmer, T., Anderson, S. A., Ekker, M. and Rubenstein, J. L. R. (2002). Ectopic expression of the Dlx genes induces glutamic acid decarboxylase and Dlx expression. *Development* **129**, 245–252.

Su, C.-Y., Bay, S. N., Mariani, L. E., Hillman, M. J. and Caspary, T. (2012). Temporal deletion of Arl13b reveals that a mispatterned neural tube corrects cell fate over time. *Development* **139**, 4062–71.

Suh, J. M., Gao, X., McKay, J., McKay, R., Salo, Z. and Graff, J. M. (2006). Hedgehog signaling plays a conserved role in inhibiting fat formation. *Cell Metab.* **3**, 25–34.

Svärd, J., Heby-Henricson, K., Henricson, K. H., Persson-Lek, M., Rozell, B., Lauth, M., Bergström, A., Ericson, J., Toftgård, R. and Teglund, S. (2006). Genetic elimination of Suppressor of fused reveals an essential repressor function in the mammalian Hedgehog

signaling pathway. *Dev. Cell* **10**, 187–97.

Taipale, J., Cooper, M. K., Maiti, T. and Beachy, P. A. (2002). Patched acts catalytically to suppress the activity of Smoothened. *Nature* **418**, 892–7.

Tamada, A., Kumada, T., Zhu, Y., Matsumoto, T., Hatanaka, Y., Muguruma, K., Chen, Z., Tanabe, Y., Torigoe, M., Yamauchi, K., et al. (2008). Crucial roles of Robo proteins in midline crossing of cerebellofugal axons and lack of their up-regulation after midline crossing. *Neural Dev.* **3**, 29.

Teperino, R., Amann, S., Bayer, M., McGee, S. L., Loipetzberger, A., Connor, T., Jaeger, C., Kammerer, B., Winter, L., Wiche, G., et al. (2012). Hedgehog partial agonism drives Warburg-like metabolism in muscle and brown fat. *Cell* **151**, 414–26.

Thomas, S., Wright, K. J., Le Corre, S., Micalizzi, A., Romani, M., Abhyankar, A., Saada, J., Perrault, I., Amiel, J., Litzler, J., et al. (2014). A homozygous PDE6D mutation in Joubert syndrome impairs targeting of farnesylated INPP5E protein to the primary cilium. *Hum. Mutat.* **35**, 137–46.

Thomas, S., Cantagrel, V., Mariani, L., Serre, V., Lee, J.-E., Elkhartoufi, N., de Lonlay, P., Desguerre, I., Munnich, A., Boddaert, N., et al. (2015). Identification of a novel ARL13B variant in a Joubert syndrome-affected patient with retinal impairment and obesity. *Eur. J. Hum. Genet.* **23**, 621–7.

Tukachinsky, H., Lopez, L. V and Salic, A. (2010). A mechanism for vertebrate Hedgehog signaling: recruitment to cilia and dissociation of SuFu-Gli protein complexes. *J. Cell Biol.* **191**, 415–28.

Tuson, M., He, M. and Anderson, K. V (2011). Protein kinase A acts at the basal body of the primary cilium to prevent Gli2 activation and ventralization of the mouse neural tube. *Development* **138**, 4921–30.

Tuz, K., Bachmann-Gagescu, R., O'Day, D. R., Hua, K., Isabella, C. R., Phelps, I. G., Stolarski, A. E., O'Roak, B. J., Dempsey, J. C., Lourenco, C., et al. (2014). Mutations in CSPP1 cause primary cilia abnormalities and Joubert syndrome with or without Jeune asphyxiating thoracic dystrophy. *Am. J. Hum. Genet.* **94**, 62–72.

Umberger, N. L. and Caspary, T. (2015). Ciliary transport regulates PDGF-AA/αα signaling via elevated mammalian target of rapamycin signaling and diminished PP2A activity. *Mol. Biol. Cell* **26**, 350–8.

Valente, E. M., Brancati, F. and Dallapiccola, B. (2008). Genotypes and phenotypes of Joubert syndrome and related disorders. *Eur. J. Med. Genet.* **51**, 1–23.

van Reeuwijk, J., Arts, H. H. and Roepman, R. (2011). Scrutinizing ciliopathies by unraveling ciliary interaction networks. *Hum. Mol. Genet.* **20**, R149–57.

vandenHeuvel, M. and Ingham, P. (1996). Smoothened encodes a serpentine protein required for hedgehog signalling. *Nature* **382**, 547–551.

Varjosalo, M., Li, S.-P. and Taipale, J. (2006). Divergence of hedgehog signal transduction mechanism between Drosophila and mammals. *Dev. Cell* **10**, 177–86.

Vierkotten, J., Dildrop, R., Peters, T., Wang, B. and Rüther, U. (2007). Ftm is a novel basal body protein of cilia involved in Shh signalling. *Development* **134**, 2569–77.

Wang, B., Fallon, J. F. and Beachy, P. A. (2000). Hedgehog-regulated processing of Gli3 produces an anterior/posterior repressor gradient in the developing vertebrate limb. *Cell* **100**, 423–34.

Wang, V. Y., Rose, M. F. and Zoghbi, H. Y. (2005). Math1 expression redefines the rhombic lip derivatives and reveals novel lineages within the brainstem and cerebellum. *Neuron* **48**, 31–43.

Wang, Y., Zhou, Z., Walsh, C. T. and McMahon, A. P. (2009). Selective translocation of intracellular Smoothened to the primary cilium in response to Hedgehog pathway modulation. *Proc. Natl. Acad. Sci. U. S. A.* **106**, 2623–8.

Wang, C., Pan, Y. and Wang, B. (2010). Suppressor of fused and Spop regulate the stability, processing and function of Gli2 and Gli3 full-length activators but not their repressors. *Development* **137**, 2001–9.

Wang, J., Morita, Y., Mazelova, J. and Deretic, D. (2012). The Arf GAP ASAP1 provides a platform to regulate Arf4- and Rab11-Rab8-mediated ciliary receptor targeting. *EMBO J.* **31**, 4057–71.

Ward, H. H., Brown-Glaberman, U., Wang, J., Morita, Y., Alper, S. L., Bedrick, E. J., Gattone, V. H., Deretic, D. and Wandinger-Ness, A. A conserved signal and GTPase complex are required for the ciliary transport of polycystin-1. *Mol. Biol. Cell* 1–36.

Ward, H. H., Brown-Glaberman, U., Wang, J., Morita, Y., Alper, S. L., Bedrick, E. J., Gattone, V. H., Deretic, D. and Wandinger-Ness, A. (2011). A conserved signal and GTPase complex are required for the ciliary transport of polycystin-1. *Mol. Biol. Cell* **22**, 3289–305.

Wen, X., Lai, C. K., Evangelista, M., Hongo, J.-A., de Sauvage, F. J. and Scales, S. J. (2010). Kinetics of hedgehog-dependent full-length Gli3 accumulation in primary cilia and subsequent degradation. *Mol. Cell. Biol.* **30**, 1910–22.

Westlake, C. J., Baye, L. M., Nachury, M. V, Wright, K. J., Ervin, K. E., Phu, L., Chalouni, C., Beck, J. S., Kirkpatrick, D. S., Slusarski, D. C., et al. (2011). Primary cilia membrane assembly is initiated by Rab11 and transport protein particle II (TRAPPII) complex-dependent trafficking of Rabin8 to the centrosome. *Proc. Natl. Acad. Sci. U. S. A.* **108**, 2759–64.

Wijgerde, M., McMahon, J. A., Rule, M. and McMahon, A. P. (2002). A direct requirement for Hedgehog signaling for normal specification of all ventral progenitor domains in the presumptive mammalian spinal cord. *Genes Dev.* **16**, 2849–64.

Wilson, N. H. and Stoeckli, E. T. (2013). Sonic hedgehog regulates its own receptor on postcrossing commissural axons in a glypican1-dependent manner. *Neuron* **79**, 478–91.

Wong, S. Y. and Reiter, J. F. (2008). The Primary Cilium: At the Crossroads of Mammalian Hedgehog Signaling. *Curr. Top. Dev. Biol.* **85**, 225–260.

Xu, Q., Zhang, Y., Wei, Q., Huang, Y., Hu, J. and Ling, K. (2016). Phosphatidylinositol phosphate kinase PIPKIγ and phosphatase INPP5E coordinate initiation of ciliogenesis. *Nat. Commun.* **7**, 10777.

Yachnis, A. T. and Rorke, L. B. (1999). Neuropathology of Joubert Syndrome. *J. Child Neurol.* **14**, 655–659.

Yam, P. T., Langlois, S. D., Morin, S. and Charron, F. (2009). Sonic hedgehog guides axons through a noncanonical, Src-family-kinase-dependent signaling pathway. *Neuron* **62**, 349–62.

Yasunaga, T., Hoff, S., Schell, C., Helmstädter, M., Kretz, O., Kuechlin, S., Yakulov, T. A., Engel, C., Müller, B., Bensch, R., et al. (2015). The polarity protein Inturned links NPHP4 to Daam1 to control the subapical actin network in multiciliated cells. *J. Cell Biol.* **211**,

963–73.

Yoshimura, S.-I., Egerer, J., Fuchs, E., Haas, A. K. and Barr, F. A. (2007). Functional dissection of Rab GTPases involved in primary cilium formation. *J. Cell Biol.* **178**, 363–9.

Yuan, S. and Sun, Z. (2013). Expanding horizons: ciliary proteins reach beyond cilia. *Annu. Rev. Genet.* **47**, 353–76.